Loss of TET2 increases B-1 cell number and IgM production while limiting CDR3 diversity

Emily Ann Dennis
Virginia Beach, VA

B.A., University of Virginia, 2017
M.S., University of Virginia, 2021

A Dissertation presented to the Graduate Faculty of the University of Virginia in Candidacy for the Degree of Doctor of Philosophy

Department of Microbiology, Immunology, and Cancer Biology

University of Virginia
July, 2024

Abstract

Ten-Eleven Translocation-2 (TET2) is an epigenetic modifier and potent regulator of immune cells, yet its role in B-1 cell biology is largely unknown. B-1 cells protect against infection and clear apoptotic cells via the production of natural Immunoglobulin M (IgM). Our study analyzed B-1 cell subsets from mice with global knockout (KO) of TET2 compared to wildtype (WT) controls using flow cytometry to determine the frequency and number of B cell subsets, RNA sequencing to determine differences in global gene expression as well as B cell receptor (BCR) repertoire analysis, and enzyme-linked immunosorbent assay (ELISA) to evaluate plasma IgM levels. Mice with TET2-KO had elevated numbers of B-1a and B-1b cells in their primary niche, the peritoneal cavity, as well as in the bone marrow and spleen. Consistent with this finding, circulating IgM was elevated in TET2-KO mice compared to WT. We observed reduced expression in both heavy and light chain immunoglobulin genes, predominantly in B-1a cells from TET2-KO mice compared to WT controls. As expected, IgM was by far the most abundant isotype expressed by genes in B-1 cells. Yet, only in B-1a cells was there a significant increase in the proportion of IgM isotypes in TET2-KO mice compared to WT. Analysis of the complementarity determining region 3 (CDR3) revealed an increased abundance of replicated CDR3 sequences in B-1 cells from TET2-KO mice, which was more clearly pronounced in B-1a compared to B-1b cells. The results from our study suggest that TET2 may regulate the pool of antigen-specific IgM-producing cells.

Acknowledgments and Dedication

It has been an honor and a privilege to be a student and employee at the University of Virginia for the past eleven years and to graduate as a “Triple Hoo.” One of the tenets of UVA that I hold most dear is the concept of lifelong learning. I am certain my scientific curiosity has been given a strong foundation and the excitement of learning and discovery will never diminish.

Coleen McNamara provided her wisdom, scientific guidance, and the supportive environment she has established with her lab at UVA, and I am profoundly grateful for her mentorship. Thank you for always being honest with me, encouraging me to follow the science, and providing an example of patience, perseverance, and optimism.

I am so fortunate to have been embraced by a team of critical thinkers and hard workers. Melissa Marshall assumed the leadership of the lab during a time of incredible upheaval, from our move across buildings to a nationwide epidemic. She has been a wonderful role model in the way she mentors everyone in the lab from postdoctoral researchers to undergraduate volunteers. Melissa has been essential to my success and a terrific friend and colleague, and I hope my future workplace is filled with clones of her. I am thankful for the many scientific discussions with lab mates Oom Pattarabanjird and Brett Ransegnola. They helped me navigate the pandemic's isolation and the hardships of starting my doctoral project from scratch. Cassidy Blackburn, I thank you for your scientific insights and friendship. You have been a role model to me as a young scientist balancing work-life and family. To Maria Murach, you were instrumental in enriching

my project with your bioinformatics expertise, and I look forward to seeing all you accomplish in the future. Katherine Root, bless you for managing the mice colony and assistance with the many takedowns.

Thank you to my committee, particularly Loren Erickson for taking the helm as my co-mentor and Chair and being so enthusiastic and encouraging about my project. The other members of my committee, Stefan Bekiranov, Melanie Rutkowski and Rusty Elliot, provided excellent advice about my projects as well as helpful counsel about career planning. In addition, the technical assistance from Mike Solga and Lesa Campbell at the UVA Flow Cytometry Core Facility was essential to the success of my experiments. I would also like to thank our collaborators at the Medical University of Vienna, Dr. Christoph Binder, his doctoral student Justine Deroissart, and lab member Maria Ozsvar Kozma, as well as Dr. Nichol Holodick from Western Michigan University and Dr. Ken Walsh here at UVA, for their scientific contributions and advice.

My friends and family, both present and no longer with me, have been a wonderful support system during my time as a doctoral student. In particular, my parents Tabatha Dennis (Frankie Rodriguez) and Stephen Dennis (Paulette Boyette), and my grandmother. I know my grandfather would be “tickled” that I am now a published author and can call myself “Doctor.” The date my first manuscript was accepted will always be bittersweet as I lost my Aunt Diane that day. I would also like to thank my family-in-law for always being there and happy to hear about my research.

Francesca Azar, whom I met during my first week as an undergraduate at UVA, encouraged me to explore the biomedical research path with her in our fourth year. I am

so incredibly honored to call you my best friend, and I can't wait to celebrate with you. Here's to many more years of friendship and matching science and cat tattoos.

To my husband, Billy Bower, who has been unfailingly supportive and never allowed me to give up my dreams, I dedicate this to you. Your patience and support have meant the world to me, as well as the boundless love you have for our menagerie of Ana, Cleo, Mister, Daphne, and Daisy (and in memoriam, Rocky, Reginald, and Poppy). I thank you from the bottom of my heart and can't wait to see where life takes us.

Table of Contents

List of Figures

List of Tables

List of Abbreviations

5mC	5-methylcytosine
5hmC	5-hydroxymethylcytosine
Ab	Antibody
AID	Activation-induced cytidine deaminase
ALCAM	Activated leukocyte cell adhesion molecule
AML	Acute myeloid leukemia
ASCVD	Atherosclerotic cardiovascular disease
ASXL1	ASXL transcriptional regulator 1
BCR	B cell receptor
BM	Bone marrow
CAD	Coronary artery disease
CCL	CC motif chemokine ligand
CCR	CC motif chemokine receptor
CDR3	Complementarity determining region 3
CHIP	Clonal hematopoiesis of indeterminate potential
CSR	Class switch recombination
CVD	Cardiovascular disease
CXCR	CXC motif chemokine receptor
DAMP	Danger-associated molecular patterns
DEG	Differentially expressed genes

D_H	Heavy chain diversity genes
DLBCL	Diffuse large B cell lymphoma
DNTM3A	DNA (cytosine-5)-methyltransferase 3A
DZ	Dark zone
ELISA	Enzyme-linked immunosorbent assay
ES	Enrichment score
FACS	Fluorescence-activated cell sorting
Fc	fragment crystallizable region of the antibody
FDR	False discovery rate
FMO	Fluorescence minus one
FO	Follicular
GC	Germinal center
GSEA	Gene set enrichment analysis
HDAC	Histone deacetylase
HSC	Hematopoietic stem cell
Ig	Immunoglobulin
IgA	Immunoglobulin class A antibody
ICAM	Intercellular adhesion molecule
IgD	Immunoglobulin class D antibody
IgG	Immunoglobulin class G antibody
IgH	Immunoglobulin heavy chain
Ig_K	Immunoglobulin kappa light chain

Ig_L	Immunoglobulin lambda light chain
IgM	Immunoglobulin class M antibody
IL	Interleukin
J_H	Heavy chain junctional genes
KO	Knockout
LDL	Low-density lipoprotein
LPS	Lipopolysaccharide
LZ	Light zone
Macs	Macrophages
MDA	Malondialdehyde
MDS	Myelodysplastic syndrome
MFI	Median fluorescence intensity
MS	Multiple sclerosis
Mx1-Cre/$Tet2^{Lox/Lox}$	Catalytically inactive TET2 mouse model
MZ	Marginal zone
MZB	Marginal zone B cell
Nab	Natural antibody
N-additions	Non-template encoded nucleotide additions
NLRP3	NLR family pyrin domain containing 3
OSE	Oxidation-specific epitope
OxLDL	Oxidized LDL
PAMP	Pathogen-associated molecular patterns

PBMC	Peripheral blood mononuclear cell
PC	Phosphorylcholine
PtC	Phosphatidylcholine
PerC	Peritoneal cavity
PRR	Pattern recognition receptor
SHM	Somatic hypermutation
SLE	Systemic lupus erythematosus
SLO	Secondary lymphoid organ
RA	Rheumatoid arthritis
RLU	Relative light units
TCR	T cell receptor
TD	T cell-dependent
TdT	Terminal deoxynucleotidyl transferase
TET2	Ten-eleven translocation 2
TET2-KO	Global TET2 knockout mouse
$Tet2^{LacZ/LacZ}$	Catalytically inactive TET2 mouse model
TET2-WT	Wildtype littermate control to TET2-KO mouse
Tfh	T follicular helper cell
Th	Helper T cell
TI	T cell-independent
TLR	Toll like receptor
VCAM	Vascular cell adhesion molecule

V-D-J	Variable-Diversity-Junctional genes
V_H	Heavy chain variable genes
WD	Western diet
WT	Wildtype

Chapter 1: Introduction

B cells are key mediators of auto-immunity

B cells are major immune cells with roles in innate and adaptive immunity. Their primary function is to secrete antibodies in response to danger or pathogen signaling via pattern recognition receptors (PRRs) or T cell-mediated activation. Several subsets of B cells exist in mice and can be broadly categorized as B-1 and B-2 due to the timing of their development, as B-1 cells arise earlier within the fetal liver and B-2 cells arise later and are repopulated by hematopoietic progenitors in the adult bone marrow (BM) [1] [2-6]. B-2 cells populate secondary lymphoid organs (SLOs) and are the main B cell type in circulation. B-2 cells can be further classified into marginal zone (MZ) and follicular (FO) B cells. Marginal zone B cells (MZB) are static and located in the marginal zone of the spleen, and show similar characteristics to B-1 cells in early participation in Type 1 T cell-independent (TI) responses, but also participate in T cell-dependent responses [1]. FO B-2 cells reside around follicular dendritic cells in the white pulp of the spleen and the cortical areas of peripheral lymph nodes, and they also circulate [1]. FO B-2 cells are dependent on T follicular helper (Tfh) cell interaction in the formation of germinal centers (GC), specialized microenvironments within SLOs, to promote effective primary immune responses and antibody isotype switching for the establishment of high-affinity B cell memory cells or long-lived plasma cells [1, 7].

There is also a subset of B cells called regulatory B cells, which secrete anti-inflammatory cytokines such as IL-10 and TGF-β and suppress effector T cell responses. They can play a role in autoimmune diseases, transplantation tolerance, and allergic

reactions. This subset of B cells is implicated in the modulation of immune responses and maintenance of immune tolerance, but they require more investigation.

B-1 cells produce natural IgM antibody

B-1 cells originate from the fetal liver and are long-lived and self-renewing [8-11]. B-1 cells can be found predominantly in the serosal spaces such as the peritoneal cavity (PerC) or the pleural cavity, but can also migrate to SLOs such as the spleen and lymph nodes, as well as into the BM [12] [13]. B-1 cells can produce antibodies via TI responses without GC formation. There are two types of TI responses. The Type 1 TI response involves activation of antibody secretion via a PRR such as toll-like receptor 4 (TLR4) or cytokine stimulation, independent from signaling through the B cell receptor (BCR) [14-18]. In this case there is limited affinity maturation (the process of increasing antibody affinity for a given antigen), so the majority of the antibodies produced have lower affinity to specific antigens but more extensive specificities for antigens as a whole [9]. In addition, B-1 cells can produce antibodies such as IgM (immunoglobulin M), which are naturally occurring (i.e. can be present even without infection) [19-21]. These natural antibodies act during the innate immune response to provide rapid protection and maintain tissue homeostasis through apoptotic cell clearance [22]. However, the Type 2 TI response signals through BCR cross-linking, which at a large enough scale overrules the need for T cell mediation to produce antigen-specific antibodies [23].

The first antibody isotype to be produced by B cells is IgM. 80% of IgM is derived from B-1 cells, where a low level of IgM is produced by B-1 cells in serosal

cavities, and the majority of IgM is produced by the few B-1 cells in the spleen and BM [19, 24-26]. IgM acts in several ways to control the immune response. The first is to bind to the complement compound C1 and activate the classical complement pathway, which results in the opsonization of antigens and subsequent cytolysis. Additionally, Fc receptors Fcα/μ-R and Fcμ-R bind to IgM, which results in the uptake of the IgM-bound antigen and endocytosis. Thus, IgM facilitates the clearance of antigens and the resolution of inflammation [27]. Another important function of B cells is the secretion of cytokines. Cytokines can influence other immune cells towards a more pro- or anti-inflammatory state, as well as serve as recruiters for additional immune cell infiltration [28]. Autoimmune disorders tend to be caused by IgG antibodies against self, while IgM antibodies tend to be protective [29-45].

Generation of diverse antibodies

B cells produce antibodies of varied specificity through their BCR. The BCR structure is complex and is critical for the recognition and resultant response of the B cell to antigens. The BCR is membrane-bound and made up of a variable region and a constant region. The variable region, which consists of heavy and light chains, binds to specific antigens. This region's diversity allows B cells to recognize a vast array of antigens. The variable region includes V (variable), D (diversity), and J (joining) segments. The light chain variable region includes V and J segments only (no D segment). The constant region determines the antibody's class (IgM, IgD, IgG, IgA, IgE)

and mediates effector functions. The constant region of the heavy chain anchors the receptor in the B cell membrane.

The BCR generates diverse antibodies through a process called VDJ recombination, resulting in millions of different specificities from a relatively small number of genes. VDJ recombination of the immunoglobulin heavy chain involves the random selection and recombination of V, D, and J gene segments to form a complete heavy chain variable region exon. The light chain also undergoes recombination of its V and J genes. Additional variability is introduced through non-template-encoded N nucleotide (N-additions) and nucleotide excisions at the junctions between V-D and D-J gene segments.

Antigen binding occurs and is determined by hypervariable regions of IgH V genes called the complementarity determining regions (CDRs), the most variable of which is CDR3. Several studies have sequenced the variable region of the heavy chain (V_H) and shown that significant heterogeneity exists in the V_H repertoire of B cell subsets from different locations.

Antibodies are unbound versions of the BCR. Sometimes, antibodies can bind to similar epitopes on different antigens, which is called cross-reactivity. Errors in VDJ recombination can potentially create self-reactive receptors, contributing to autoimmune diseases. The severity of autoimmune disorders like systemic lupus erythematosus (SLE) are often dependent on the titer of auto-antibody in circulation or in the disease-targeted tissues.

Atherosclerosis is an autoimmune disorder

Atherosclerosis (ASCVD), the major type of cardiovascular disease (CVD), is a disease of chronic systemic inflammation and is characterized by the formation of lipid-laden lesions which occlude the blood vessel lumen, reducing blood flow past the lesions. As the disease progresses, thromboembolic events such as stroke or heart attack risk increases and is the leading cause of death worldwide [46]. ASCVD is widely becoming accepted as being classified as an autoimmune disorder [47-50]. The development of atherosclerosis begins with an accumulation of low-density lipoprotein (LDL) in the artery wall, which can become oxidized [51]. Oxidized LDL (oxLDL) activates the endothelial cells lining the artery wall, which induces adhesive membrane glycoproteins that serve as sites of attachment for circulating immune cells such as monocytes to extravasate from the vessel into the lesion. OxLDL is then taken up by scavenger receptors on monocyte-derived macrophages [52]. Eventually, when a macrophage has engulfed a large amount of oxLDL, there is a phenotypic change, and the heavily lipid-laden cell becomes a foam cell and forms fatty streaks. Other immune cells infiltrate the artery wall as atherosclerosis progresses, including neutrophils, T cells, and B cells, which increases inflammation. As foam cells accumulate and die, the lesion grows, and smooth muscle cells surrounding the blood vessel migrate to the surface of the lesion to form a stabilizing fibrous cap. As the lesion grows, the fibrous cap can become destabilized, and rupture and a blood clot can lead to stroke or heart attack. Connections among the immunologic side to activated endothelium, local inflammation, and infiltration of immune cells have received great attention.

B cells in atherosclerosis

While the role of monocytes and macrophages has been extensively studied in atherosclerosis inflammation research, more recently lymphocytes have been shown to contribute to the inflammation landscape [53]. Evidence demonstrates a role for B cell subsets in atherosclerosis progression [54-72]. B-2 cells can be atherogenic by influencing CD4 helper T cell differentiation towards a pro-inflammatory Th1 fate through IgG secretion, and an additional study which depleted B-2 cells showed attenuated atherosclerosis [28, 64, 67, 73]. However, further studies are needed to identify the specific mechanisms involved in B-2-mediated atherosclerosis progression.

B-1 cells can be divided further into B-1a and B-1b B cell subsets based on surface expression of CD5 (B-1a cells are $CD5^+$ and B-1b cells are $CD5^-$), but both are atheroprotective and produce IgM [8, 16, 25, 61, 63]. Passive and active immunization of mice with IgM specific to LDL or oxLDL attenuated atherosclerosis and established that IgM is atheroprotective [73-79]. IgM to oxidation-specific epitopes (OSEs) that amass during atherosclerosis, such as malondialdehyde (MDA) and oxidized phospholipids present on oxLDL, can reduce macrophage lipid uptake, thereby preventing foam cell formation and subsequent inflammatory cytokine production [74, 75, 77, 80, 81].

Our lab discovered that the B-1b B cell subset produces ample IgM to OSE and protects Apoe-/- mice from diet-induced atherosclerosis [61]. A putative human equivalent to the murine B-1 cell was recently identified through its ability to produce IgM spontaneously; plasma levels of IgM to MDA-LDL in humans are associated with

less coronary artery disease (CAD) and fewer adverse events [82]. In addition, IgM to MDA-LDL can predict 15-year CVD outcomes, potentially providing clinical assistance to reassign a significant number of individuals into adjusted risk categories following a traditional risk assessment [78, 83-85]. Altogether, these data provide evidence that IgM to MDA-LDL-producing B cells in humans may be atheroprotective.

TET2 loss of function is associated with CVD research

Researchers have discovered a novel risk factor that could increase CVD risk by two- to four-fold: Clonal Hematopoiesis of Indeterminate Potential (CHIP) [86-98]. CHIP is the occurrence of a clonal population of blood cells with somatic mutations detected at a variant allele frequency of 2% or higher [86]. Overwhelmingly, CHIP mutations accumulate with age [86, 88, 92, 94, 95, 99, 100]. Individuals with CHIP and a conventionally low risk of CVD exhibit a significant level of atherosclerosis [87-91, 94-96, 99-103]. Furthermore, somatic mutations in candidate driver genes such as Ten-Eleven Translocation 2 (*TET2*), DNA Methyl Transferase 3A (*DNMT3A*), and Additional Sex Combs-Like protein 1 (*ASXL1*), are canonically associated with hematological malignancies, and are implicated in this increased CVD risk. Additionally, individuals with CHIP have an unexpected and noteworthy increase in mortality attributed to the increase in CVD prevalence among individuals with CHIP.

The TET family of proteins act enzymatically as α-ketoglutarate-dependent cytosine dioxygenases that promote DNA demethylation by oxidizing the methyl group of 5-methylcytosine (5mC) to 5-hydroxymethylcytosine (5hmC) [104-107]. The methylation status of DNA is important in recruiting proteins for gene repression or inhibition of transcription factor binding. Additionally, TET proteins enlist chromatin modifying proteins to histones, which can affect gene expression via physical accessibility for transcription [108, 109]. Thus, TET proteins are potent epigenetic modulators.

TET2 deficiency accelerates atherosclerosis in mice

Murine BM chimera studies showed a connection between deficiency in TET2 and acceleration of atherosclerosis through an increase in inflammatory macrophage production of IL-1 β and activation of the NLRP3 inflammasome [110, 111]. While macrophages are an important cell type in atherogenesis, so too are B cells; B cells are known to play a role in modulating inflammation in atherosclerotic plaques, as mentioned earlier. We posit that macrophages are not the only immune cells involved in atherosclerosis progression via TET2 deficiency. We hypothesize that B cells could assist in shaping the inflammatory landscape in atherosclerosis in subjects with TET2 CHIP. Gathering more data and developing information about the mechanistic regulation of other immune cells by TET2 will enable precision medicine to emerge further in the treatment of CVD.

TET2 regulation of myeloid cells

TET2 is highly involved in hematopoietic cell development and differentiation [112-114]. Dysfunction in TET2 is well characterized in hematological malignancies like acute myeloid leukemia (AML) and myelodysplastic syndromes [115-122], as well as autoimmune disorders like systemic lupus erythematosus (SLE) and rheumatoid arthritis (RA) [123-127].

In the myeloid lineage, which consists of monocytes, macrophages, and granulocytes, TET2 loss can affect inflammatory response via altered cytokine secretion (Figure 1) [110, 111, 116, 128]. Research has shown that TET2 can repress macrophage

and dendritic cell expression of IL-6, a major pro-inflammatory cytokine, in two ways [116, 129]. The first is through interacting with Iκbζ, an inhibitor of NFκB, to bind to the IL-6 promoter. The second way is through recruiting histone deacetylase 2 (HDAC2) to repress IL-6 expression. Additionally, as mentioned earlier, TET2 suppresses NLRP3-inflammasome-mediated IL-1B production in macrophages [110, 111]. TET2 and its effects on myeloid cells have been widely studied [114, 116, 118, 119, 126, 130-133].

TET2 regulation of lymphocytes

In the lymphoid lineage, which consists of T cells and B cells, there is less known about the role TET2 plays in development and differentiation (Figure 1). In T cells, 5hmC is elevated during their development in the thymus, specifically in regions where transcription factors influence CD4 and CD8 differentiation commitment [134]. Loss of TET2 in T cells can reduce commitment towards Th1 and Th17 CD4 helper T cell subsets and increase CD8 T cell differentiation, impair regulatory T cell stability, and aberrantly activate and increase effector function [135-137].

In B cells, TET2 has been implicated in B cell lymphomas and systemic autoimmunity. A study investigating TET2/3 loss during B cell development using a Mb1-Cre system found that loss of TET2 and TET3 together impairs B cell development at the pro-B to pre-B transition in a cell-autonomous manner due to decreased immunoglobulin kappa light chain (Ig_K) rearrangement and expression [109]. In addition, the investigators noted a reduction in mature B cell number in the double knockout which was age-related, and suggested that TET2 and TET2 play a role in maintaining B cell

homeostasis [109]. Another study corroborated the above results with a double knockout of TET2/3 and found that TET2/3-dependent demethylation is necessary to properly control gene expression and normal developmental progression in B cells [138]. In a study of diffuse large B cell lymphomas (DLBCLs), about 10% of patients with DLBCL had mutations in TET2 [139]. In a B cell-specific TET2-deficiency model using a CD19-Cre system, GC formation was disrupted, and plasma cell differentiation was prevented. GCs are transiently formed structures where B cells undergo clonal expansion, class switch recombination (CSR) at the IgH locus, somatic hypermutation (SHM) of V_H genes, and selection for increased affinity of a BCR for its unique antigenic epitope through affinity maturation [1]. GC B cells intermittently migrate between the GC dark zone (DZ), where they undergo clonal expansion and SHM, and the GC light zone (LZ) where cells expressing a high-affinity BCR are positively selected. Successful exit from a GC is necessary for plasma cell differentiation. The study showed that TET2 loss results in reduction in the 5hmC mark leading to aberrant repression of enhancers for genes that must be induced to resolve the GC phenotype and mediate the plasma cell phenotype [140, 141]. It was also shown that TET activity was required for CSR from IgM to IgG1 [139]. Furthermore, activation-induced cytidine deaminase (AID) was involved in SHM and immunoglobulin class switching of GC B cells via DNA hypomethylation, and has been shown to be dependent on TET2 enhancer elements within the *Aicda* locus [108, 142, 143].

Another study using two models of TET2 knockout, Mx1-Cre/$Tet2^{Lox/Lox}$ and $Tet2^{LacZ/LacZ}$, resulted in elevated frequency of B cells in both of the knockouts compared

to the WT; however, the sample size for this experiment was very low (n=2) and bears repeating with a larger sample size [144]. Tanaka and colleagues utilized a CD19-Cre system to make a double knockout of TET2 and TET3, and they found that there was aberrant T cell activation through B cells. Further, they observed that repression of CD86 in self-tolerant B cells was dependent on TET2/3 to prevent autoimmunity [124]. All the above-mentioned studies primarily focused on B-2 cells and suggest reduced production of high-affinity IgG (an isotype associated with increased atherosclerosis). Our results focusing on B-1 cells with TET2 deficiency will fill the knowledge gap that currently exists in the field and reveal how TET2 loss in B-1 cells affects cell number and function.

Figure 1. TET2 regulation of immune cells. TET2-mediated DNA demethylation regulates gene expression programs critical for many different immune cells' development, differentiation, homeostasis, activation, proliferation, and function. TET2 is involved in regulating the development and differentiation of T cells from hematopoietic progenitors in the thymus. Loss of TET2 function in early T cell progenitors can affect lineage commitment and skew T cell differentiation towards specific subsets. TET2-deficient T cells may exhibit altered cytokine production, proliferation, and effector functions, affecting their ability to mount effective immune responses. TET2-deficient B cells may exhibit dysregulated gene expression profiles and altered antibody responses, affecting their ability to mount effective immune responses against pathogens. Loss of TET2 function in myeloid cells such as macrophages may exacerbate inflammatory responses and contribute to the pathogenesis of inflammatory diseases and myeloid-related disorders. It is unknown if a phenotype change manifests in B-1 cells with TET2 deficiency. Figure schematic made with BioRender.

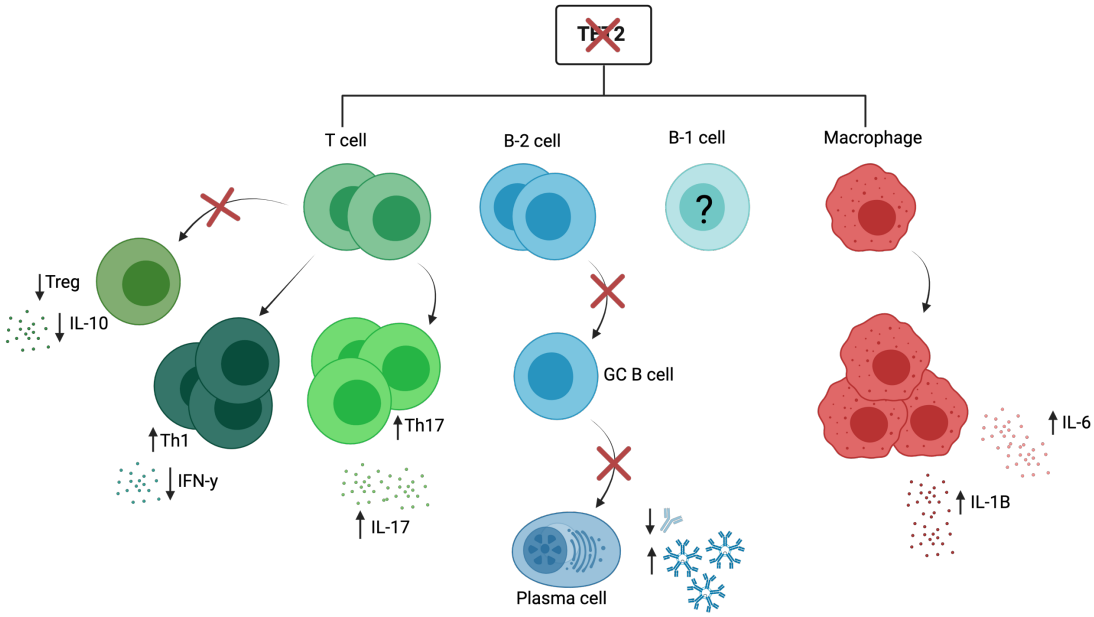
T cell
B-2 cell
B-1 cell
Macrophage
?
Treg
IL-10
Th1
IFN-y
Th17
IL-17
GC B cell
Plasma cell
IL-6
IL-1B

Project Rationale

Specific Aims

Cardiovascular disease (CVD) is the leading cause of death in individuals over 60 years old and affects more than 100 million Americans. Recent research has shown that somatic mutations in candidate driver genes for hematopoietic malignancies, or Clonal Hematopoiesis of Indeterminate Potential (CHIP), are associated with a two- to four-fold increased risk of CVD. Ten-Eleven Translocation 2 (TET2) is a candidate driver gene associated with CHIP and increased risk of CVD. Mechanisms mediating TET2 effects on atherosclerosis have largely focused on myeloid cells. TET2 can also play a regulatory role for B cells. B cells clearly regulate the formation of atherosclerosis and do so in a subset-dependent manner. B-2 cells aggravate atherosclerosis, while B-1 cells are atheroprotective through a mechanism mediated at least in part by the production of IgM to oxidation-specific epitopes (OSEs). While the role of TET2 in B-2 cells has been somewhat explored, little is known about TET2 regulation of B-1 cells. Further investigations to elucidate the mechanisms mediating the changes in B-1 cell number and to determine the impact on atherosclerosis are important, as they may provide evidence that TET2 function in B-1 cells could be targeted in the development of new anti-inflammatory therapies to reduce the risk of CVD.

I hypothesized that loss of TET2 in B-1 cells will differentially induce frequency, epigenetic, transcriptional, and functional changes in B-1 cell subtypes (Figure 2). I tested this hypothesis and gained insights with the following aims:

Aim 1: To investigate biological processes and Ig clonality affected by changes in gene expression and methylation in peritoneal B-1 cells from TET2-KO mice compared to WT controls using RNA sequencing and DNA methylation assays.

I collaborated with bioinformatics experts to leverage computational tools to test the hypothesis that genes differentially expressed and/or methylated in B-1 cell subtypes from TET2-KO mice will be associated with immune molecular and functional pathways implicated in atherosclerosis and will have a different repertoire of Igs.

Aim 2. To characterize immune cell type frequency in the peritoneal cavity, spleen, and bone marrow using flow cytometry and to measure Ig profiles using ELISA in mice with global TET2-KO compared to WT controls.

I hypothesized that TET2-KO mice would have increased frequencies in the known B-1 cell niches compared to WT, which would result in elevated IgM production.

Figure 2. Loss of TET2 in B-1 cells project rationale. Since the loss of TET2 in hematopoietic stem cells results in augmented proliferation, and loss of TET2 in B-2 cells restricts IgG production, I hypothesized that loss of TET2 will result in elevated B-1 cells and increased IgM production. I planned to test this hypothesis by analyzing gene expression and interrogating the BCR repertoire, characterizing the B-1 cell niches for immune cell composition, and measuring circulating Ig levels. Figure schematic made with BioRender.

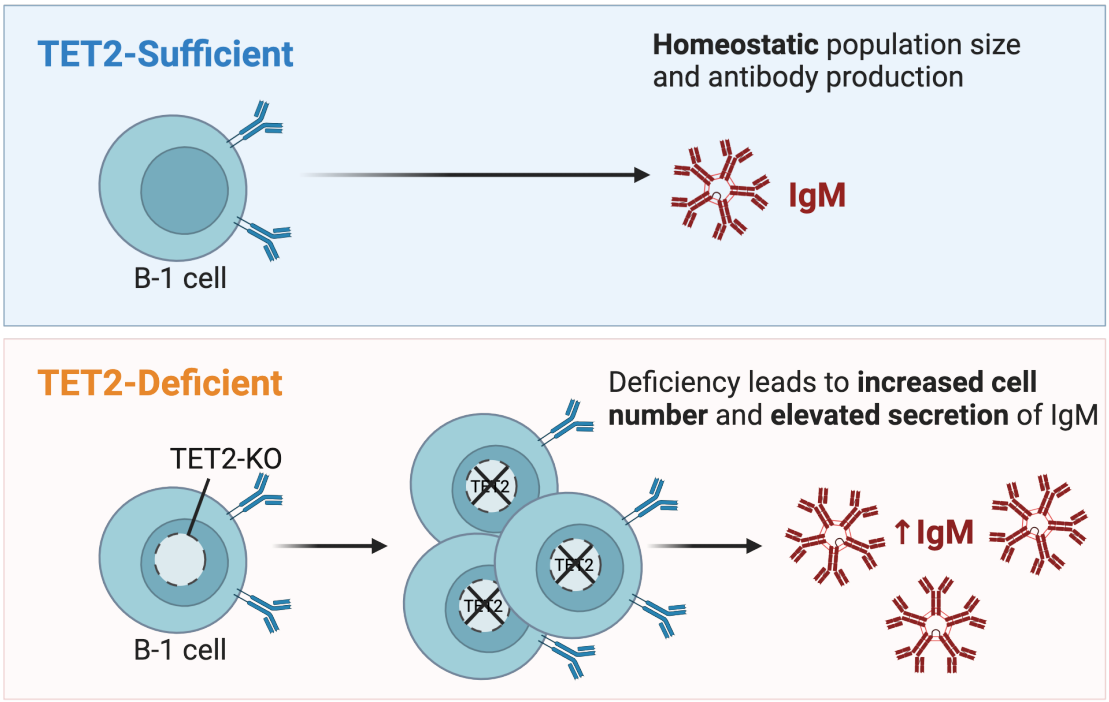

Aim 1
Leverage bioinformatic tools to analyze differential gene expression and BCR repertoire

Aim 2
Utilize flow cytometry and ELISA to determine immune cell populations and immunoglobulin levels

Chapter 2: Materials and Methods

Reagents

Prepared Buffers and Media

Peritoneal lavage media:

5% HI-FBS
1x Pen/strep
in DMEM

AKC lysis buffer:

0.15 M NH4Cl
0.01 M $KHCO_3$
0.1 mM EDTA
in ddH_2O

Flow buffer:

0.05% NaN_3
1% BSA
in PBS

FACS buffer:

1% BSA
in PBS

Sort collection buffer:

20% HI-FBS
1 mM HEPES
1x NEAA

100 μM NA-pyruvate
40 μg/ml Gentamycin
55μM β-mercaptoethanol
in RPMI

Fixation buffer:

2% PFA
in PBS

Mice

All animal protocols were approved by the Animal Care and Use Committee at the University of Virginia. TET2-KO mice [112] were provided by Dr. Kenneth Walsh (University of Virginia). The model was generated by Ko *et al.* and targeted the endogenous *TET2* locus to create a conditional allele that enabled the deletion of exons 8, 9, and 10, the catalytic region of TET2 [112]. Mice were maintained on a 12-h light/dark schedule in a specific pathogen-free animal facility and given food (standard chow diet, Tekland 7012) and water *ad libitum*. The number of mice included in each study is indicated in the figures or the associated legends.

Sample Preparations for Flow Cytometry and Live Cell Sorting

Bone marrow, spleen, and peritoneal cavity cells were processed for flow cytometry as previously described [61]. Briefly, following sacrifice by CO_2 overdose, peritoneal cells were harvested by flushing the peritoneal cavity with 10 mL FACS buffer (PBS containing 1% BSA, 0.05% NaN_3). The spleen and one femur and tibia were

removed. Spleens and flushed bone marrow were filtered through a 70 μm cell strainer. Red blood cells were lysed from single-cell suspensions of bone marrow and spleen using a lysis buffer containing 155 mM NH_4Cl, 10 mM $KHCO_3$, and 0.1 mM EDTA. Cell surface Fc receptors were blocked using anti-CD16/32 (clone:93, 4 eBioscience), then cells were stained with fluorescently conjugated antibodies against cell surface markers. Cells were stained with fixable Live/Dead Zombie NIR (Life Technologies) for dead cell discrimination, then fixed in 2% PFA in PBS. For FAC sorting, cells were resuspended in modified FACS buffer (PBS with 1% BSA) and 4',6-Diamidino-2-Phenylindole (DAPI) live/dead stain then immediately taken to the University of Virginia Flow Cytometry Core for sorting. B-1a and B-1b cells were sorted to better than 99% purity from their parent gate. Clone and fluorophore information for the flow cytometry antibodies used in murine experiments to immunophenotype or FAC-sort B cell subsets are given in Table 1 and Table 2 respectively.

All flow cytometry was conducted at the University of Virginia Flow Cytometry Core Facility. Immunophenotyping was performed on an Aurora Borealis 5-laser (Cytek) cytometer. FAC-sorting was performed on an Influx Cell Sorter (Becton Dickinson). Data analysis and flow plots were generated using OMIQ software (Dotmatics). Representative flow plots were chosen based on the samples whose population frequencies were closest to the mean for that group. Gates on flow plots were set using fluorescence minus one (FMO) controls.

Table 1. Murine immunophenotyping panel used for flow cytometry of the peritoneal cavity, bone marrow, and spleen.

Marker	**Fluorophore**	**Clone**	**Vendor**
CD45	PerCP	30-F11	BD
B220	APC	RA3-6B2	eBioscience
CD19	APCefl780	1D3	eBioscience
IgM	PECF594	R6-60.2	BD
IgD	efl450	11-26	eBioscience
CD8	BV510	53-6.7	BioLegend
CD4	PECy5.5	GK1.5	SouthernBiotech
CD44	BV785	IM7	BioLegend
CD62L	BV570	MEL-14	BioLegend
CD25	BB515	PC61	BD
F4/80	PECy7	BM8	eBioscience
CD11b	PerCPCy5.5	M1/70	BD
CD11c	AF647	N418	BioLegend
CD138	PE	281-2	BD
Ly6c	BV711	HK1.4	BioLegend
NK1.1	BV480	PK136	BD
CD5	BV605	53-7.3	BD
CD21	FITC	4E3	eBioscience
CD23	BUV737	B3B4	BD
Zombie NIR Fixable Viability Dye			BioLegend

Table 2. Murine FACS panel used for sorting B cell subsets from the peritoneal cavity.

Marker	**Fluorophore**	**Clone**	**Vendor**
IgD	FITC	11-26	eBioscience
CD5	PE	53-7.3	eBioscience
CD23	PE-CY7	B3B4	eBioscience
B220	APC	RA3-6B2	eBioscience
CD19	APC-EF780	1D3	eBioscience
DAPI Staining Solution			Miltenyi Biotec

ELISA for quantification of total IgM in mice

Total IgM in mouse plasma was measured using colorimetric ELISA as described previously [61]. Briefly, EIA/RIA high-binding microplates were coated with goat anti-mouse IgM, capture antibody (Southern Biotech, 1020-01). Mouse IgM standards (Southern Biotech, 0101-01), or plasma samples were detected with alkaline phosphatase-conjugated goat anti-mouse IgM secondary antibody (Southern Biotech, 1020-04;) and pNPP substrate (Southern Biotech 0201-01). Absorbance measurements were analyzed with a SpectraMAX 190 microplate reader (Molecular Devices) at 405 nm. The standard curve was determined using a 4-parameter function and concentration measurements were extrapolated using Softmax Pro 3.1.2 software. Only samples with CV<15% and within the standard curve were included in the analysis.

Sample Preparation for Bulk RNA Sequencing

Peritoneal B-1a, B-1b, and B-2 cells obtained from *TET2*-KO and *TET2*-WT C57BL/6 mice were sort-purified directly into RLT Plus Buffer (Qiagen). RNA and DNA were extracted using the Qiagen AllPrep kit. The purified RNAs were stored at −80 °C before being sent to Novogene for sequencing. Total RNA was stored in RNase-free water to directly synthesize first strand, followed by the whole-length LD-PCR amplification. The amplified ds-cDNA(double-stranded DNA) is purified with AMPure XP beads and quantified with Qubit. The cDNA samples were sheared by the Covaris system, and then the sheared fragments were end-repaired, A-tailed, and ligated to

sequencing adaptors. A size selection of about 200 bp was performed before the PCR enrichment. Library concentration was first quantified using a Qubit 2.0 fluorometer (Life Technologies), and then diluted to 2 ng/µl before checking insert size on an Agilent 2100 and quantifying to greater accuracy by qPCR. Ultra-low input bulk RNA sequencing was performed on the NovaSeq 6000 PE150 (Illumina).

DEG and Pathway Analysis

The quality trimming was performed using fastp [145] with default settings. Mapping to the GRCm39 genome was performed with STAR [146], followed by featureCounts [147] to count reads mapped to genes. DESeq2 [148] was used for differential analysis, followed by pathway analysis using clusterProfiler [149] with the Gene Ontology (GO) [150] database.

BCR Analysis

For BCR analysis, quality trimming was performed using fastp [145] and TRUST4 [151] was subsequently used to identify BCR repertoire in paired sequencing reads using the international ImMunoGeneTics (IMGT) information system database as a reference. Results were analyzed using R and circus plots were made using circos Bioconductor package [152]. The code developed for these analyses will be available on the following Github page: https://github.com/mariamurach/TET2 and https://github.com/mariamurach/bcr_R.

Statistics

In Figure 4, Figure 8D, and Figure 11C, comparisons were conducted between the TET2-KO and WT strains using Prism 10.0 with unpaired, two-tailed Mann-Whitney U-tests. Values shown are mean±SD. In Figures 3B and 4A Wilcoxon Rank Sum and Signed Rank Tests were used to determine the significance of differences in proportions of unique CDR3 sequences, isotypes, and usages of specific V, D, and J chains between TET2-KO and WT groups. In Figure 13B, chi-squared test was performed to assess the significance of the association between the number of unique CDR3 amino acid sequences in B-1a and B-1b cells from TET2-KO and WT mice.

Data availability

The datasets generated and analyzed in this study are available from the corresponding author upon reasonable request (C.A.M).

Chapter 3: Loss of TET2 increases B-1 cell number and IgM production while limiting CDR3 diversity

Modified from Dennis E and Murach M et al. (2024) Loss of TET2 increases B-1 cell number and IgM production while limiting CDR3 diversity. Front. Immunol. 15:1380641. doi: 10.3389/fimmu.2024.1380641

Abstract

Recent studies have demonstrated a role for Ten-Eleven Translocation-2 (TET2), an epigenetic modulator, in regulating germinal center formation and plasma cell differentiation in B-2 cells, yet the role of TET2 in regulating B-1 cells is largely unknown. Here, B-1 cell subset numbers, IgM production, and gene expression were analyzed in mice with global knockout of TET2 compared to wildtype (WT) controls. Results revealed that TET2-KO mice had elevated numbers of B-1a and B-1b cells in their primary niche, the peritoneal cavity, as well as in the bone marrow (B-1a) and spleen (B-1b). Consistent with this finding, circulating IgM, but not IgG, was elevated in TET2-KO mice compared to WT. Analysis of bulk RNASeq of sort purified peritoneal B-1a and B-1b cells revealed reduced expression of heavy and light chain immunoglobulin genes, predominantly in B-1a cells from TET2-KO mice compared to WT controls. As expected, the expression of IgM transcripts was the most abundant isotype in B-1 cells. Yet, only in B-1a cells there was a significant increase in the proportion of IgM transcripts in TET2-KO mice compared to WT. Analysis of the CDR3 of the BCR revealed an increased abundance of replicated CDR3 sequences in B-1 cells from TET2-KO mice, which was more clearly pronounced in B-1a compared to B-1b cells. V-D-J usage and circos plot analysis of V-J combinations showed enhanced usage of V_H11 and V_H12 pairings. Taken together, our study is the first to demonstrate that global loss of TET2 increases B-1 cell number and IgM production and reduces CDR3 diversity, which could impact many biological processes and disease states that are regulated by IgM.

Introduction

B cells participate in both innate and adaptive immunity through the secretion of antibodies. B cells are broadly divided into B-1 and B-2 subtypes. B-2 cells are derived from hematopoietic progenitor cells in the bone marrow (BM) and function predominantly in T cell-dependent responses for antibody production [1, 7]. B-1 cells originate during early fetal life, are long-lived, and self-renew [8-11]. B-1 cells can be found predominantly in serosal spaces such as the peritoneal cavity (PerC) or the pleural cavity but can also be found in secondary lymphoid organs such as the spleen, lymph nodes, and the BM [13]. B-1 cells are further subtyped into B-1a or B-1b cells depending on the expression of CD5 (B-1a are CD5+). B-1 cells produce about 80% of circulating serum IgM (immunoglobulin M). A low level of IgM is produced by B-1 cells in serosal cavities, and the majority of circulating serum IgM is produced by B-1 cells in the spleen and BM [24-26]. IgM antibodies produced by B-1a cells are thought to be naturally occurring (i.e., present at birth, in gnotobiotic mice and without antigen exposure) [19-21]. These natural antibodies provide rapid protection from infections and maintain tissue homeostasis through apoptotic cell clearance [26, 77]. However, recent evidence identified the VDJ region in B-1a cells as having N additions [8, 153-156], an event due to the action of the DNA polymerase TdT which is only expressed after birth. This suggests more complexity to the regulation of the CDR3 in B-1a cells than previously thought.

The TET family of proteins act enzymatically as α-ketoglutarate-dependent cytosine dioxygenases that promote DNA demethylation by oxidizing the methyl group of 5-methylcytosine (5mC) to 5-hydroxymethylcytosine (5hmC) [105-107]. The methylation status of DNA is important in recruiting proteins for gene repression or inhibition of transcription factor binding. Additionally, TET proteins enlist chromatin-modifying proteins to histones, which can affect gene expression via physical accessibility for transcription [108, 109]. Thus, TET proteins are potent epigenetic modulators. TET2 is involved in hematopoietic cell development and differentiation [112-114]. Dysfunction in TET2 is well characterized in hematological malignancies including acute myeloid leukemia (AML) [119, 121, 122, 157] and myelodysplastic syndrome (MDS) [117-119, 158, 159]. TET2 loss can affect inflammatory responses via altered cytokine secretion [110, 111] and other biological processes in myeloid cells [114, 116, 119, 126, 130, 131]. TET2 has also been implicated in B cell lymphomas [108, 139-141, 143, 160-162]. Most studies of TET2 in B cells primarily focused on B-2 cells and suggested reduced production of high-affinity IgG [139-141]. Only one study to date has briefly investigated TET2 loss in B-1 cells, and that was with a focus on diffuse large B cell lymphoma and chronic lymphocytic leukemia development [162]. In contrast, our study focuses on B-1 cells in young mice without evidence of tumor, allowing for the identification of key homeostatic processes that may be altered by loss of TET2. Our novel findings characterize the impact of global loss of TET2 on B-1 cell biology at homeostasis, revealing that global TET2 loss leads to increased B-1 cell number, IgM production, and the number of replicated complementarity-determining region 3 (CDR3)

sequences, which could impact diseases that are modulated by IgM antibodies to specific antigens.

Materials and Methods

Mice

All animal protocols were approved by the Animal Care and Use Committee at the University of Virginia. TET2-KO mice [112] were provided by Dr. Kenneth Walsh (University of Virginia). The model was generated by Ko *et al.* and targeted the endogenous *TET2* locus to create a conditional allele that enabled the deletion of exons 8, 9, and 10, the catalytic region of TET2 [112]. Mice were maintained on a 12-h light/dark schedule in a specific pathogen-free animal facility and given food (standard chow diet, Tekland 7012) and water *ad libitum*. The number of mice included in each study is indicated in the figures or the associated legends.

Sample Preparations for Flow Cytometry and Live Cell Sorting

Bone marrow, spleen, and peritoneal cavity cells were processed for flow cytometry as previously described [61]. Briefly, following sacrifice by CO_2 overdose, peritoneal cells were harvested by flushing the peritoneal cavity with 10 mL FACS buffer (PBS containing 1% BSA, 0.05% NaN_3). The spleen and one femur and tibia were removed. Spleens and flushed bone marrow were filtered through a 70 μm cell strainer. Red blood cells were lysed from single-cell suspensions of bone marrow and spleen using a lysis buffer containing 155 mM NH_4Cl, 10 mM $KHCO_3$, and 0.1 mM EDTA. Cell surface Fc receptors were blocked using anti-CD16/32 (clone:93, 4 eBioscience), then cells were stained with fluorescently conjugated antibodies against cell surface markers.

Cells were stained with fixable Live/Dead Zombie NIR (Life Technologies) for dead cell discrimination, then fixed in 2% PFA in PBS.

For FAC sorting, cells were resuspended in modified FACS buffer (PBS with 1% BSA) and 4',6-Diamidino-2-Phenylindole (DAPI) live/dead stain then immediately taken to the University of Virginia Flow Cytometry Core for sorting. B-1a and B-1b cells were sorted to better than 99% purity from their parent gate. Clone and fluorophore information for the flow cytometry antibodies used in murine experiments to immunophenotype or FAC-sort B cell subsets are given in Table 1 and Table 2 respectively. All flow cytometry was conducted at the University of Virginia Flow Cytometry Core Facility. Immunophenotyping was performed on an Aurora Borealis 5-laser (Cytek) cytometer. FAC-sorting was performed on an Influx Cell Sorter (Becton Dickinson). Data analysis and flow plots were generated using OMIQ software (Dotmatics). Representative flow plots were chosen based on the samples whose population frequencies were closest to the mean for that group. Gates on flow plots were set using fluorescence minus one (FMO) controls.

ELISA for quantification of total IgM in mice

Total IgM in mouse plasma was measured using colorimetric ELISA as described previously [61]. Briefly, EIA/RIA high-binding microplates were coated with goat anti-mouse IgM, capture antibody (Southern Biotech, 1020-01). Mouse IgM standards (Southern Biotech, 0101-01), or plasma samples were detected with alkaline phosphatase-conjugated goat anti-mouse IgM secondary antibody (Southern Biotech,

1020-04;) and pNPP substrate (Southern Biotech 0201-01). Absorbance measurements were analyzed with a SpectraMAX 190 microplate reader (Molecular Devices) at 405 nm. The standard curve was determined using a 4-parameter function and concentration measurements were extrapolated using Softmax Pro 3.1.2 software. Only samples with CV<15% and within the standard curve were included in the analysis.

Sample Preparation for Bulk RNA Sequencing

Peritoneal B-1a, B-1b, and B-2 cells obtained from *TET2*-KO and *TET2*-WT C57BL/6 mice were sort-purified directly into RLT Plus Buffer (Qiagen). RNA and DNA were extracted using the Qiagen AllPrep kit. The purified RNAs were stored at −80 °C before being sent to Novogene for sequencing. Total RNA was stored in RNase-free water to directly synthesize first strand, followed by the whole-length LD-PCR amplification. The amplified ds-cDNA(double-stranded DNA) is purified with AMPure XP beads and quantified with Qubit. The cDNA samples were sheared by the Covaris system, and then the sheared fragments were end-repaired, A-tailed, and ligated to sequencing adaptors. A size selection of about 200 bp was performed before the PCR enrichment. Library concentration was first quantified using a Qubit 2.0 fluorometer (Life Technologies), and then diluted to 2 ng/μl before checking insert size on an Agilent 2100 and quantifying to greater accuracy by qPCR. Ultra-low input bulk RNA sequencing was performed on the NovaSeq 6000 PE150 (Illumina).

DEG and Pathway Analysis

The quality trimming was performed using fastp [145] with default settings. Mapping to the GRCm39 genome was performed with STAR [146], followed by featureCounts [147] to count reads mapped to genes. DESeq2 [148] was used for differential analysis, followed by pathway analysis using clusterProfiler [149] with the Gene Ontology (GO) [150] database.

BCR Analysis

For BCR analysis, quality trimming was performed using fastp [145] and TRUST4 [151] was subsequently used to identify BCR repertoire in paired sequencing reads using the international ImMunoGeneTics (IMGT) information system database as a reference. Results were analyzed using R and circus plots were made using circos Bioconductor package [152]. The code developed for these analyses will be available on the following Github page: https://github.com/mariamurach/TET2 and https://github.com/mariamurach/bcr_R.

Statistics

In Figure 4, Figure 8D, and Figure 11C, comparisons were conducted between the TET2-KO and WT strains using Prism 10.0 with unpaired, two-tailed Mann-Whitney U-tests. Values shown are mean±SD. In Figures 3B and 4A Wilcoxon Rank Sum and Signed Rank Tests were used to determine the significance of differences in proportions of unique CDR3 sequences, isotypes, and usages of specific V, D, and J chains between

TET2-KO and WT groups. In Figure 13B, chi-squared test was performed to assess the significance of the association between the number of unique CDR3 amino acid sequences in B-1a and B-1b cells from TET2-KO and WT mice.

Results

Global loss of TET2 results in increased numbers of all B cell subtypes in the peritoneal cavity compared to WT

To determine the impact of the loss of TET2 on major immune cell subtypes in the peritoneal cavity, BM, and spleen of TET2-KO and littermate control mice, spectral flow cytometry was performed. B cells were defined as CD45+ CD19+; T cells were defined as CD45+ CD5+ CD19-; Macrophages (Macs) were defined as CD45+ CD5- CD19- F4-80+ CD11b+; and NK cells were defined as CD45+ CD5- CD19- NK1.1+ (Figure 3). We found that there was a higher B cell frequency and number in the peritoneal cavity (Figure 4A&D), but not in the BM (Figure 4B&E) or spleen (Figure 4C&F) of TET2-KO mice compared to controls. Numbers of T cells (p-value = 0.0043), and NK cells (p-value = 0.0152) from TET2-KO mice in the peritoneal cavity (Figure 4D) were also greater than controls. There were no significant differences in immune cell numbers from TET2-KO mice in the bone marrow (Figure 4E), while in the spleen there was a trending increase in B cells (p-value = 0.0649) with a significant increase in T cells (p-value = 0.0260) and a trending increase in NK cells (p-value = 0.0649) compared to WT (Figure 4F). Upon examination of B cell subsets specifically, we found that in the peritoneal cavity, all B cell subsets were significantly increased in frequency (B-1a p-value = 0.0152, B-1b p-value = 0.0411, B-2 p-value = 0.0260) and in number (B-1a p-value = 0.0022, B-1b p-value = 0.0043, B-2 p-value = 0.0022) in TET2-KO mice compared to WT (Figure 4G&J). However, in the BM (Figure 4H&K) only the B-1a cell subset frequency was significantly increased in TET2-KO compared to WT mice (p-value =

0.0260). In the spleen (Figure 4I&L) B-1b cells but not B-1a cells were elevated in both frequency and number (p-value = 0.0173, 0.0043, respectively). There was no difference in TET2-KO B-2 cell frequency in the spleen, although the total number of B-2 cells was significantly increased (p-value = 0.0260).

Figure 3. Gating strategy for immunophenotyping the Figure 4. RNASeq analysis of differentially expressed genes in peritoneal B-1a and B-1b cells from TET2-KO and WT mice. peritoneal cavity, bone marrow, and spleen of TET2-KO and WT mice. Representative plots are displayed from a peritoneal sample. B cells were defined as CD45+ CD19+; T cells were defined as CD45+ CD5+ CD19-; Macrophages (Macs) were defined as CD45+ CD5- CD19- F4-80+ CD11b+; and NK cells were defined as CD45+ CD5- CD19- NK1.1+.

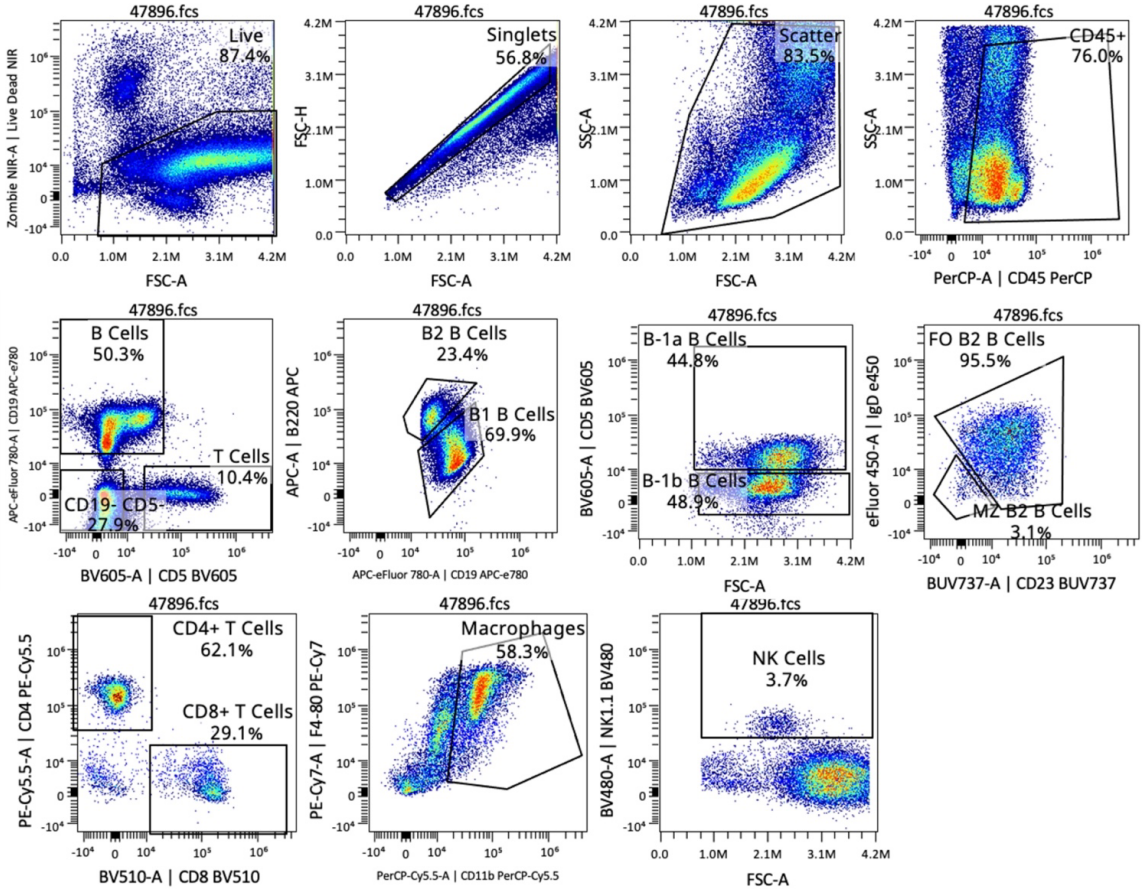
47896.fcs
Live
87.4%
Zombie NIR-A | Live Dead NIR
FSC-A
47896.fcs
Singlets
56.8%
FSC-H
FSC-A
47896.fcs
Scatter
83.5%
SSC-A
FSC-A
47896.fcs
CD45+
76.0%
SSC-A
PerCP-A | CD45 PerCP
47896.fcs
B Cells
50.3%
T Cells
10.4%
CD19- CD5-
27.9%
APC-eFluor 780-A | CD19 APC-e780
BV605-A | CD5 BV605
47896.fcs
B2 B Cells
23.4%
B1 B Cells
69.9%
APC-A | B220 APC
APC-eFluor 780-A | CD19 APC-e780
47896.fcs
B-1a B Cells
44.8%
B-1b B Cells
48.9%
BV605-A | CD5 BV605
FSC-A
47896.fcs
FO B2 B Cells
95.5%
M2 B2 B Cells
3.1%
eFluor 450-A | IgD e450
BUV737-A | CD23 BUV737
47896.fcs
CD4+ T Cells
62.1%
CD8+ T Cells
29.1%
PE-Cy5.5-A | CD4 PE-Cy5.5
BV510-A | CD8 BV510
47896.fcs
Macrophages
58.3%
PE-Cy7-A | F4-80 PE-Cy7
PerCP-Cy5.5-A | CD11b PerCP-Cy5.5
47896.fcs
NK Cells
3.7%
BV480-A | NK1.1 BV480
FSC-A

Figure 4. Immune subtypes in TET2-KO compared to WT mice. (**A - L**) Flow cytometry characterization of the number and frequency of immune cell types in the (**A, D**) peritoneal cavity; (**B, E**) bone marrow; (**C, F**) spleen. Deeper gating into B cell subset frequency and number in the (**G, J**) peritoneal cavity; (**H, K**) bone marrow; (**I, L**) spleen, respectively, from TET2-KO (n = 6) and WT (n = 6) mice. Blue and orange represent WT and TET2-KO mice, respectively. Data are representative of four independent experiments. Significance was determined with two-tailed Mann-Whitney U-tests (* $p < 0.05$, ** $p < 0.01$).

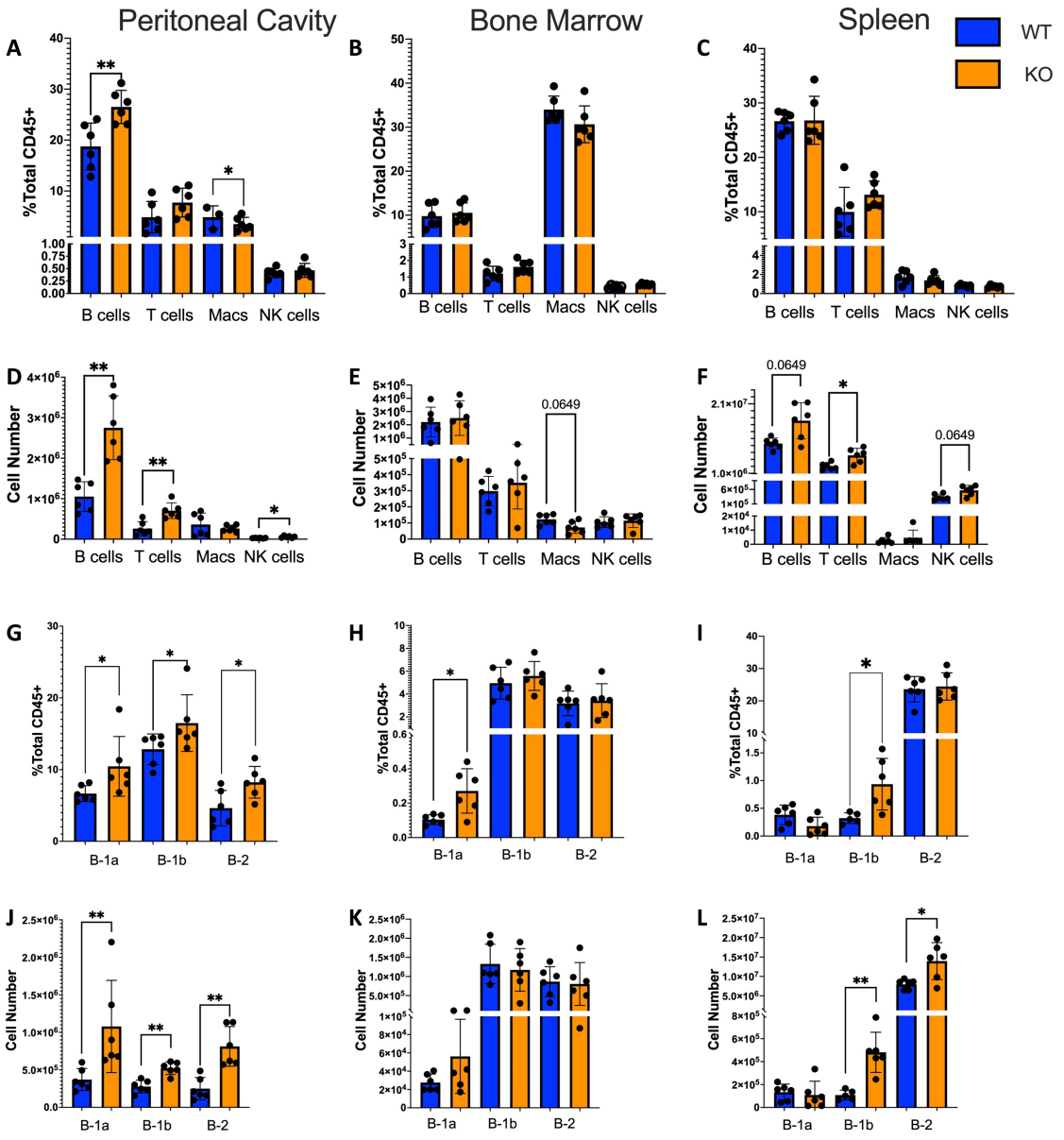
Peritoneal Cavity
Bone Marrow
Spleen
WT
KO
A
B
C
D
E
F
G
H
I
J
K
L
%Total CD45+
Cell Number
B cells
T cells
Macs
NK cells
B-1a
B-1b
B-2
0.0649

Peritoneal B-1a cells from TET2-KO mice have lower expression of immunoglobulin genes compared to WT

To identify genes differentially expressed in B cell subtypes in mice with TET2-KO compared to WT control, we performed RNA-sequencing (RNASeq) on sort-purified peritoneal B-1a and B-1b cells from TET2-KO and WT mice (Figure 5A-B, Figure 6). We utilized peritoneal B-1 cells due to their abundance in this specific niche, as well as due to the phenotypic changes we observed in Figure 4. We found that the global knockout of TET2 had a more significant impact on gene expression within B-1a cells compared to B-1b cells. Specifically, we observed a downregulation in the expression of several immunoglobulin genes in B-1a cells (and to a lesser extent in B-1b cells) from TET2-KO mice compared to their WT counterparts (Figure 5C-D, Figure 7). Consistent with this finding, Gene Set Enrichment Analysis (GSEA) revealed that TET2 loss markedly affects pathways linked to immunoglobulin production and immune response activation, primarily within B-1a cells. Indeed, the expression of numerous V genes (from both heavy and light chains) was decreased in B-1a cells from TET2-KO mice (Figure 8B-C). Similarly, the expression of genes involved in the activation of molecular mediators of the immune response was also decreased in these cells (Figure 7, Figure 9). Interestingly, significant enrichment in neurotransmitter and synapse-related pathways was seen in both B-1a and B-1b cells from the TET2-KO animals compared to the control animals (Figure 7B, Figure 10) These GSEA results provide potential avenues for further hypothesis-driven studies of the role of TET2 in sensory-neural control of B cells, an emerging area of potential significance, recently also connected to

cardiovascular disease development via other immune cells (57-59). Notably, while there are too many differentially expressed genes (DEGs) to test all at the protein level, one of the proteins encoded by our DEG, Sell, also known as CD62L, was also in our flow panel, allowing us to determine if the change in gene expression was also accompanied by changes in the protein level. Indeed, consistent with the decrease in CD62L RNA, we also saw a decrease in CD62L on the surface B-1a and B-1b cells in TET2-KO mice (Figure 8C-D).

Figure 5. RNASeq analysis of differentially expressed genes in peritoneal B-1a and B-1b cells from TET2-KO and WT mice. (**A**) Schematic of experimental design. B-1a and B-1b cells from the peritoneal cavity of TET2-KO and WT mice were sort-purified and RNA-extracted for RNASeq. (**B**) Gating strategy for sort. B-1a cells are CD19+, IgD-lo, CD23-lo, B220-lo, CD5+ while B-1b cells are CD19+, IgD-lo, CD23-lo, B220-lo, CD5-. (**C, D**) Differentially expressed genes are visualized with volcano plots of the B-1a (**C**) and B-1b (**D**) cells from TET2-KO mice compared to WT. Color legend for volcano plots: Grey: NS, Green: log2FC > 1, Blue: p-value < 0.05 and log2FC < 1, Red: p-value < 0.05 and log2FC > 1. n: B-1a: WT = 4, KO = 4, B-1b: WT = 4, KO = 3. All p-values are False Discovery Rate (FDR)-adjusted. Figure schematic made with BioRender.

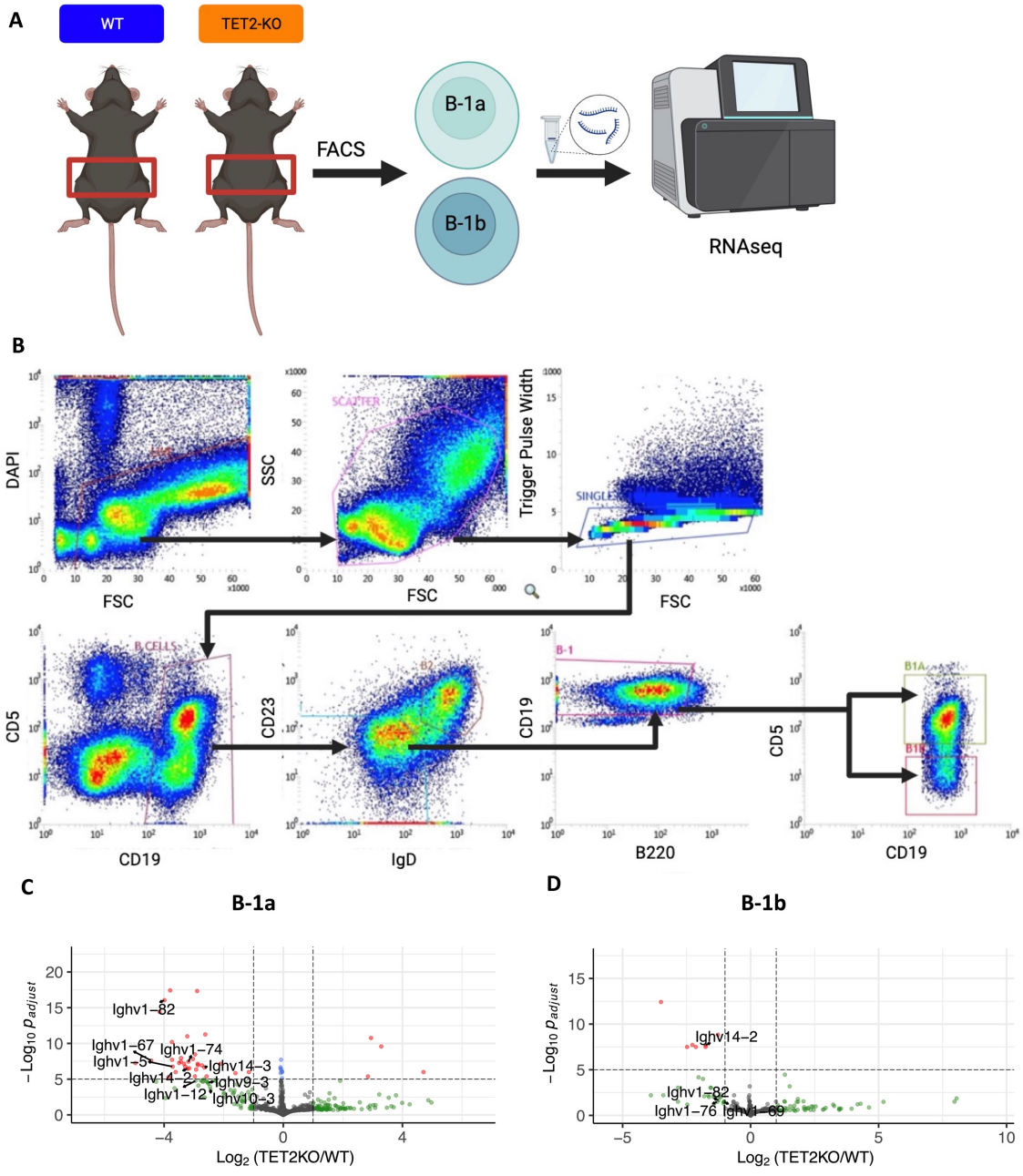
A
WT
TET2-KO
FACS
B-1a
B-1b
RNAseq
B
DAPI
FSC
SSC
SCATTER
Trigger Pulse Width
SINGLE
B CELLS
CD5
CD19
CD23
IgD
B-1
B220
B1A
B1B
C
B-1a
Ighv1−82
Ighv1−67
Ighv1−74
Ighv1−5
Ighv14−3
Ighv14−2
Ighv9−3
Ighv1−12
Ighv10−3
−Log10 padjust
Log2 (TET2KO/WT)
D
B-1b
Ighv14−2
Ighv1−82
Ighv1−76
Ighv1−69
−Log10 padjust
Log2 (TET2KO/WT)

Figure 6. Purity checks for the peritoneal FAC-sort. B-1a cells (**top**) and B-1b cells (**bottom**). We used the following gating strategy: live → scatter → singlets → total B cells → CD23lo IgDlo B-1 cells → B220lo B-1 cells → CD5+ B-1a cells or CD5- B-1b cells.

B-1a Purity Check

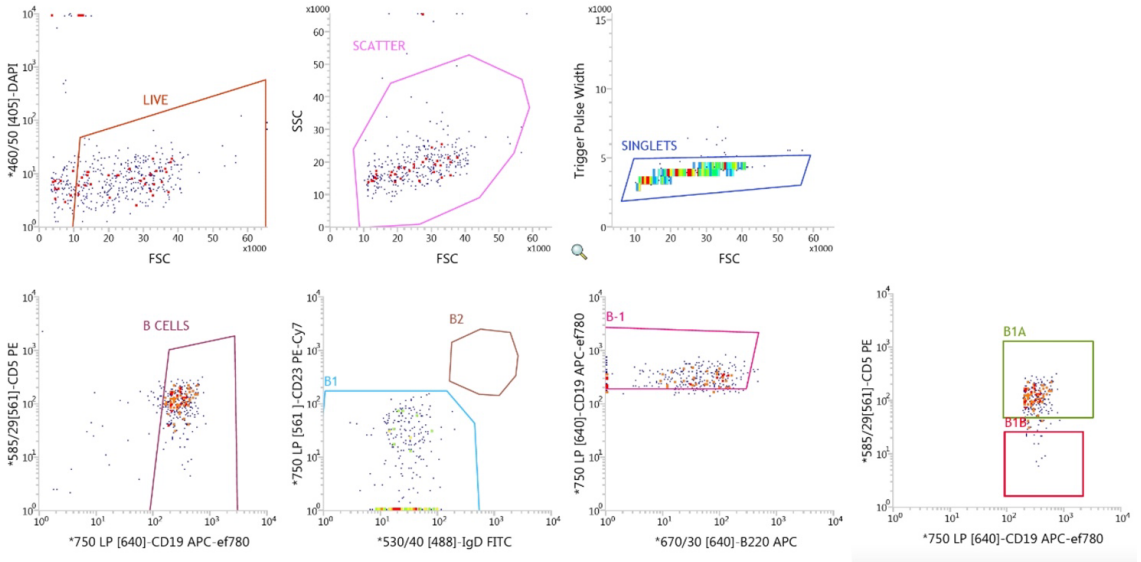

B-1b Purity Check

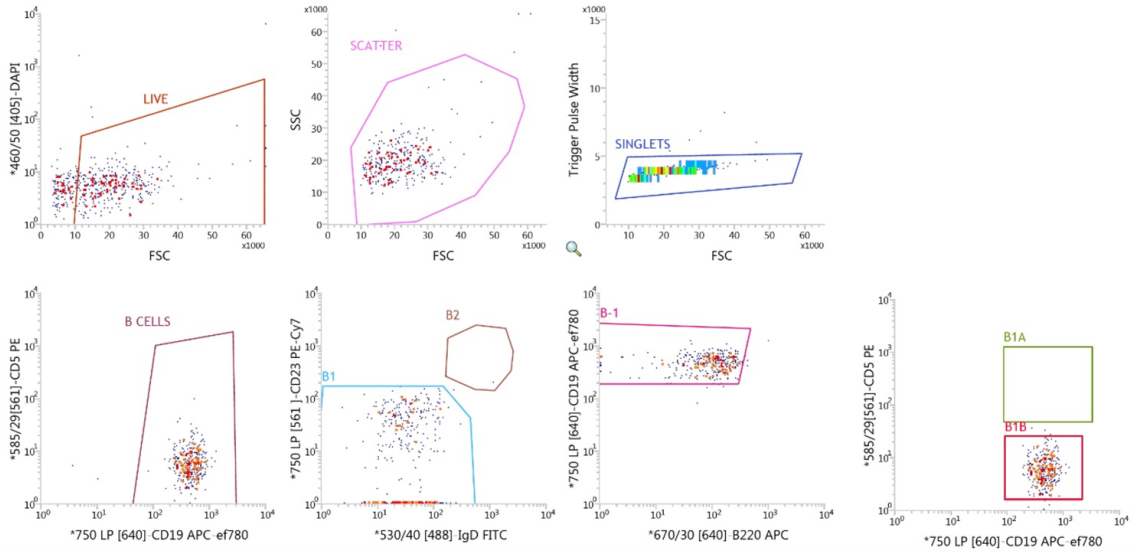

Figure 7. Differentially expressed genes in B-1a cells from TET2-KO and WT mice. (**A**) Scaled expression of all differentially expressed in B-1a cells from TET2-KO and WT mice. Each column corresponds to a gene, and each row represents a sample from WT or TET2-KO. The expression was scaled for each gene (from -2 to 2) and is represented by red for high and blue for low expression values. (**B**) Scaled expression of differentially expressed genes related to sensory perception of smell/sensory perception of chemical stimulus/olfactory receptor activity pathways.

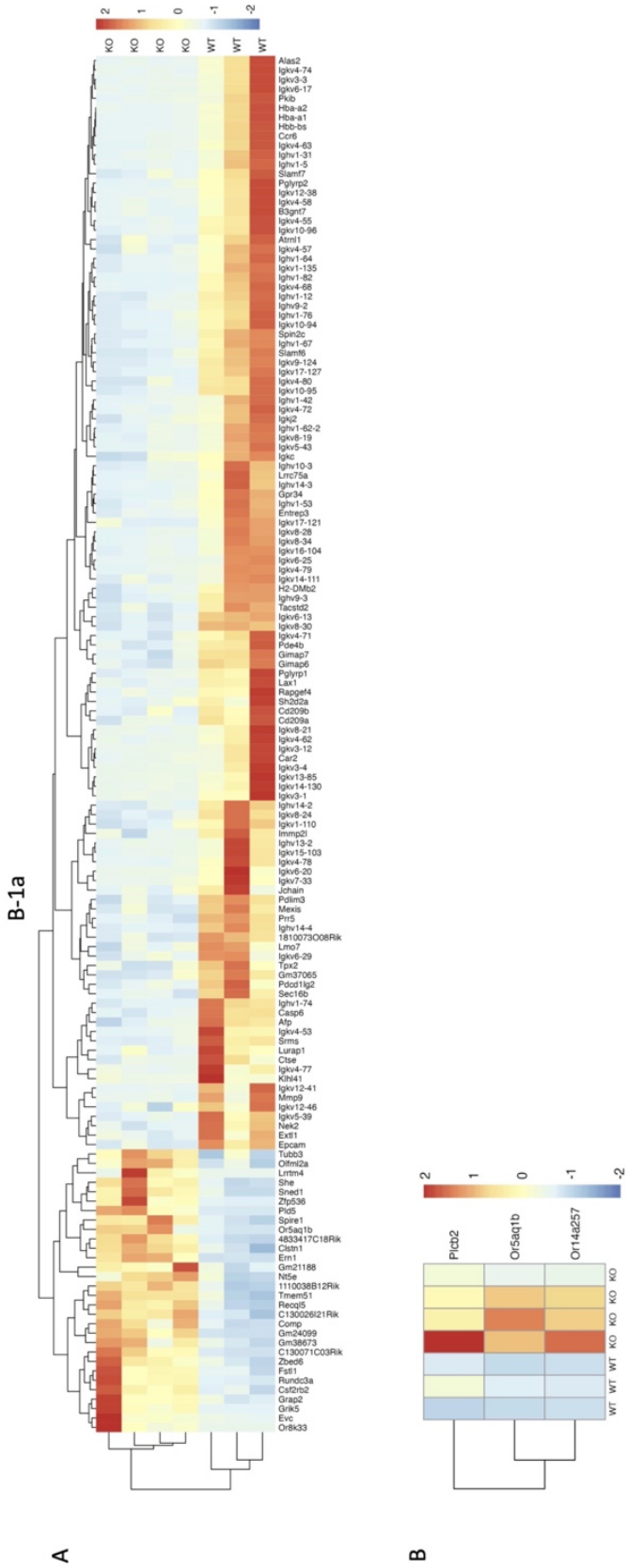
2
1
0
-1
-2
KO KO KO KO WT WT WT
B-1a
Alas2
Igkv4-74
Igkv3-3
Igkv6-17
Pkib
Hba-a2
Hba-a1
Hbb-bs
Ccr6
Igkv4-63
Ighv1-31
Ighv1-5
Slamf7
Pglyrp2
Igkv12-38
Igkv4-58
B3gnt7
Igkv4-55
Igkv10-96
Atrnl1
Igkv4-57
Ighv1-64
Igkv1-135
Ighv1-82
Igkv4-68
Ighv1-12
Ighv9-2
Ighv1-76
Igkv10-94
Spin2c
Ighv1-67
Slamf6
Igkv9-124
Igkv17-127
Igkv4-80
Igkv10-95
Ighv1-42
Igkv4-72
Igkj2
Ighv1-62-2
Igkv8-19
Igkv5-43
Igkc
Ighv10-3
Lrrc75a
Ighv14-3
Gpr34
Ighv1-53
Entrep3
Igkv17-121
Igkv8-28
Igkv8-34
Igkv16-104
Igkv6-25
Igkv4-79
Igkv14-111
H2-DMb2
Ighv9-3
Tacstd2
Igkv6-13
Igkv8-30
Igkv4-71
Pde4b
Gimap7
Gimap6
Pglyrp1
Lax1
Rapgef4
Sh2d2a
Cd209b
Cd209a
Igkv8-21
Igkv4-62
Igkv3-12
Car2
Igkv3-4
Igkv13-85
Igkv14-130
Igkv3-1
Ighv14-2
Igkv8-24
Igkv1-110
Immp2l
Ighv13-2
Igkv15-103
Igkv4-78
Igkv6-20
Igkv7-33
Jchain
Pdlim3
Mexis
Prr5
Ighv14-4
1810073O08Rik
Lmo7
Igkv6-29
Tpx2
Gm37065
Pdcd1lg2
Sec16b
Ighv1-74
Casp6
Afp
Igkv4-53
Srms
Lurap1
Ctse
Igkv4-77
Klhl41
Igkv12-41
Mmp9
Igkv12-46
Igkv5-39
Nek2
Ext1
Epcam
Tubb3
Olfml2a
Lrrtm4
She
Sned1
Zfp536
Pld5
Spire1
Or5aq1b
4833417C18Rik
Clstn1
Ern1
Gm21188
Nt5e
1110038B12Rik
Tmem51
Reql5
C130026I21Rik
Comp
Gm24099
Gm38673
C130071C03Rik
Zbed6
Fstl1
Rundc3a
Csf2rb2
Grap2
Grik5
Evc
Or8k33
A
2
1
0
-1
-2
Plcb2
Or5aq1b
Or14a257
KO
KO
KO
KO
WT
WT
WT
B

Figure 8. Pathway and Gene Set Enrichment Analysis (GSEA) of peritoneal B-1a cells from TET2-KO mice. (**A**) Plot of enrichment scores from GSEA on differentially expressed genes in B-1a cells from TET2-KO and WT mice. The axis represents the enrichment score (ES). Higher scores indicate greater enrichment of the gene set at one end of the ranked list of genes. ES measure the degree to which a gene set is overrepresented at the extremes of the entire ranked list. ES are colored based on FDR-adjusted p-values. (**B**) Scaled expression of genes involved in the production of molecular mediators of immune response and immunoglobulin production pathways. Each row corresponds to a gene, and each column represents a WT or TET2-KO sample. The expression was scaled for each gene (from -2 to 2) and is represented by red for high and blue for low expression values. (**C**) Scaled expression of genes differentially expressed and found on the cell surface. Each row corresponds to a gene, and each column represents a WT or TET2-KO sample. The expression was scaled for each gene (from -2 to 2) and is represented by red for high and blue for low expression values. (**D**) Bar chart displaying Median Fluorescence Intensity (MFI) of CD62L (Sell) in peritoneal B-1a cells and B-1b cells from TET2-KO and WT mice. Blue and orange represent WT (n = 6) and TET2-KO mice (n = 6), respectively. Significance was determined with two-tailed Mann-Whitney U-tests (* $p < 0.05$). n: B-1a: WT = 4, KO = 4 for panels A-C.

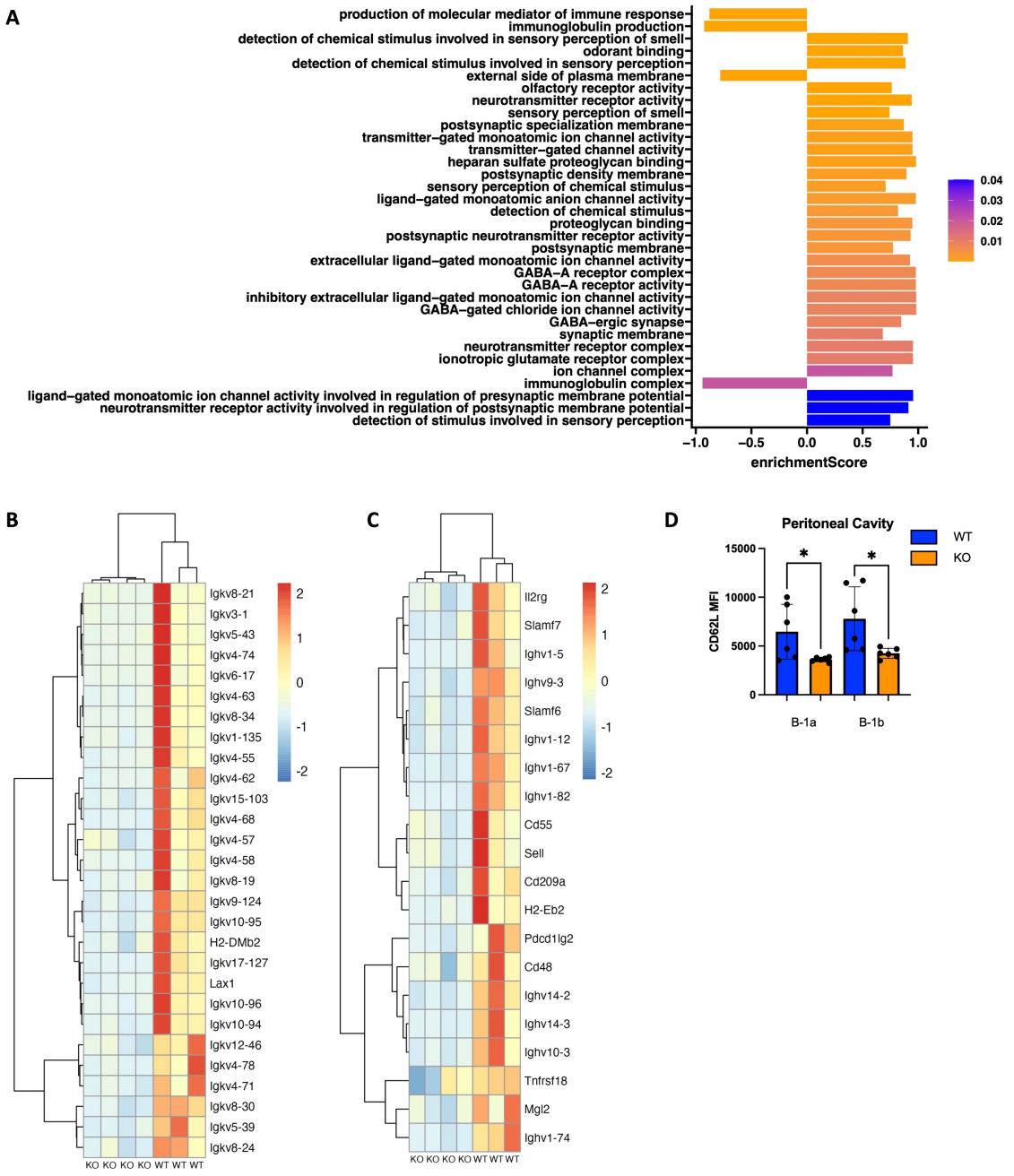
A
production of molecular mediator of immune response
immunoglobulin production
detection of chemical stimulus involved in sensory perception of smell
odorant binding
detection of chemical stimulus involved in sensory perception
external side of plasma membrane
olfactory receptor activity
neurotransmitter receptor activity
sensory perception of smell
postsynaptic specialization membrane
transmitter−gated monoatomic ion channel activity
transmitter−gated channel activity
heparan sulfate proteoglycan binding
postsynaptic density membrane
sensory perception of chemical stimulus
ligand−gated monoatomic anion channel activity
detection of chemical stimulus
proteoglycan binding
postsynaptic neurotransmitter receptor activity
postsynaptic membrane
extracellular ligand−gated monoatomic ion channel activity
GABA−A receptor complex
GABA−A receptor activity
inhibitory extracellular ligand−gated monoatomic ion channel activity
GABA−gated chloride ion channel activity
GABA−ergic synapse
synaptic membrane
neurotransmitter receptor complex
ionotropic glutamate receptor complex
ion channel complex
immunoglobulin complex
ligand−gated monoatomic ion channel activity involved in regulation of presynaptic membrane potential
neurotransmitter receptor activity involved in regulation of postsynaptic membrane potential
detection of stimulus involved in sensory perception
−1.0
−0.5
0.0
0.5
1.0
enrichmentScore
0.04
0.03
0.02
0.01
B
Igkv8-21
Igkv3-1
Igkv5-43
Igkv4-74
Igkv6-17
Igkv4-63
Igkv8-34
Igkv1-135
Igkv4-55
Igkv4-62
Igkv15-103
Igkv4-68
Igkv4-57
Igkv4-58
Igkv8-19
Igkv9-124
Igkv10-95
H2-DMb2
Igkv17-127
Lax1
Igkv10-96
Igkv10-94
Igkv12-46
Igkv4-78
Igkv4-71
Igkv8-30
Igkv5-39
Igkv8-24
KO KO KO KO WT WT WT
2
1
0
-1
-2
C
Il2rg
Slamf7
Ighv1-5
Ighv9-3
Slamf6
Ighv1-12
Ighv1-67
Ighv1-82
Cd55
Sell
Cd209a
H2-Eb2
Pdcd1lg2
Cd48
Ighv14-2
Ighv14-3
Ighv10-3
Tnfrsf18
Mgl2
Ighv1-74
KO KO KO KO WT WT WT
2
1
0
-1
-2
D
Peritoneal Cavity
WT
KO
CD62L MFI
15000
10000
5000
0
*
*
B-1a
B-1b

Figure 9. Differentially expressed genes in B-1b cells from TET2-KO and WT mice. Scaled expression of differentially expressed in B-1b cells from TET2-KO and WT mice. Each column corresponds to a gene, and each row represents a sample from WT or TET2-KO. The expression was scaled for each gene (from -2 to 2) and is represented by red for high and blue for low expression values.

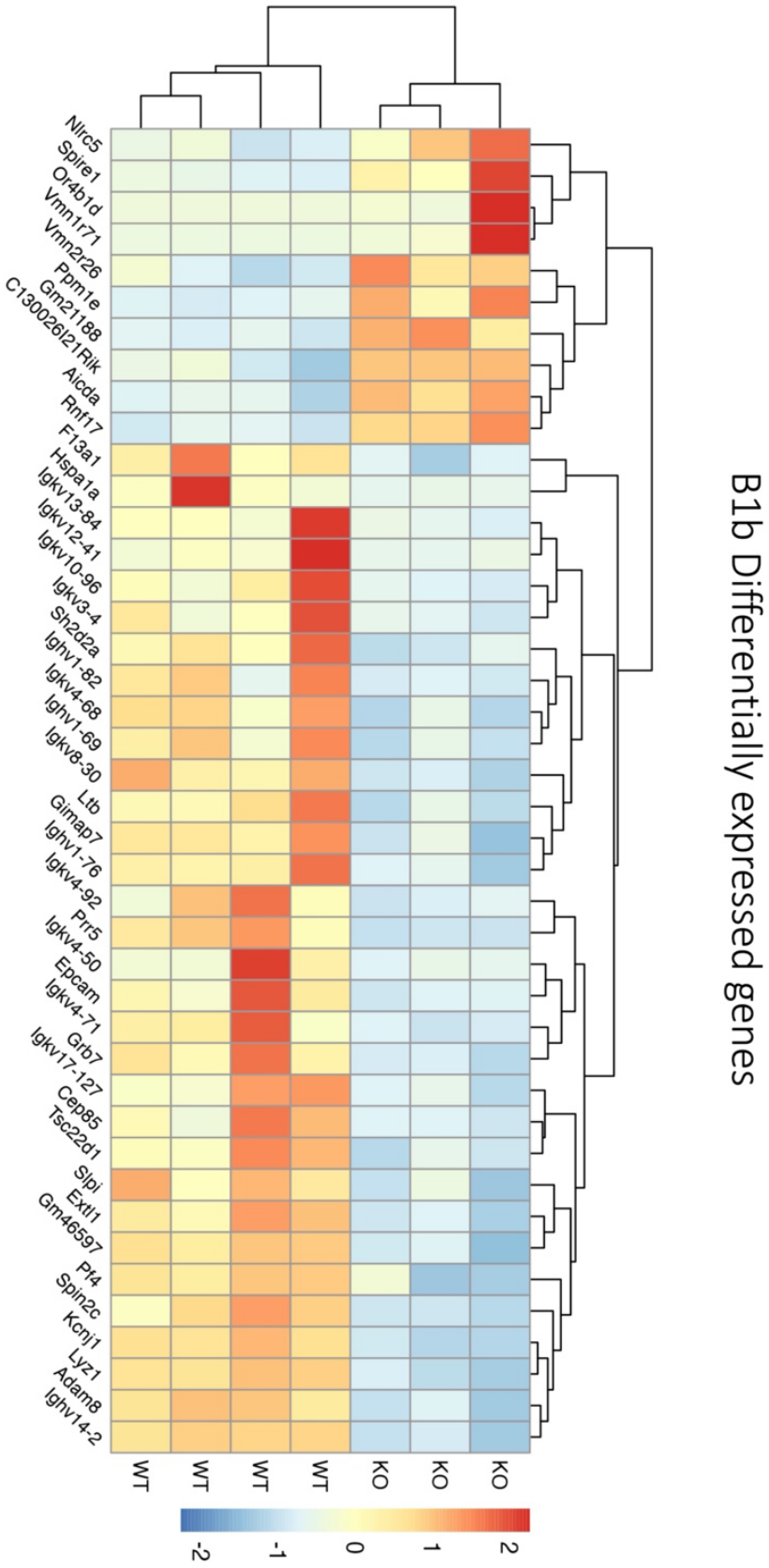
B1b Differentially expressed genes
Nlrc5
Spire1
Or4b1d
Vmn1r71
Vmn2r26
Ppm1e
Gm21188
C130026I21Rik
Aicda
Rnf17
F13a1
Hspa1a
Igkv13-84
Igkv12-41
Igkv10-96
Igkv3-4
Sh2d2a
Ighv1-82
Igkv4-68
Ighv1-69
Igkv8-30
Ltb
Gimap7
Ighv1-76
Igkv4-92
Prr5
Igkv4-50
Epcam
Igkv4-71
Grb7
Igkv17-127
Cep85
Tsc22d1
Slpi
Extl1
Gm46597
Pf4
Spin2c
Kcnj1
Lyz1
Adam8
Ighv14-2
WT
WT
WT
WT
KO
KO
KO
-2
-1
0
1
2

Figure 10. Pathway analysis on differentially expressed genes in B-1b cells from TET2-KO and WT mice. Plot of enrichment scores from Gene Set Enrichment Analysis on differentially expressed genes in B-1b cells from TET2-KO and WT mice. The axis represents the enrichment score (ES). Higher scores indicate greater enrichment of the gene set at one end of the ranked list of genes. ES measures the degree to which a gene set is overrepresented at the extremes of the entire ranked list. Enrichment scores are colored based on FDR-adjusted p-values.

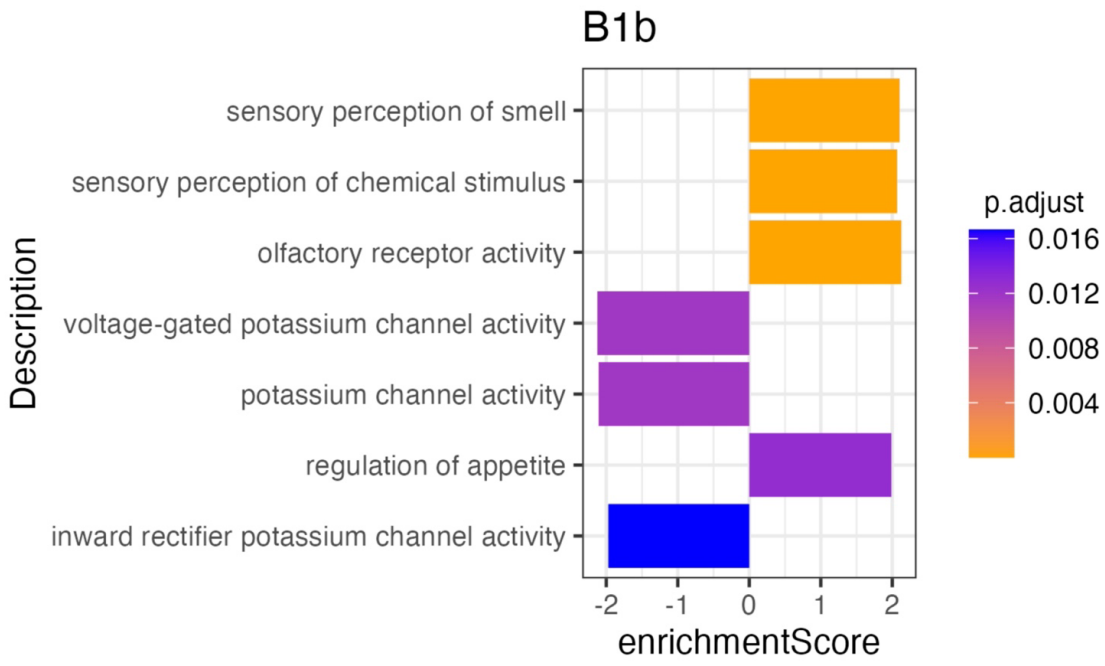
B1b
sensory perception of smell
sensory perception of chemical stimulus
olfactory receptor activity
voltage-gated potassium channel activity
potassium channel activity
regulation of appetite
inward rectifier potassium channel activity
Description
-2
-1
0
1
2
enrichmentScore
p.adjust
0.016
0.012
0.008
0.004

Global loss of TET2 results in higher expression of IgM antibody isotype in peritoneal B-1a cells compared to WT

Using TRUST4, a tool for analyzing the B cell receptor (BCR) using bulk RNASeq [163] and the IMGT [164] database, we were able to identify Ig isotype transcripts present in sequencing data and their distribution across B-1a and B-1b cells from TET2-KO and WT mice (Figure 11A). We found that there was a statistically significant increase in the expression of IgM in the B-1a cells from TET2-KO mice, but we do not see that effect in B1-b cells which is in accordance with the increase expression of *AIDCA*, a gene involved in class-switch recombination (Figure 9, Figure 11B). In contrast, there was no significant change in the distribution of IgD, IgG, or IgA isotypes expressed by the different B-1 cells in TET2-KO and WT mice (Figure 11A). Consistent with the increase in B-1 cells that we observed in niches that support antibody production, such as the spleen and BM (Figure 4E&F), and the increase in the IgM transcript in B-1a cells, the circulating plasma IgM levels were higher in the TET2-KO compared to WT mice (p-value = 0.0075) (Figure 11C). Marginal zone B-2 cells (MZB) are another source of IgM and we did observe an increase in MZB cell number in TET2-KO mice compared to controls, which could contribute to the overall increase in circulating IgM (Figure 12). We observed no change in circulating IgG levels.

Figure 11. Immunoglobulin isotype analysis in peritoneal B-1a and B-1b cells from TET2-KO and WT mice. (**A**) Bar chart showing the distribution of Ig isotypes identified by TRUST4 in B-1a and B-1b cells from TET2-KO and WT mice. (**B**) Proportion of IgM expression in B-1a and B-1b cells from TET2-KO and WT mice. (**C**) Enzyme-linked immunosorbent assay (ELISA) of total IgM (**left**) and IgG (**right**) from plasma of TET2-KO (n = 26) and WT (n = 26) mice. Blue and orange represent WT and TET2-KO mice, respectively. Significance was calculated using Wilcoxon Rank Sum (* $p < 0.05$, ** $p < 0.01$) for panel B. Significance was determined with two-tailed Mann-Whitney U-tests (* $p < 0.05$, $p < 0.01$) for panel C. n: B-1a: WT = 4, KO = 4, B-1b: WT = 4, KO = 3 in panels A and B.

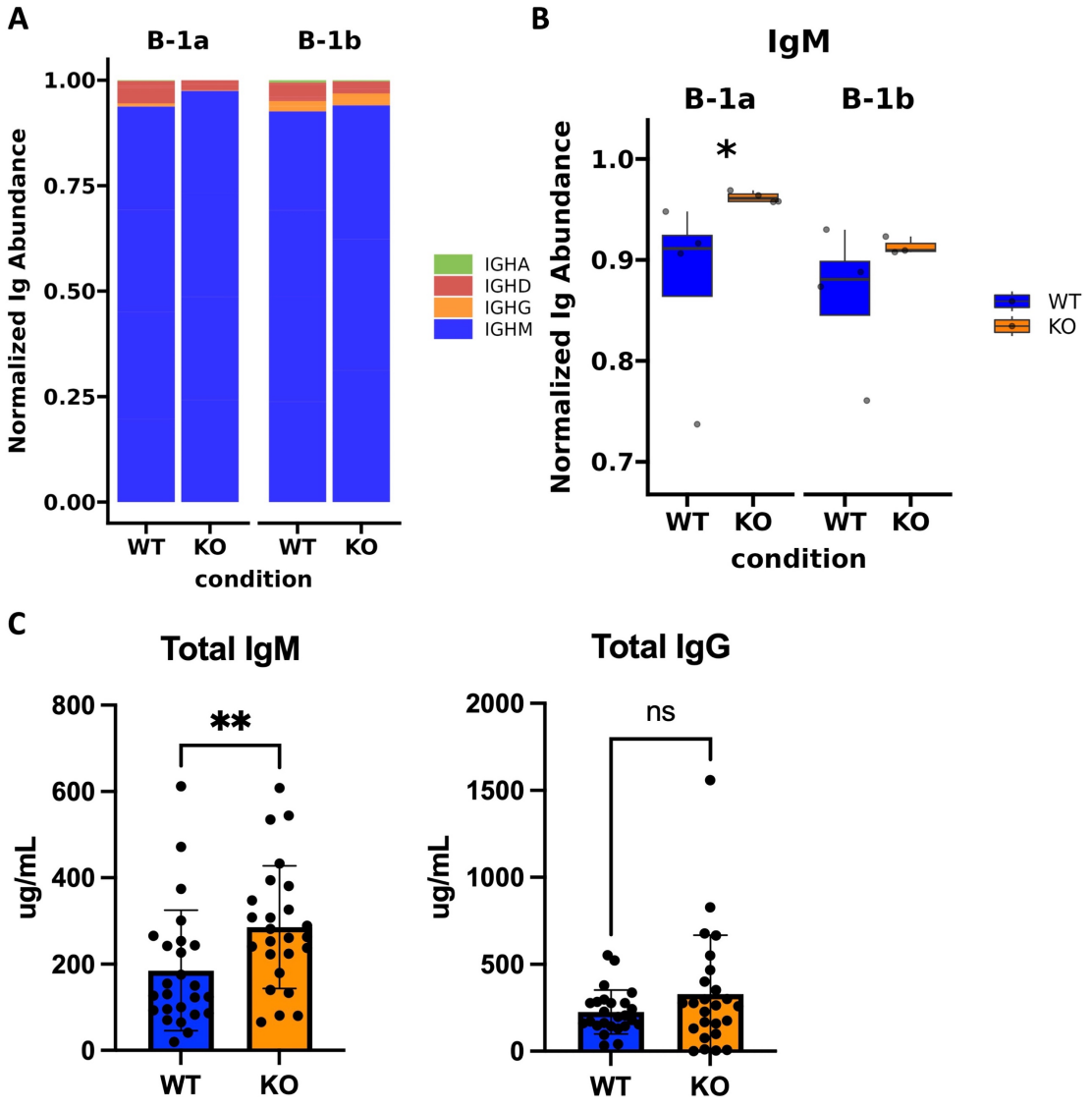
A
B-1a
B-1b
1.00
0.75
0.50
0.25
0.00
Normalized Ig Abundance
WT
KO
WT
KO
condition
IGHA
IGHD
IGHG
IGHM
B
IgM
B-1a
B-1b
*
1.0
0.9
0.8
0.7
Normalized Ig Abundance
WT
KO
WT
KO
condition
WT
KO
C
Total IgM
**
800
600
400
200
0
ug/mL
WT
KO
Total IgG
ns
2000
1500
1000
500
0
ug/mL
WT
KO

Figure 12. Flow cytometry analysis of splenic Marginal Zone B-2 (MZB) cell population from TET2-KO and WT mice. (**A, B**) Density scatterplots display MZB cells from the spleens of TET2-KO (**B**) and WT mice (**A**). The gate percentage displayed on the plot is from the total B-2 cell population. (**C**) Bar chart displaying the total number of MZB cells from the spleens of TET2-KO and WT mice. Blue and orange represent WT (n = 6) and TET2-KO mice (n = 6), respectively. Statistical significance was assessed using the Mann Whitney Signed Rank Test between WT and KO conditions (* $p < 0.05$).

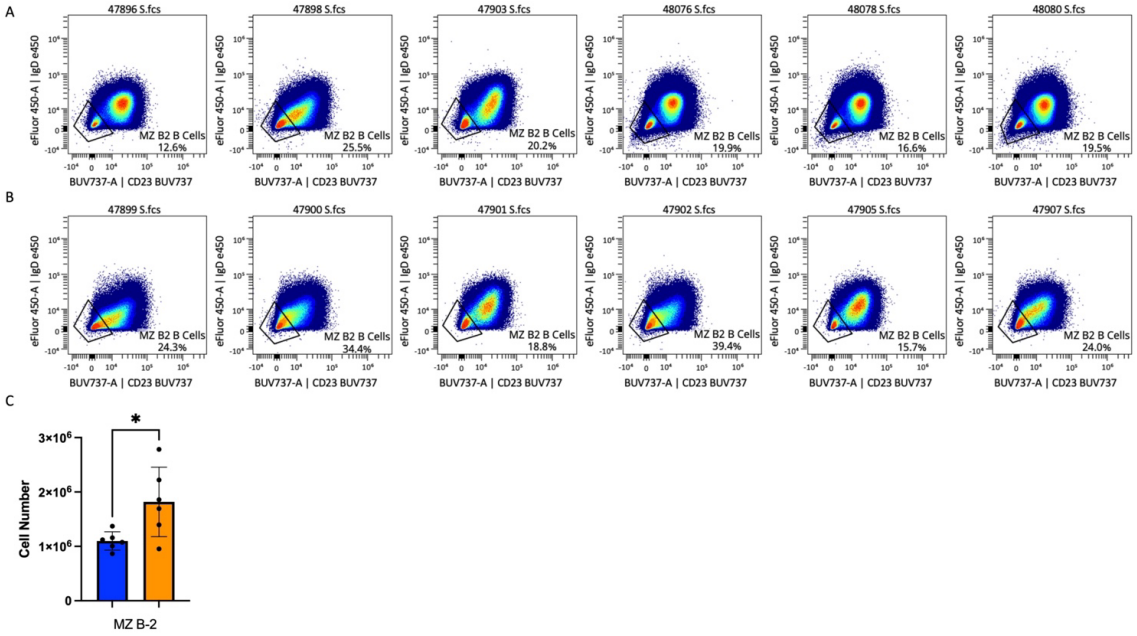
A
47896 S.fcs
47898 S.fcs
47903 S.fcs
48076 S.fcs
48078 S.fcs
48080 S.fcs
eFluor 450-A | IgD e450
BUV737-A | CD23 BUV737
MZ B2 B Cells
12.6%
25.5%
20.2%
19.9%
16.6%
19.5%
B
47899 S.fcs
47900 S.fcs
47901 S.fcs
47902 S.fcs
47905 S.fcs
47907 S.fcs
24.3%
34.4%
18.8%
39.4%
15.7%
24.0%
C
Cell Number
3×10^6
2×10^6
1×10^6
0
MZ B-2
*

Global loss of TET2 results in a reduced number of unique heavy chain CDR3 sequences and an increased number of replicated heavy chain CDR3 sequences in peritoneal cavity B-1a cells compared to WT

To assess differences in the heavy chain BCR repertoire in B-1 cells from TET2-KO and WT mice, we performed an analysis of the CDR3 sequences using our bulk RNASeq data and TRUST4 [163]. Results demonstrated that in both B-1a and B-1b cells from TET2-KO mice, CDR3 diversity was reduced compared to WT mice (Figure 13A). The reduction in CDR3 sequence diversity in the B-1a cells from TET2-KO mice compared to WT was statistically significant (p-value = 0.02857) (Figure 13A), while the reduction in unique CDR3 sequences in TET2-KO B-1b cells compared to WT was trending (p-value = 0.05714) (Figure 13A).

It is not feasible to establish the presence of clonal expansion based on bulk RNASeq data, due to the inability to determine the absolute number of cells and their level of expression of each Ig transcript at a single-cell resolution in a given B cell population. However, a high proportion of replicated sequences suggests the presence of clonally dividing, or self-renewing B-1a cells, as they are known to do. Here we define replicated sequences as those whose frequency is greater than 1% of all sequences. In B-1a cells from TET2-KO mice, we observed that 72% of the CDR3 sequences were replicated, compared to B-1a cells from WT mice which only had 15% of the total CDR3 sequences replicated (Figure 13B, Figure 14A). Thirteen unique CDR3 sequences covered 72% of all CDR3s in B-1a cells from TET2-KO mice, while 4972 CDR3 sequences made up the other 28% of the total number of identified CDR3s (Figure 13B,

Figure 14A). In B-1b cells from TET2-KO mice, 25% of all CDR3 sequences are made up of 12 unique CDR3 sequences, while 11107 CDR3 sequences made up the rest of the 75% (Figure 13B, Figure 14B). Differences in the number of replicated unique CDR3 sequences were significant based on Chi-squared tests for B-1a (p-value = $3.2x10^{-13}$) and B-1b cells (p-value = $3.1x10^{-6}$) from TET2-KO mice compared to WT (Figure 13B). An analysis of the commonality of replicated CDR3 sequences revealed that there was minimal overlap in the CDR3 sequence between B-1a cells from TET2-KO and WT mice or in B-1b cells from TET2-KO and WT mice, respectively (Figure 13C). Interestingly, there was a greater degree of commonality in the CDR3 sequence comparing B-1a and B-1b cells from TET2-KO mice. We visualized the proportion of replicated CDR3 sequences across B-1 cell subsets in TET2-KO and WT mice using pie charts (Figure 14A-B). Consistent with our findings in Figure 13C, the CDR3 sequences that were most abundantly represented in B-1a cells from WT mice were represented in B-1a cells from TET2-KO mice at different proportions, and there were more similarities in replicated CDR3 sequences between B-1a and B-1b cells from TET2-KO mice.

Since antigen binding specificity is not just determined by the heavy chain CDR3, we performed an analysis of the light chain BCR repertoire from our bulk RNASeq data with TRUST4. Results demonstrated that in both B-1a and B-1b cells from TET2-KO mice, CDR3 diversity was reduced compared to WT mice (Figure 15). The reduction in CDR3 sequence diversity in the B-1a cells from TET2-KO mice compared to WT was statistically significant (p-value = 0.029) (Figure 15A). The reduction in CDR3 sequences in B-1b cells from TET2-KO mice compared to WT was trending (p-value = 0.133)

(Figure 15A). Similar to what we observed in the heavy chain CDR3 sequences, the number of replicated light chain CDR3 sequences was over 2-fold greater in B-1a cells from TET2-KO compared to WT mice (Figure 15B-D). The number of unique CDR3 sequences from the light chain accounted for a similar percentage of total CDR3 sequences as seen in the heavy chain results in B-1a cells from TET2-KO mice (Figure 15B-D). Differences in the number of replicated unique CDR3 sequences were significant based on Chi-squared tests for B-1a (p-value = 0.01) and B-1b cells (p-value = 0.02) from TET2-KO mice compared to WT. While the role of the light chain in antigen binding and specificity remains less well-known compared to the heavy chain, it still contributes to those functions [165]. These results in the light chain CDR3 provide additional support that B-1a cells are more profoundly impacted by loss of TET2 than B-1b cells, and the diversity of antigen-specific IgMs may be affected as a result.

Figure 13. Heavy chain CDR3 sequence analysis reveals restricted BCR repertoire in peritoneal B-1a and B-1b cells from TET2-KO and WT mice. (**A**) The number of unique CDR3 sequences identified by TRUST4 in B-1a and B-1b cells from TET2-KO and WT mice. (**B**) Contingency tables derived to assess the association between the number of unique CDR3 amino acid sequences (**left**) and total number of CDR3 amino acid sequences (**right**) with the mutant status of the mice (i.e., WT or TET2-KO) in B-1a (**top**) and B-1b cells (**bottom**). Chi-squared test was used to assess the significance of these associations. Significance in panel A was calculated using Wilcoxon Rank Sum (* $p < 0.05$). (**C**) Venn diagrams that examine the shared repertoire of unique CDR3 sequences in the different B cell subsets. Blue represents CDR3 AA sequences from B-1a cells from WT mice, orange from B-1a cells from TET2-KO mice, red B-1b cells from WT mice, and green B-1b cells from TET2-KO mice, respectively. A shared sequence was defined as one expressed at least once in each of the subsets being compared. The number of shared sequences is represented by the overlapping region in each Venn diagram. Numbers and percentages of nonshared sequences of each cell subset in every comparison are indicated. For panels B-C, sequences were pooled from mice from the same cell type and condition (n: B-1a: WT = 4, KO = 4, B-1b: WT = 4, KO = 3).

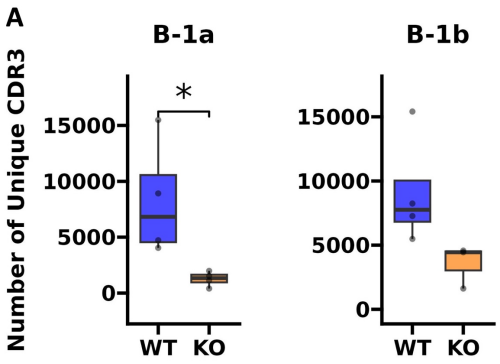

B

Number of unique CDR3aa sequences

B-1a

	not replicated	replicated
WT	34705	5
KO	4972	13

Chi-squared test p= 3.2e-13

B-1b

	not replicated	replicated
WT	37416	4
KO	11107	12

Chi-squared test p=3.1e-06

Total number of CDR3aa sequences

B-1a

	not replicated	replicated
WT	154022 (85%)	25855 (15%)
KO	37761 (28%)	95578 (72%)

B-1b

	not replicated	replicated
WT	165901 (89%)	20369 (11%)
KO	83633 (75%)	28183 (25%)

C

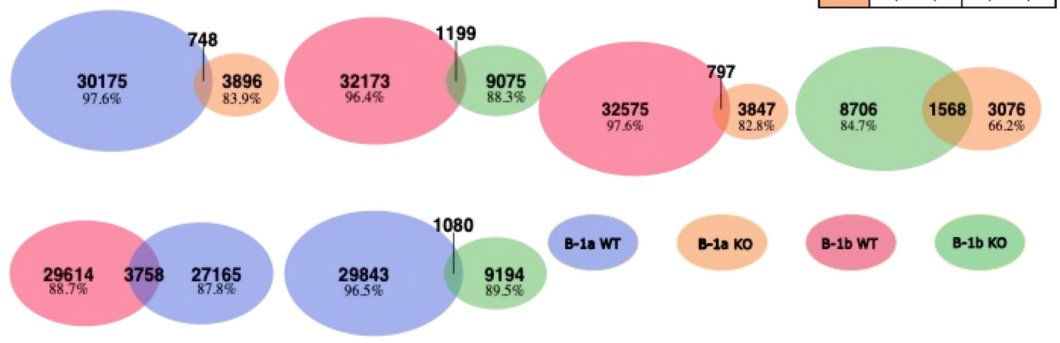

Figure 14. Heavy chain CDR3 sequence analysis reveals differences in most abundant CDR3 sequences in peritoneal B-1a and B-1b cells from TET2-KO and WT mice. (**A, B**) Annotated pie charts depicting the proportion of CDR3 sequences that are unique and the sequence and proportion of the replicated sequences in B-1a (**A**) and B-1b (**B**) cells from WT (**top**) and TET2-KO mice (**bottom**). (**C**) Bar chart comparing the proportion of the top-most abundant CDR3 sequence in B-1a cells from WT mice from of all CDR3 sequences in B-1a and B-1b cells from TET2-KO and WT mice. (**D** Bar chart comparing the proportion of the second-most abundant CDR3 sequence in B-1a cells from WT mice from of all CDR3 sequences in B-1a and B-1b cells from TET2-KO and WT mice. Blue and orange represent WT and TET2-KO mice, respectively. Sequences were pooled from mice from the same cell type and condition (n: B-1a: WT = 4, KO = 4, B-1b: WT = 4, KO = 3).

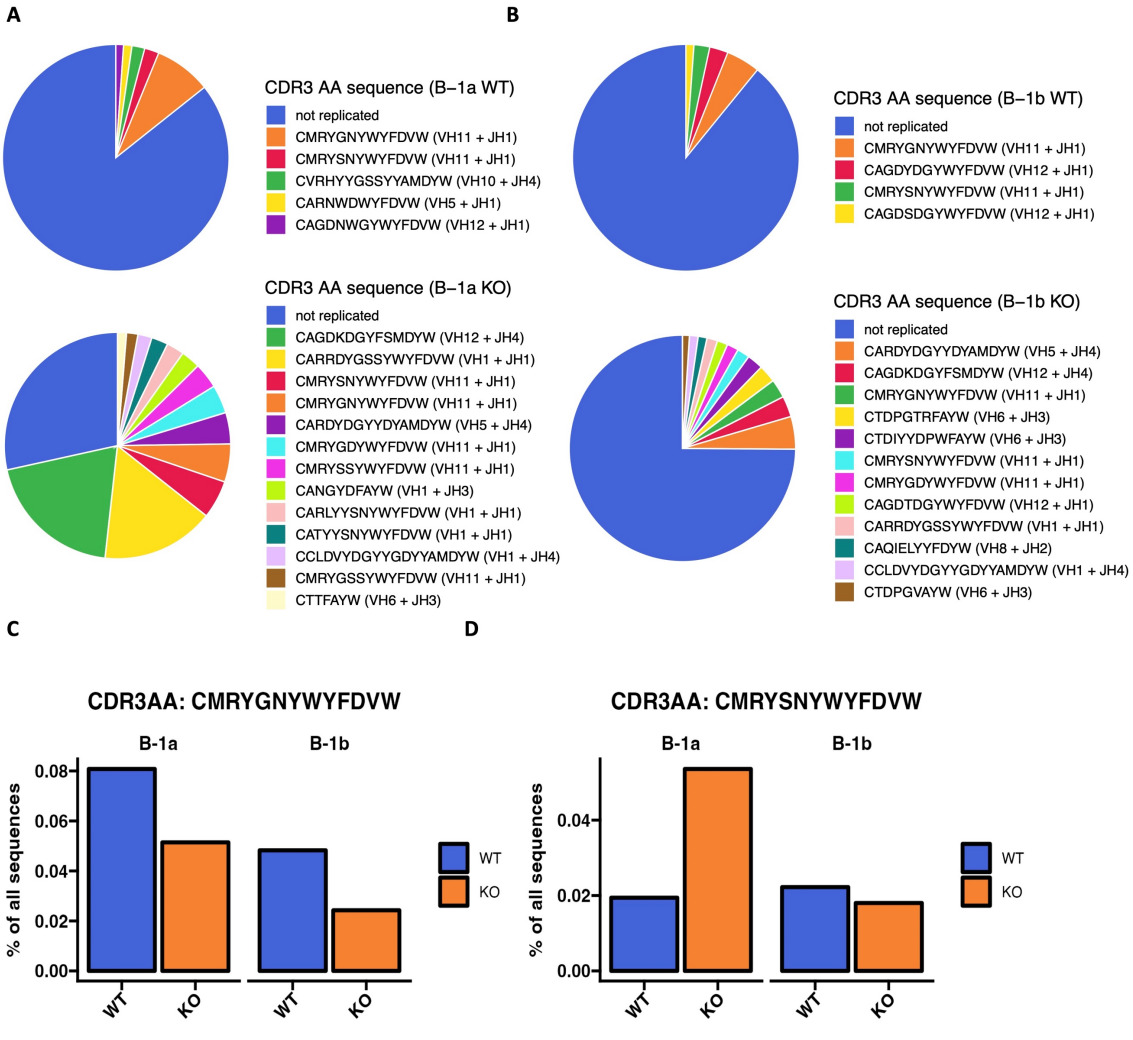
A
CDR3 AA sequence (B−1a WT)
not replicated
CMRYGNYWYFDVW (VH11 + JH1)
CMRYSNYWYFDVW (VH11 + JH1)
CVRHYYGSSYYAMDYW (VH10 + JH4)
CARNWDWYFDVW (VH5 + JH1)
CAGDNWGYWYFDVW (VH12 + JH1)
CDR3 AA sequence (B−1a KO)
not replicated
CAGDKDGYFSMDYW (VH12 + JH4)
CARRDYGSSYWYFDVW (VH1 + JH1)
CMRYSNYWYFDVW (VH11 + JH1)
CMRYGNYWYFDVW (VH11 + JH1)
CARDYDGYYDYAMDYW (VH5 + JH4)
CMRYGDYWYFDVW (VH11 + JH1)
CMRYSSYWYFDVW (VH11 + JH1)
CANGYDFAYW (VH1 + JH3)
CARLYYSNYWYFDVW (VH1 + JH1)
CATYYSNYWYFDVW (VH1 + JH1)
CCLDVYDGYYGDYYAMDYW (VH1 + JH4)
CMRYGSSYWYFDVW (VH11 + JH1)
CTTFAYW (VH6 + JH3)
B
CDR3 AA sequence (B−1b WT)
not replicated
CMRYGNYWYFDVW (VH11 + JH1)
CAGDYDGYWYFDVW (VH12 + JH1)
CMRYSNYWYFDVW (VH11 + JH1)
CAGDSDGYWYFDVW (VH12 + JH1)
CDR3 AA sequence (B−1b KO)
not replicated
CARDYDGYYDYAMDYW (VH5 + JH4)
CAGDKDGYFSMDYW (VH12 + JH4)
CMRYGNYWYFDVW (VH11 + JH1)
CTDPGTRFAYW (VH6 + JH3)
CTDIYYDPWFAYW (VH6 + JH3)
CMRYSNYWYFDVW (VH11 + JH1)
CMRYGDYWYFDVW (VH11 + JH1)
CAGDTDGYWYFDVW (VH12 + JH1)
CARRDYGSSYWYFDVW (VH1 + JH1)
CAQIELYYFDYW (VH8 + JH2)
CCLDVYDGYYGDYYAMDYW (VH1 + JH4)
CTDPGVAYW (VH6 + JH3)
C
CDR3AA: CMRYGNYWYFDVW
B-1a
B-1b
% of all sequences
0.08
0.06
0.04
0.02
0.00
WT
KO
WT
KO
WT
KO
D
CDR3AA: CMRYSNYWYFDVW
B-1a
B-1b
% of all sequences
0.04
0.02
0.00
WT
KO
WT
KO
WT
KO

Figure 15. Light chain CDR3 sequence analysis in B-1a and B-1b cells from TET2-KO and WT mice. (**A**) The number of unique CDR3 sequences identified by TRUST4 in B-1a and B-1b cells from TET2-KO and WT mice. (**B**) Contingency tables derived to assess the association between the number of unique CDR3 amino acid sequences (**left**) and total number of unique CDR3 amino acid sequences (**right**) with the mutant status of the mice (i.e., WT or TET2-KO) in B-1a (**top**) and B-1b cells (**bottom**). Chi-squared test was used to assess the significance of these associations. (**C, D**) Annotated pie charts depicting the proportion of CDR3 sequences that are unique and the sequence and proportion of the replicated sequences in B-1a (**C**) and B-1b (**D**) cells from WT (**top**) and TET2-KO mice (**bottom**). Statistical significance was assessed using the Mann Whitney Signed Rank Test between WT and KO conditions (* $p < 0.05$).

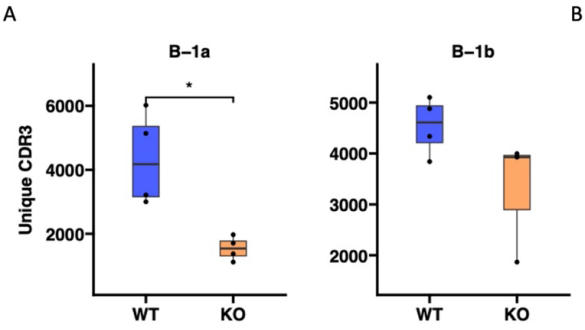

B

Number of unique CDR3aa sequences

B-1a

	not replicated	replicated
WT	15644	13
KO	5267	12

Chi-squared test p= 0.01

B-1b

	not replicated	replicated
WT	16119	13
KO	9374	18

Chi-squared test p=0.02

Total number of CDR3aa sequences

B-1a

	not replicated	replicated
WT	688241 (69%)	311759 (31%)
KO	219492 (22%)	780508 (78%)

B-1b

	not replicated	replicated
WT	688180 (67%)	311820 (33%)
KO	601748 (60%)	398252 (40%)

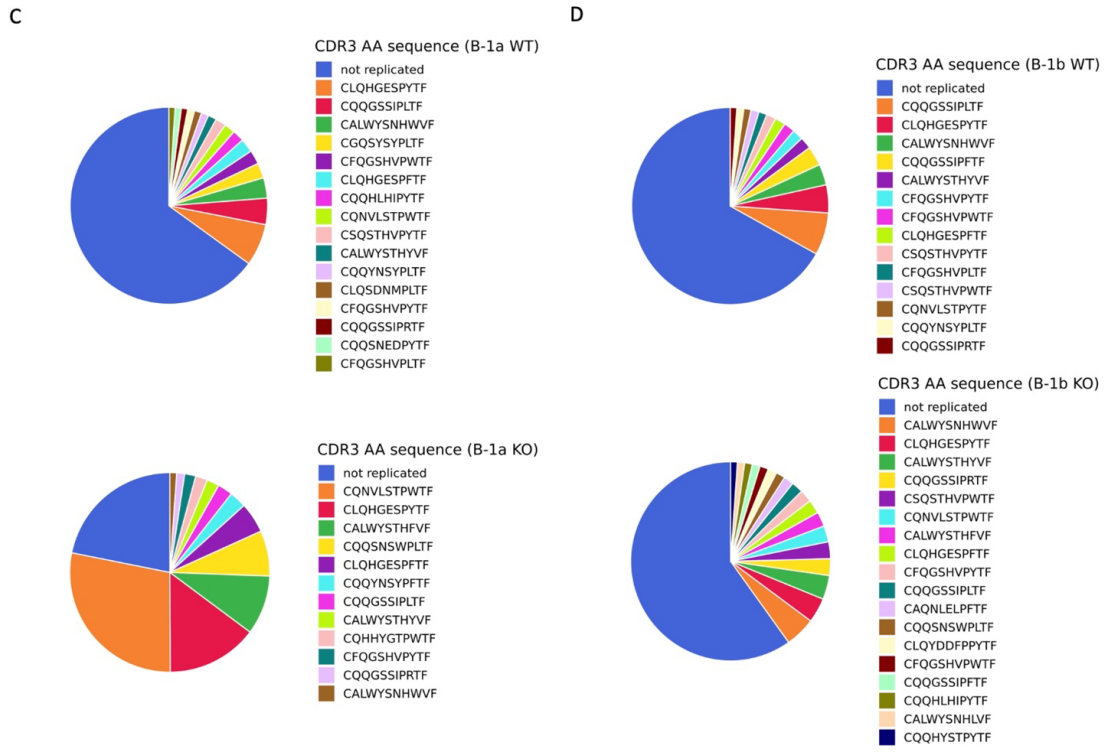

VH–DH–JH usage shows differences between TET2-KO and WT BCR repertoires

Analysis of specific V_H–D_H–J_H gene region usage in B-1a and B-1b cells from TET2-KO and WT mice revealed high usage of V_H1, V_H11, and V_H12 in B-1 cells consistent with prior findings (Figure 16) [4, 156, 166]. The B-1a cells from the TET2-KO mouse appeared to have greater usage of these regions. There were also several reductions in V_H region usage in the B-1a cells from the TET2-KO mice, but these were regions of minimal usage and of unclear significance. We also analyzed differences in the specific $V_{K/L}$–$J_{K/L}$ gene regions of the light chain CDR3 sequence in B-1a and B-1b cells from TET2-KO or WT mice (Figure 17) and similarly found differences in V_K and J_K usage predominantly in B-1a compared to B-1b cells. An analysis of kappa and lambda ratio revealed that there is more lambda light chain utilization in B-1b cells from TET2-KO mice compared to WT despite not reaching significance, while showing no difference in kappa/lambda ratio in B-1a cells (Figure 17E).

Circos plots (Figure 18), measuring the relative frequency of each V-J pairing revealed a greater abundance of V_H1-J_H1, V_H11-J_H1, and V_H12-J_H4 in B-1a cells from TET2-KO mice compared to control, suggesting that TET2 has an important role in specific V-J recombination of B-1a cells. These specific recombination events could be important for creating the over-representation of the specific CDR3s in B-1a cells from TET2-KO mice. The increase in V_H12-J_H4 pairing in TET2-KO mice was also seen in the B-1b cells but only constituted 5% of all pairings compared to over 20% in the B-1a cells. These data are consistent with the loss of TET2 generating a more pronounced effect on the BCR in B-1a cells compared to B-1b cells.

Figure 16. V_H - D_H - J_H analysis of B-1a and B-1b cells from TET2-KO and WT mice. (**A-F**) The percentage of CDR3 sequences identified by TRUST4 utilizing V segments is displayed for B-1a (**A**) and B-1b cells (**B**), D segments for B-1a (**C**) and B-1b cells (**D**), and J segments for B-1a (**E**) and B-1b cells (**F**) from TET2-KO and WT mice. Each pair of bars represents the distribution of frequency values for a specific V, D, or J gene based on pooled gene frequencies from mice from the same cell type and condition. Blue and orange represent WT and TET2-KO mice, respectively.

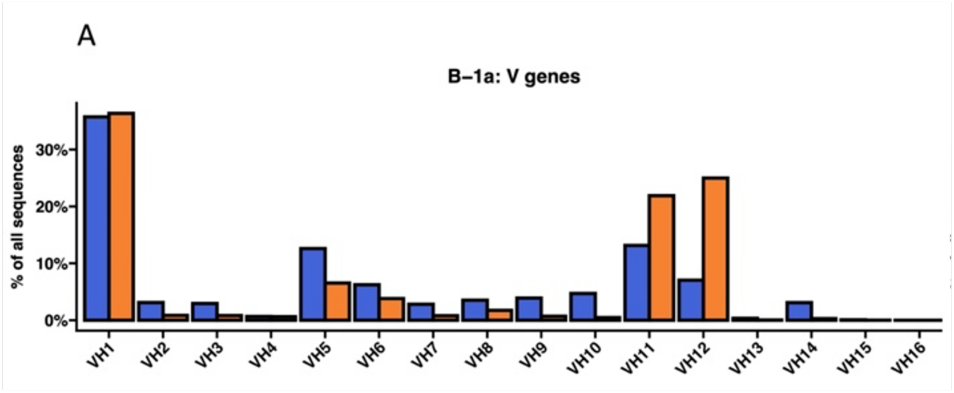
A
B–1a: V genes
% of all sequences
30%
20%
10%
0%
VH1
VH2
VH3
VH4
VH5
VH6
VH7
VH8
VH9
VH10
VH11
VH12
VH13
VH14
VH15
VH16

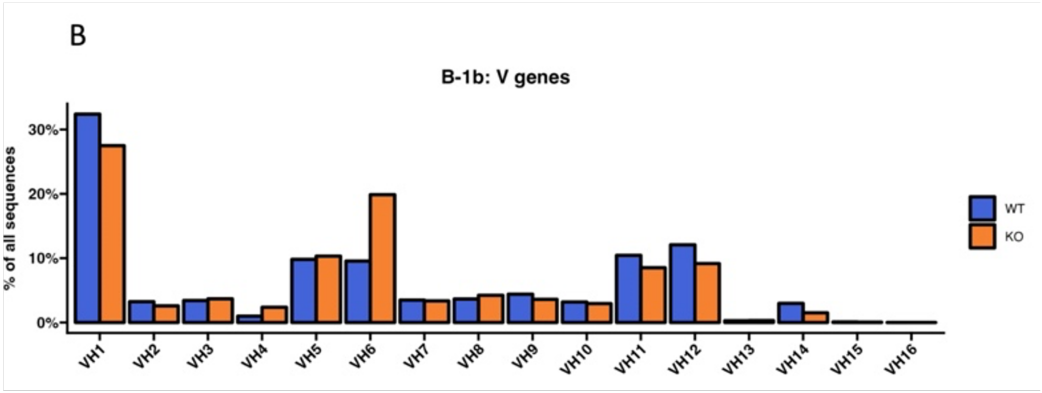
B
B-1b: V genes
% of all sequences
30%
20%
10%
0%
VH1
VH2
VH3
VH4
VH5
VH6
VH7
VH8
VH9
VH10
VH11
VH12
VH13
VH14
VH15
VH16
WT
KO

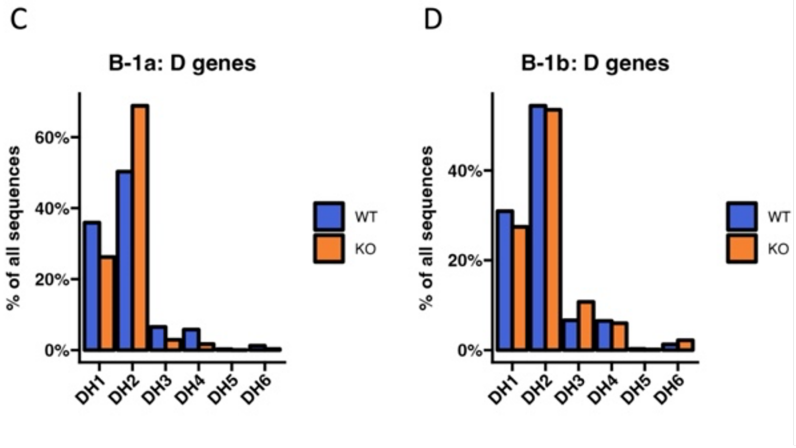
C
B-1a: D genes
% of all sequences
60%
40%
20%
0%
DH1
DH2
DH3
DH4
DH5
DH6
WT
KO
D
B-1b: D genes
% of all sequences
40%
20%
0%
DH1
DH2
DH3
DH4
DH5
DH6
WT
KO

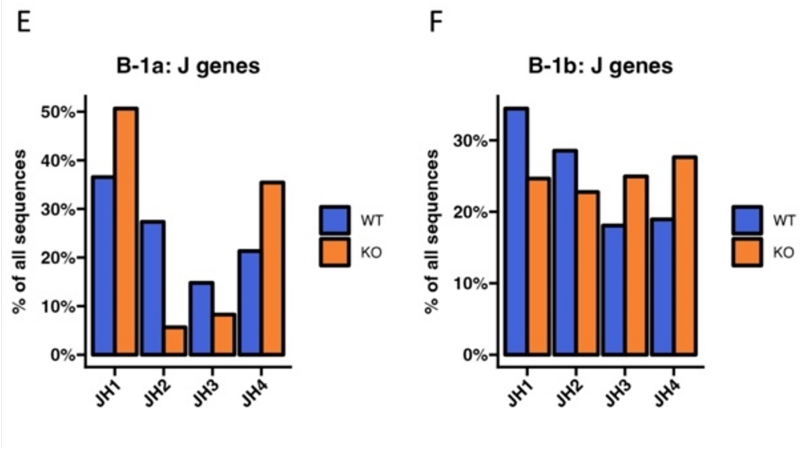
E
B-1a: J genes
% of all sequences
50%
40%
30%
20%
10%
0%
JH1
JH2
JH3
JH4
WT
KO
F
B-1b: J genes
% of all sequences
30%
20%
10%
0%
JH1
JH2
JH3
JH4
WT
KO

Figure 17. $V_{K/L}$ – $J_{K/L}$ and kappa/lambda analysis of B-1a and B-1b cells from TET2-KO and WT mice. (**A-D**) The percentage of CDR3 sequences identified by TRUST4 utilizing V segments is displayed for B-1a (**A**) and B-1b cells (**B**) and J segments for B-1a (**C**) and B-1b cells (**D**) from TET2-KO and WT mice. (**E**) Bar chart showing the distribution of kappa and lambda usage identified by TRUST4 in B-1a and B-1b cells from TET2-KO and WT mice. Each pair of bars represents the distribution of frequency values for a specific V or J gene based on pooled gene frequencies from mice from the same cell type and condition. Blue and orange represent WT and TET2-KO mice, respectively.

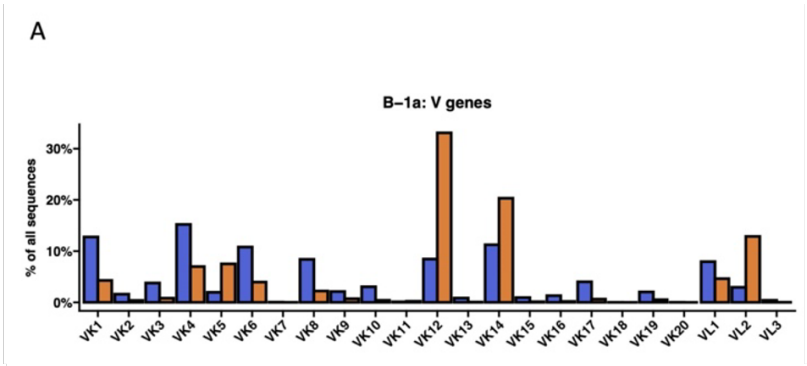
A
B–1a: V genes
% of all sequences
30%
20%
10%
0%
VK1 VK2 VK3 VK4 VK5 VK6 VK7 VK8 VK9 VK10 VK11 VK12 VK13 VK14 VK15 VK16 VK17 VK18 VK19 VK20 VL1 VL2 VL3

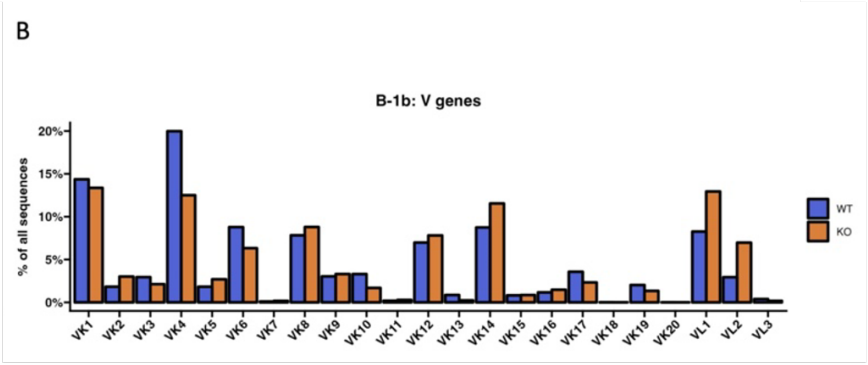
B
B-1b: V genes
% of all sequences
20%
15%
10%
5%
0%
VK1 VK2 VK3 VK4 VK5 VK6 VK7 VK8 VK9 VK10 VK11 VK12 VK13 VK14 VK15 VK16 VK17 VK18 VK19 VK20 VL1 VL2 VL3
WT
KO

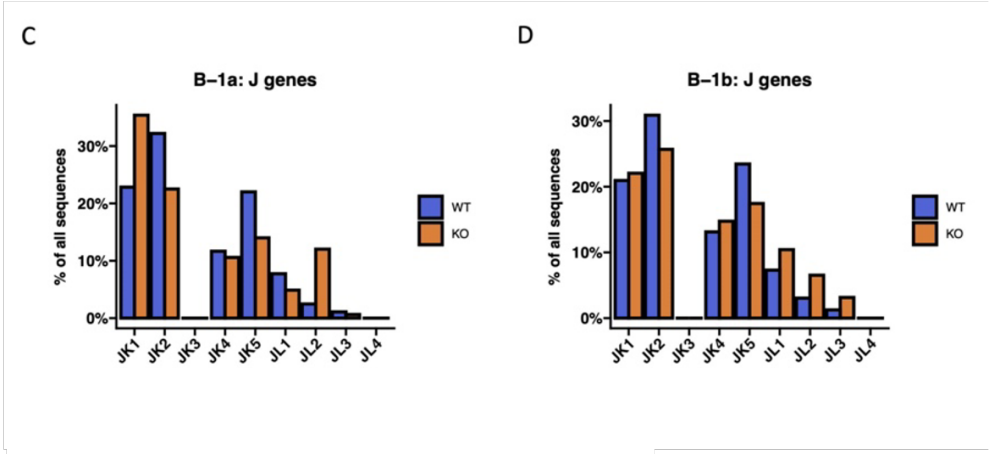
C
B–1a: J genes
% of all sequences
30%
20%
10%
0%
JK1 JK2 JK3 JK4 JK5 JL1 JL2 JL3 JL4
WT
KO
D
B–1b: J genes
% of all sequences
30%
20%
10%
0%
JK1 JK2 JK3 JK4 JK5 JL1 JL2 JL3 JL4
WT
KO

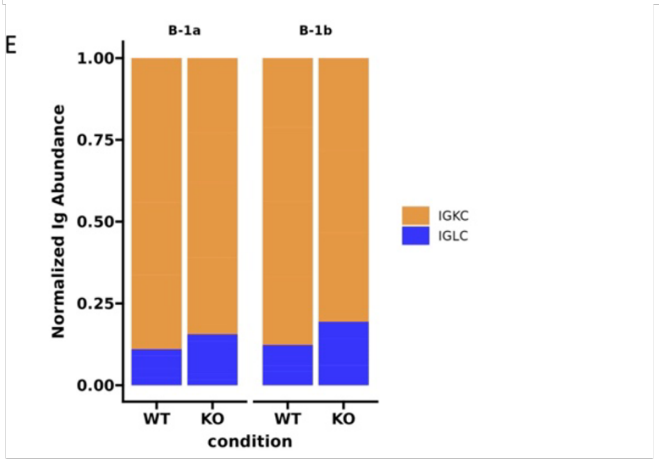
E
B-1a
B-1b
Normalized Ig Abundance
1.00
0.75
0.50
0.25
0.00
WT KO WT KO
condition
IGKC
IGLC

Figure 18. V-J Gene Association analysis of B-1a and B-1b cells from TET2-KO and WT mice. (**A-H**) Circos plot of V-J gene associations of CDR3 sequences identified by TRUST4 utilizing specific V-J gene segment pairs is displayed for B-1a cells from TET2-KO (**B, D**) and WT mice (**A, C**) from all CDR3 sequences (**A, B**) and replicated CDR3 sequences (**C, D**). Circos plot of V-J gene associations of CDR3 sequences identified by TRUST4 utilizing specific V-J gene segment pairs is displayed for B-1b cells from TET2-KO (**F, H**) and WT mice (**E, G**) from all CDR3 sequences (**E, F**) and replicated CDR3 sequences (**G, H**). Cables connect V and J gene segments that are observed together within the same CDR3 region, with the thickness of each cable indicating the relative frequency of each V-J pairing. (**I, J**) The abundance of V-J gene connections identified in replicated CDR3s presented as percent abundance of all CDR3 sequences in B-1a (**I**) and B-1b cells (**J**) from TET2-KO and WT mice. Each pair of bars represents the count of V-J associations combined from all samples. Blue and orange represent WT and TET2-KO mice, respectively. Sequences were pooled from mice from the same cell type and condition (n: B-1a: WT = 4, KO = 4, B-1b: WT = 4, KO = 3).

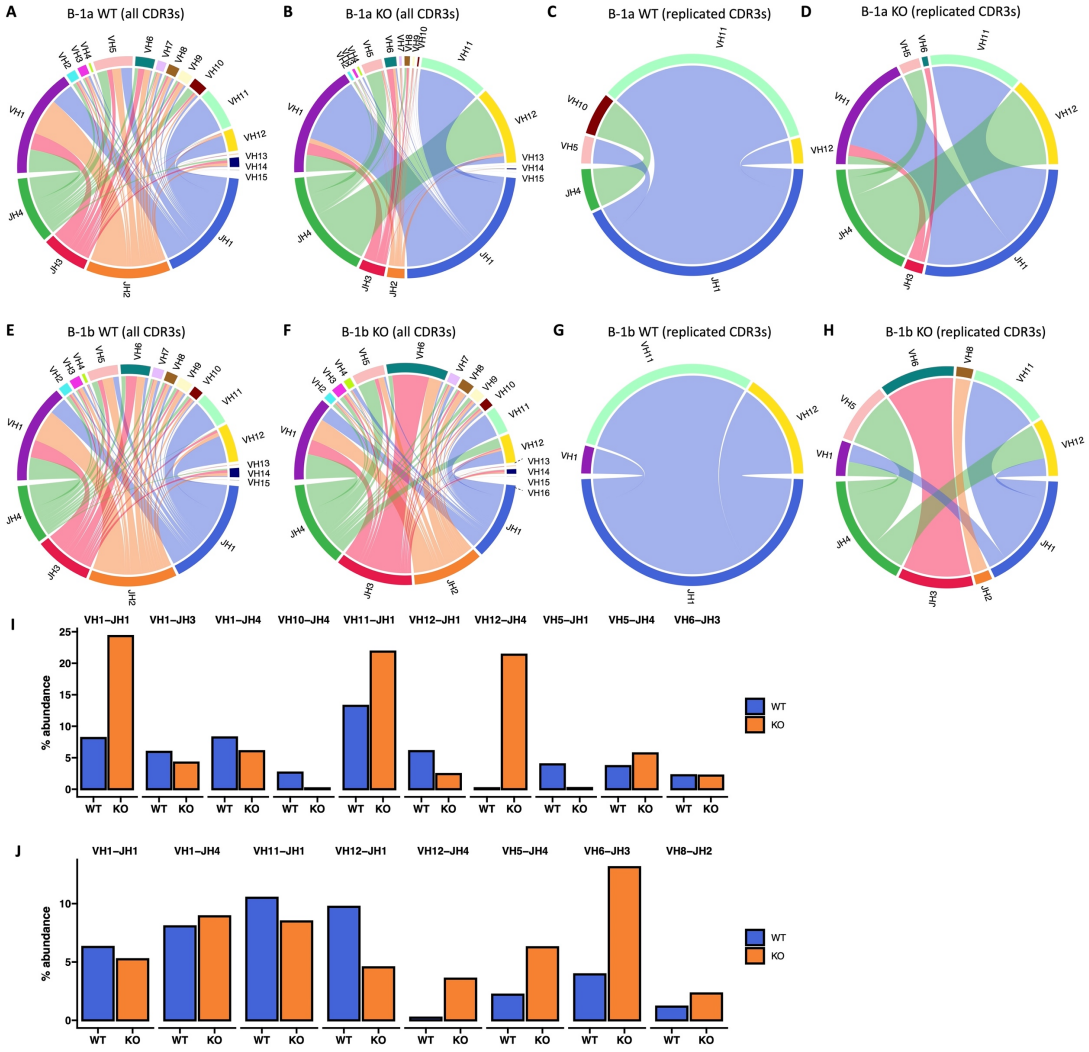
A
B-1a WT (all CDR3s)
B
B-1a KO (all CDR3s)
C
B-1a WT (replicated CDR3s)
D
B-1a KO (replicated CDR3s)
E
B-1b WT (all CDR3s)
F
B-1b KO (all CDR3s)
G
B-1b WT (replicated CDR3s)
H
B-1b KO (replicated CDR3s)
I
VH1–JH1
VH1–JH3
VH1–JH4
VH10–JH4
VH11–JH1
VH12–JH1
VH12–JH4
VH5–JH1
VH5–JH4
VH6–JH3
% abundance
WT
KO
J
VH1–JH1
VH1–JH4
VH11–JH1
VH12–JH1
VH12–JH4
VH5–JH4
VH6–JH3
VH8–JH2
% abundance
WT
KO

Discussion

Murine B cells can broadly be divided into B-2 cells, which are derived from BM precursors and include conventional follicular and marginal zone B cells, and B-1 cells, which are largely fetal liver-derived and persist in adults through self-renewal [2-6]. These B cell subtypes are developmentally, functionally, and phenotypically distinct [13, 156, 167-171]. Given their self-renewal capacity, we hypothesized that B-1 cells may be regulated by TET2, an epigenetic modulator that has been implicated in the clonal expansion of hematopoietic cells leading to disorders such as myelodysplastic syndromes (MDS) [117-119, 158, 159] and acute myeloid leukemia (AML) [119, 121, 122, 157]. Indeed, the results of the present study identified an important role for TET2 in regulating B cell numbers in specific niches. However, further studies are needed to determine if this is an effect intrinsic to the loss of TET2 specifically in B cells. Even if these findings are secondary to TET2 loss in another cell type, they still have potential relevance to diseases regulated by IgMs produced by B-1 cells such as infection [16, 17, 172-176], atherosclerosis [85, 177-182], and obesity-related metabolic dysfunction [81, 183]. Several human genetic variants of TET2 with loss of function have been identified [184-186] and these could have a broad impact similar to global TET2 deletion in mice, resulting directly or indirectly in modulating the anti-inflammatory effects of IgM-producing B cells.

B-1 cells have been shown to have important roles in the first line of defense against pathogens [16, 17, 172-176] and in mediating a reduction of inflammation [4, 24, 71, 154, 177, 183]. One of the major mechanisms mediating this effect is their production

of IgM that can recognize pattern-associated molecular pattern (PAMPs) and danger-associated molecular patterns (DAMPs) such as phosphorylcholine on the cell wall of *Streptococcus pneumoniae* [16, 174, 187] and oxidation-specific epitopes (OSEs) on lipoproteins [188, 189]. OSEs on lipoproteins and apoptotic cells can fuel disease-associated inflammation [189, 190] and IgM to these neoepitopes can inhibit their induction of inflammatory responses [191, 192]. Our study presents novel findings that the global loss of TET2 increased B-1 cell number, circulating IgM level, and BCR specificity, all factors that could affect the immune response against PAMPs and DAMPs.

The first major phenotype we observed due to the global loss of TET2 was an elevation in the frequency and number of all B cell subtypes in the peritoneal cavity (Figure 4G&J). Yet, in the specialized niches that promote B cell effector function, such as antibody production, only the frequency of B-1a cells in the BM (Figure 4H), and B-1b frequency and number in the spleen (Figure 4I&L), were higher in the TET2-KO compared to WT mice. The mechanism responsible for these subset and niche-specific increases in cell number remains unclear and requires further study to determine if proliferation, increased cell survival, or migration are responsible. As B-1a cells self-renew like hematopoietic stem cells (HSCs) [3, 153, 193-196], and this self-renewal property is enhanced in HSCs with TET2-KO [112, 113, 118, 119, 197, 198], enhanced self-renewal of B-1a cells from TET2-KO animals may explain the increase in B-1a cells in the peritoneal cavity.

The genes and pathways that were different in B-1 cells from TET2-KO mice compared to control, particularly in the B-1a cells, were immunoglobulin-related and they were expressed at a lower level (Figure 5C, Figure 8). There was a predominance of kappa light chain genes that were less expressed, in addition to several V_H genes, leading us to hypothesize that loss of TET2 may be limiting the expression of certain variable region genes, which allows for specific antigen recognition of foreign or neo-antigens [153, 199-202]. To further investigate those differences, we performed BCR analysis using our RNASeq data.

Historically, BCR identification from sequencing was facilitated by well-established algorithms like MiXCR [203] or BALDR [204] using V-D-J enriched or single-cell RNASeq data. However, the associated costs and impracticality of research studies focusing on low-frequency cell populations were limiting factors for broader application. The introduction of the TRUST4 algorithm by Song *et al.* [163] enabled the accurate detection of BCR and TCR repertoire from bulk RNASeq data. This innovation diminished the financial burden of data generation and allowed for the re-utilization of previously generated data, limiting redundancy and resources required for BCR/TCR analysis and providing opportunities for potential clinical applications. While the results are not at single-cell resolution, they offer valuable insight into the diversity of immune cell receptor repertoire and specificity. To date, a limited number of studies have performed an analogous analysis in bulk RNASeq data [205-207].

The constant region of the BCR determines the effector function of the antibody. There were no differences in the transcript expression levels of antibody isotypes IgG,

IgD, and IgA (Figure 11A). However, there was a statistically significant increase in transcript expression of IgM, the main isotype produced by B-1 cells [26, 63, 71, 154], in the B-1a cells from TET2-KO compared to WT mice suggesting that TET2 may inhibit factors responsible for encoding the constant region downstream of the V region on chromosome 14 that determines antibody isotype or TET2 may limit isotype switching in B-1a cells (Figure 11B). These data are consistent with no changes observed in the circulating IgG level while there was an increase in circulating IgM in the TET2-KO mice compared to the control. We could not conclude if the increase in total IgM was due to increased IgM secretion on a per-cell basis or due to the increase in overall cell number (Figure 11C). However, increased IgM levels could also be due to the increase in B-1 numbers in the spleen and bone marrow. Additionally, there was an increase in MZB cell number in the spleens from TET2-KO mice compared to WT, another potential source of IgM from TET2-KO and WT mice (Figure 12).

While much more has been documented about the role of the heavy chain variable region, specifically the CDR3 of the BCR, less is known about the purpose of the light chain regarding its role in binding antigens [165, 202, 208-213]. A study by Lio *et al.* revealed that double knockout of TET2 and TET3 in the early B cell stage impaired rearrangement at the Igκ locus [109]. Our findings support previous research by detecting the lower expression of many Igκ genes, and indeed, while not reaching significance, overall kappa immunoglobulin usage is reduced in B-1b cells, but surprisingly not B-1a cells from TET2-KO mice compared to WT (Figure 17E). There was also a significant reduction in the number of unique CDR3 sequences in B-1a cells and a trending

reduction in B-1b cells from TET2-KO mice compared to WT (Figure 5, Figure 16). Consistent with the reduced variety of CDR3 sequences, there is a higher number of replicated sequences in the light chain observed in the B-1a cells from the TET2-KO mice compared to WT, and the effect was also observed in B-1b cells to a lesser extent (Figure 16). These data suggest that the BCR repertoire in the light chains of B-1a cells is more sensitive to loss of TET2 than in B-1b cells.

B-1a cells from TET2-KO mice had significantly fewer unique CDR3 sequences with 72% of the total CDR3 sequences representing replicates, suggesting that loss of TET2 impacts the diversity of antigen specificity in B-1 cells, particularly B-1a cells (Figure 5B). The more marked lack of antigen diversity in the B-1a cells from TET2-KO mice is consistent with B-1a cells predominantly originating from the fetal liver and persisting through self-renewal, and a role for TET2 in promoting expansion of rapidly self-renewing cells. While our study isolated B cells from the global TET2-KO and WT mice, it must be considered that the effects of loss of TET2 in other cells, such as cytokine-secreting macrophages, could be playing a role in influencing the selection of the B cell repertoire. Additionally, the presence of IgM itself can influence the selection of the B cell repertoire [214]. In an analysis of V_H–D_H–J_H gene regions of the heavy chain, our data suggest that the restricted associations of V_H–D_H–J_H gene regions in the B-1a cells from TET2-KO mice could be responsible for the reduction in the number of unique CDR3 sequences. A study by Wong *et al.* identified a pathway whereby B-1a cells can bypass the need for a pre-BCR and generate a mature, albeit somewhat self-reactive, BCR directly [215]. The V_H12/V_K4 pairing is typical for binding

phosphatidylcholine, a lipid present in many bacteria membranes, and while V_H12 frequency of use is increased in B-1a cells from TET2-KO mice, V_K4 frequency of use is lower in B-1a cells from TET2-KO mice compared to WT (Figure 16-9) [215]. It should be noted that both V_H11 and J_H1 are associated with early fetal characteristics, which supports the potential enhancement of self-renewal that loss of TET2 regulation may foster [6, 156, 170, 210]. Our CDR3 and VDJ association data from the heavy chain provide further evidence in addition to the light chain data that B-1a cells are more profoundly impacted by global loss of TET2 compared to B-1b cells. The reason for this remains to be determined but may be due to the expression of CD5 by B-1a cells, given that studies have shown many of the malignant B cell samples with loss of TET2 express CD5 [197, 216, 217], but this connection requires further study.

Taken together, our data reveals that loss of TET2 influences IgM level and BCR repertoire, particularly in B-1a cells, which are key producers of natural IgM. Alteration to the antigen-specificity or abundance of B-1a-produced IgM may have consequences in the response to PAMPs and DAMPs and in regulating antigen-driven inflammation. Our data demonstrating that loss of TET2 increased B-1 cell subset numbers in antibody-producing niches and reduced CDR3 diversity suggests that TET2 may regulate the pool of antigen-specific IgM produced by B-1 cells (Figure 19) and underscores the need for further study of the impact and mechanisms whereby TET2 regulates B-1 cells, especially in the context of infection and diseases involving chronic inflammation.

Figure 19. Graphical abstract of key findings. Peritoneal B cell number is increased, circulating IgM levels are elevated, and CDR3 sequence diversity is reduced in mice null for TET2 compared to WT mice. Figure made with BioRender.

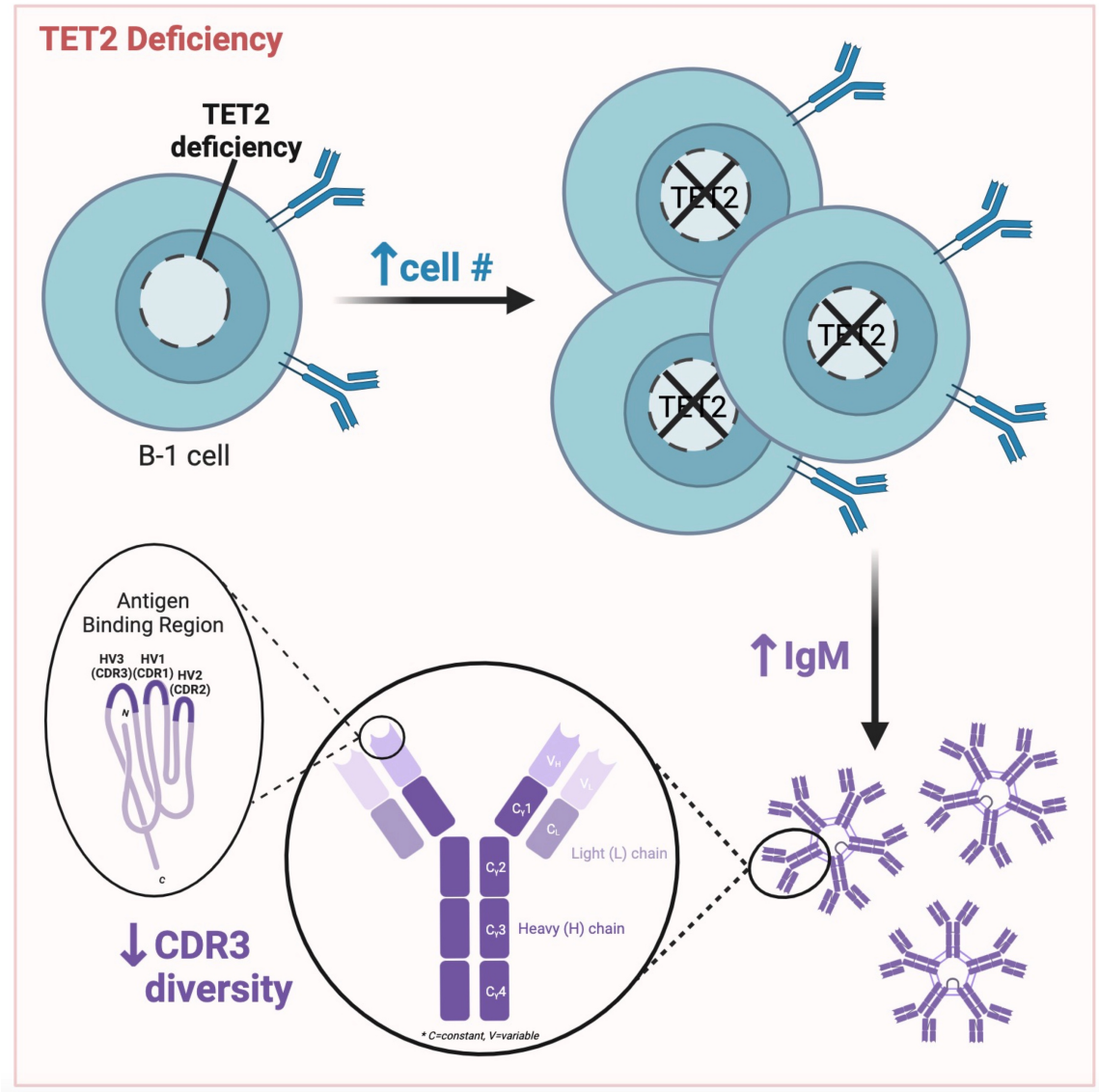
TET2 Deficiency
TET2 deficiency
B-1 cell
↑cell #
TET2
TET2
TET2
↑IgM
Antigen Binding Region
HV3 (CDR3)
HV1 (CDR1)
HV2 (CDR2)
N
C
↓CDR3 diversity
Light (L) chain
Heavy (H) chain
* C=constant, V=variable

Conflict of Interest

The authors declare that the research was conducted in the absence of any commercial or financial relationships that could be construed as a potential conflict of interest.

Author Contributions

Conceptualization, E.D. and C.M.; investigation, E.D., M.M., C.M.R.B., M.A.M., K.R.; data curation, M.M.; formal analysis, E.D. and M.M.; writing—original draft preparation, E.D.; writing—review and editing, M.M, C.M., S.B., L.E., T.P., C.J.B., J.D.; visualization, M.M. and E.D.; supervision, C.M. and S.B.; funding acquisition, C.M., E.D., M.M., C.J.B.

Funding

This work was supported by National Institutes of Health grants R01-HL148109 and 5R01HL141123 (C.A.M.) and a LeDucq Foundation Transatlantic Network of Excellence grant: ‘B cells in cardiovascular disease’ (C.A.M. and C.J.B.), T32 HL007284 (E.D.) and UVA iPRIME Fellowship (E.D. and M.M.).

Acknowledgments

The authors would like to thank Dr. Nichol Holodick (Western Michigan University Homer Stryker M.D. School of Medicine) for robust intellectual discussions about our data and comments on the manuscript. We thank Dr. Kenneth Walsh

(University of Virginia) for the donation of the global TET2-KO mice. We thank Maria Ozsvar Kozma (Medical University of Vienna) for technical support with plasma Ig analysis. The data for this manuscript were generated in the University of Virginia Flow Cytometry Core Facility (RRid:SCR_017829) and is partially supported by the NCI Grant (P30-CA044579).

Chapter 4: Discussion and Future Directions

B cell-produced IgM against OSEs is protective in atherosclerosis

B cell subtypes are developmentally, functionally, and phenotypically distinct [13, 156, 167-171]. Given their self-renewal capacity, we hypothesized that B-1 cells may be regulated by TET2, an epigenetic modulator that has been implicated in the clonal expansion of hematopoietic cells leading to disorders such as myelodysplastic syndromes (MDS) [117-119, 158, 159] and acute myeloid leukemia (AML) [119, 121, 122, 157]. Indeed, the results of the present study identified an important role for TET2 in regulating B cell number in specific niches. As prior studies have mostly reported on the effects of TET2 on B-2 cells [108, 109, 124, 132, 139-141, 162] and on hematological malignancy [108, 112, 140, 141, 162, 218], we focused our study on the B-1 B cell subtype at homeostasis. B-1 cells have been shown to have important roles in mediating the reduction of inflammation [4, 13, 24, 71, 154, 168, 219-221]. One of the major mechanisms mediating this effect is the production of IgM that can recognize danger-associated molecular patterns (DAMPs) such as oxidation-specific epitopes (OSEs) [188] and inhibit their induction of inflammatory responses [191, 192].

In atherosclerosis, a cardiovascular disease of chronic inflammation, OSEs on low-density lipoprotein and apoptotic cells can fuel disease-associated inflammation [190]. B-1 cell-derived IgMs that recognize these epitopes constitute an abundant portion of the IgM pool and can blunt the pro-inflammatory effect of these OSEs [21, 182, 222] and limit atherosclerosis [61, 63, 71, 77, 154, 223-227]. This study presented novel findings about the role of TET2 in modulating B-1 cell number, immunoglobulin production, and BCR specificity, all factors that could affect the immune response against

OSE. In humans, plasma levels of IgM to OSE are inversely associated with atherosclerotic cardiovascular disease (ASCVD) [73, 78, 182, 228] and TET2 mutations are linked to ASCVD [87, 110, 229, 230]. While the findings of this study are novel and contribute to our broader understanding of cell type-specific roles of TET2, we have not yet reported a causal link to ASCVD. Additional experiments utilizing induced hyperlipidemia and Western Diet could assess if the elevated IgM observed in TET2-KO mice exhibit attenuated atherosclerotic plaque burden, and those future experiments could then potentially advance our understanding of the complex role of TET2 in ASCVD (Figure 20).

Figure 20. Loss of TET2 in B-1 cells may attenuate atherosclerosis. Wildtype IgM-secreting B-1 cells are considered atheroprotective and the binding of IgM to oxLDL helps reduce atherosclerosis plaque progression. Loss of TET2 in B-1 cells may result in increased cell numbers and enhanced function as described in macrophages from murine models with TET2 deficiency. This growth in the B-1 cell population combined with elevated IgM secretion might further reduce atherosclerosis burden by reducing the accumulation of foam cells and overall plaque size. Further investigation of if the IgM levels observed in TET2-KO mice are sufficient to attenuate atherosclerosis is needed to confirm any causal link. Figure schematic made with BioRender.

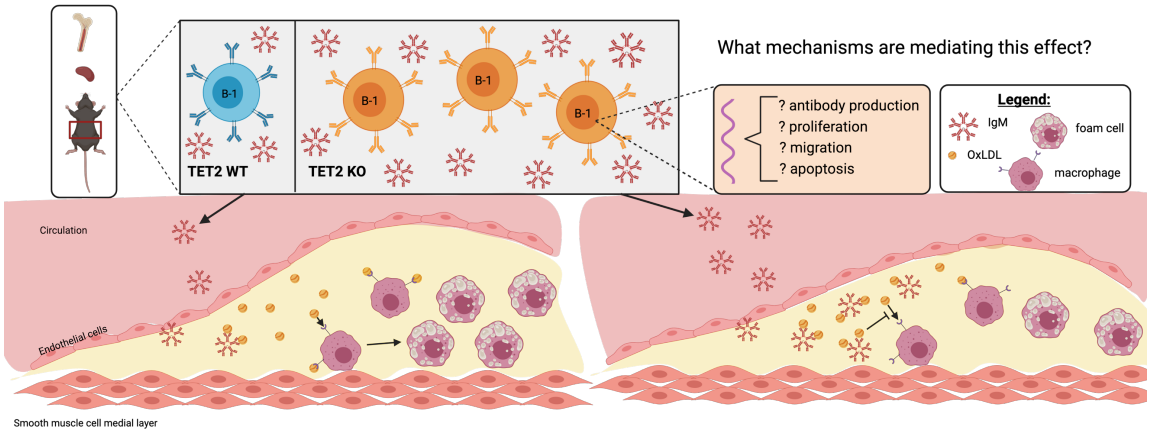

Atheroprotective B-1 cells from the bone marrow, spleen, and peritoneal cavity secrete IgM, which binds to oxidized LDL (oxLDL) and prevents macrophage uptake, subsequent foam cell formation, and lesion growth. Changes in B-1 cells due to loss of TET2 may result in attenuation of atherosclerosis progression.

The mechanism behind the B-1 cell number augmentation in mice with loss of TET2 remains to be determined

The first major phenotype we observed due to the global loss of TET2 was an elevation in the frequency and number of all B cell subtypes in the peritoneal cavity (Figure 4A, 4D, 4G). Yet, in the specialized niches that promote B cell effector function, such as antibody production, only the frequency of B-1a cells in the BM (Figure 4B, 4E, 4H), and B-1b number in the spleen (Figure 4C, 4F, 4I), were higher in the TET2-KO compared to WT mice. The mechanism responsible for these subset and niche-specific increases remains unclear and requires further study to determine if proliferation, increased cell survival, or migration are responsible. As B-1a cells self-renew like hematopoietic stem cells (HSCs) [3, 153, 193-196], and this self-renewal property is enhanced in HSCs with TET2-KO [112, 113, 118, 119, 197, 198], enhanced self-renewal of B-1a cells from TET2-KO animals may explain the increase in B-1a cells in the peritoneal cavity. To address the questions raised by the elevated numbers of B-1 cells from TET2-KO mice, experiments assessing augmented proliferative capacity or enhanced cell survival would be informative. Intercalating DNA dyes such as CellTrace or CFSE can measure differences in the number of replication cycles each B-1 cell subset underwent; alternatively, Ki-67 could be measured via flow cytometry or immunohistochemistry for a snapshot profile of actively proliferating cells. Additionally, cell survival assays using Annexin V and a viability dye can be used to identify apoptotic and/or necrotic cell populations and assess overall cell health in B-1 cell subsets from mice with TET2-KO compared to WT controls.

Immunoglobulin-related genes were downregulated in B-1 cells null for TET2 compared to WT controls, particularly in the B-1a cells (Figure 5A). A majority of kappa light chain genes were downregulated, in addition to several V_H genes, leading us to hypothesize that TET2 may be restraining the expression of certain variable region genes, which allows for specific antigen recognition of foreign or neo-antigens [153, 199-202]. To further investigate those differences, we performed B-cell Receptor (BCR) analysis using our RNASeq data.

BCR analysis can be performed with bulk RNAseq data

Traditionally, BCR identification from sequencing is executed by well-established algorithms like MiXCR [203] or BALDR [204] using V-D-J enriched or single-cell RNASeq data. However, the associated costs and impracticality for research studies focusing on low-frequency cell populations were limiting factors for its broader application. Song and colleagues introduced the TRUST4 algorithm and enabled the accurate detection of the BCR and TCR repertoire from bulk RNASeq data [163]. This innovation reduces the financial burden of data generation and allows for re-utilization of previously generated data, limiting redundancy and resources required for BCR/TCR analysis and providing opportunities for potential clinical applications. While the results are not on a single-cell resolution, they offer valuable insight into the diversity of immune cell receptor repertoire and specificity. The number of studies that have performed an analogous analysis in bulk RNASeq data is growing [205-207].

Loss of TET2 impacts antigen diversity in B-1 cells

In an analysis of the immunoglobulin heavy chain, B-1a cells from TET2-KO mice had significantly fewer unique CDR3 sequences with 72% of the total CDR3 sequences representing replicates, suggesting that loss of TET2 impacts the diversity of antigen specificity in B-1 cells, particularly B-1a cells. The restricted associations of V_H–D_H–J_H gene regions in the B-1a cells from TET2-KO mice could be responsible for the reduction in the number of unique CDR3 sequences. It should be noted that both V_H11 and J_H1 are associated with early fetal characteristics, which supports the potential enhancement of self-renewal that loss of TET2 regulation may allow. The more marked lack of antigen diversity in the B-1a cells from TET2-KO mice is consistent with B-1a cells emerging from the fetal liver and maintaining their population through self-renewal and presents a role for TET2 in promoting expansion of rapidly self-renewing B-1 cells. .

Other cell types could contribute to our observed phenotype

Since our study isolated B cells from the global TET2-KO and WT mice, we cannot conclude that the effects of loss of TET2 in other cells, such as cytokine-secreting macrophages, do not take part in shaping the selection of the BCR repertoire. Additionally, Holodick and colleagues reported that the presence of IgM itself can influence the selection of the B cell repertoire [214]. Future studies utilizing B cell-specific knockouts to control for non-cell autonomous effects, for example with a CD19-cre strain crossed with TET2 fl/fl mice, or tamoxifen-inducible B cell-specific knockouts to control for B cell development, would be ideal to determine the mechanism of TET2's

influence over IgM production and the BCR repertoire. Should investigators fail to achieve a knockout restricted to the B cell population, B-1 cells sort-purified from TET2-KO and WT mice could be adoptively transferred into Rag1-/- mice, which lack B and T cells and thus would provide a clear background for measuring effects due to loss of TET2 in B cells, as the recipient mice would be TET2-WT.

Loss of TET2 increases the transcriptional output of IgM in B-1 cells

There were no differences in the transcript expression of antibody isotypes including IgG, IgD, and IgA (data not shown). However, there was a statistically significant increase in transcript expression of IgM, the main isotype produced by B-1 cells [26, 63, 71, 154, 231], in the B-1a cells from TET2-KO compared to WT mice. This increase in the IgM RNA expression could indicate that TET2 may inhibit factors responsible for encoding the constant region downstream of the V region on chromosome 14 which determines antibody isotype, or that TET2 may limit isotype switching in B-1a cells as it does in GC B cells.

This finding is consistent with most of the pool of B-1a cells having originated from the fetal liver and undergone self-renewal to maintain numbers, usually with little introduced variation in the BCR. B-1b cells can be repopulated more easily than B-1a cells from the bone marrow, and with the activity of the enzyme TdT, which is only active after birth, can introduce variety in the BCR and thus reduce the proportion of replicate CDR3 sequences [1, 6, 9, 10, 156, 169-171, 194, 210, 211, 232].

These data are strengthened by the observed increase in circulating IgM in the TET2-KO mice compared to the controls. While increased circulating IgM levels could also be due to the increase in B-1 numbers in the spleen and bone marrow, there was no difference in the frequency of the other potential source of IgM frequency, MZBs, from TET2-KO and WT mice (Figure 12). Changes in the proportion of specific antibody isotypes encoded by the constant region could result in physiological changes due to the effector functions associated with each isotope. To assess if there are changes directly to antigen-binding capacity or specificity of the antibodies produced by B-1 cells with TET2 deficiency, agents that induce inflammation or are commonly characterized as infectious agents could be used to challenge the cells *in vitro* or mice *in vivo*. Antibodies binding to antigens such as PC are well-documented, and protein precipitation assays can be used to assess the fraction of free-antigen versus bound antigens. Alternatively, downstream processes following antibody-antigen binding, such as neutralization, opsonization, and complement activation, could also be utilized in determining if the quality of antibody response exhibits differences due to loss of TET2 in B-1 cells.

Loss of TET2 also reduces BCR diversity via the immunoglobulin light chain

While much more has been documented about the role of the heavy chain variable region, specifically the CDR3 of the BCR, less is known about the purpose of the light chain regarding its role in binding antigens [165, 202, 208-213]. The light chain repertoire is more limited due to the absence of the Diversity segments and N-additions [202]. Kappa (Ig_K) and lambda (Ig_L) gene rearrangements are also required to minimize

BCR self-reactivity. A study by Lio *et al.* revealed that double knockout of TET2 and TET3 in the early B cell stage impaired rearrangement at the Ig_K locus [109].

Our findings support previous research by detecting the downregulation of many Ig_K genes, as well as a significant reduction in the number of unique CDR3 sequences in B-1a cells and a trending reduction in B-1b cells from TET2-KO mice compared to WT (Figure 5, Figure 15). Our data suggest that the BCR repertoire in both the heavy and light chains in B-1a cells was more sensitive to loss of TET2 than in B-1b cells.

In an analysis of $V_{K/L}$ and $J_{K/L}$ segment use, we found that many $V_{K/L}$ genes are significantly different between B-1a cells from TET2-KO and WT mice, although only three of the $V_{K/L}$ gene segments make up the majority proportion of the expressed genes. V_K9 is considered the "prototypic" light chain for B cells, but in the peritoneal B-1a cells from our data there was minimal expression of this gene, although there was a slightly higher expression in B-1b cells (~5%) in both TET2-KO and WT mice (Figure 17) [168]. Two BCR combinations are associated with the production of a natural autoantibody associated with autoimmunity: the first and most abundant is V_H11-V_K9; this BCR specificity plays a role in additional B-1a generation [168]. The second combination is V_H12-V_K4, and in our samples, V_K4 was represented as the top third most frequently expressed in B-1a cells while it was the topmost expressed in B-1b cells (Figure 17). In the B-1a cells from TET2-KO mice, there was a significant reduction in the expression frequency of V_K4 compared to WT, while there was no difference in expression frequency in B-1b cells from TET2-KO mice compared to WT (Figure 17).

Many potential experiments could address the potential consequences of increased autoimmunity due to TET2 deficiency in B-1 cells. Kidney dysfunction is a symptom shared by many autoimmune diseases, such as systemic lupus erythematosus (SLE), which affects about 73 cases per 100,000 people in the United States. Including the kidneys at terminal tissue collection would provide a wealth of information about potential autoimmunity effects in the TET2-KO model. Gross measurements of the organ would allow for reporting overt kidney disease, which is characterized by reduced organ size. Digestion and preparation of kidney cells for flow cytometry would allow measurement of activation or expansion of leukocytes in that tissue. Similarly, immunohistochemistry of kidney sections could provide spatial resolution and organization of immune cell infiltration, as well as identify autoantibodies against dsDNA, which are commonly elevated in autoimmune disorders. The collection of urine is possible at time points throughout the animals' lifespans and at terminal tissue harvest. Utilizing reported urine biomarkers for nephritis, such as proteins ALCAM, CD163, CCL2, SELL, ICAM1, and VCAM1, as well as measuring levels of IgA, which accumulates in the kidney and causes inflammation and nephropathy, are additional methods to assess autoimmunity severity. The contribution of TET2 regulation of B-1 cell-mediated autoimmunity remains to be revealed, and additional study would further illuminate mechanisms of TET2 and B-1 cell influence in the pathology of autoimmune diseases.

TET2 moderation of IgM to OSEs may have profound effects on disease states

Taken together, our data reveals that loss of TET2 influences Ig production and BCR repertoire, particularly in B-1a cells, which are key producers of natural IgM and help attenuate atherosclerotic plaque development. Alteration to the antigen-specificity or abundance of B-1a-produced IgM due to TET2's regulation of the BCR may have consequences in the development or severity of atherosclerosis, however we cannot yet make a claim that loss of TET2 in B-1 cells is atheroprotective. The recent evidence implicating TET2 in the pathogenesis of CVD [86, 87, 110, 111], and our data demonstrating that loss of TET2 increases B-1 cell subset numbers in antibody-producing niches which suggest that TET2 could regulate the pool of antigen-specific IgM produced by B-1 cells (Figure 19) underscores the need for further study of the impact and mechanisms whereby TET2 regulates B-1 cells, especially in the context of diseases involving chronic inflammation, like atherosclerosis. Experiments inducing hyperlipidemia, for instance with the viral delivery of AAV-PCSK9 which effectively knocks out the LDL receptor, paired with Western diet (WD) could assess if atherosclerotic plaque burden is altered due to increased levels of IgM circulating in TET2-KO mice compared to WT mice. In addition, chimeric adoptive transfers modeling CHIP could be useful, using transfer ratios of 10-20% cells from TET2-KO mice and 80-90% cells from WT mice compared to 100% WT mice which more closely resemble population distributions of TET2 mutant clones in humans. However, an ideal experiment would be to use CRISPR/Cas9 to replicate a specific SNP mutation in TET2 in the mice which has been reported in humans with TET2 CHIP, and then to induce hyperlipidemia

and use WD to assess atherogenesis. Much remains to be discovered about the contribution of TET2-regulated, B-1 cell-produced IgM to the severity of atherosclerosis.

Interestingly, when we measured IgM specific to certain antigens including MDA-LDL, Cu-oxLDL, PC-BSA, and T15-E06 idiotype, the level of plasma IgM was affected in an antigen-specific-IgM manner (Figure 24). Malondialdehyde-modified low-density lipoprotein (MDA-LDL) and Copper-oxidized LDL (Cu-oxLDL) are oxidation-specific epitopes (OSEs) that IgM binds, preventing uptake by macrophages and plaque generation in atherosclerosis. E06 is a T15 idiotype IgM natural antibody (Nab) exclusively produced by B-1 cells, which recognizes the phosphocholine (PC) head group in oxidized phospholipids on the surface of apoptotic cells, and the PC present on the cell wall of *Streptococcus pneumoniae* thus facilitating apoptotic cell clearance and protection from infectious pathogens [77].

Recently it has been shown that patients with an autoimmune disorder SLE are more likely to have low levels of anti-PC IgM, which also increases the risk of plaque accumulation in atherosclerosis [233]. While there were no differences in secreted IgM against the T15-E06 idiotype, significance was trending with Cu-oxLDL and was trending even closer to significance with PC-BSA. IgM against MDA-LDL was the only IgM that was significantly elevated in the TET2-KO mice compared to WT (Figure 24). This could indicate that TET2 may play a role in augmenting the production of IgM specifically against MDA-LDL, which protects from atherogenesis. In our study we utilized young adult mice to avoid the potential for malignant hematological effects due to loss of TET2. The mice were fed a normal chow diet, without stimulation or antigen

challenge to measure the role loss of TET2 plays in B-1 cell homeostasis. Future studies with stimulation using LPS or inducing hyperlipidemia with a high-fat diet would be useful to assess how TET2 loss in B-1 cells modulates cell number and function in an infectious or inflammatory state (Figure 21).

Loss of TET2 and altered BCR repertoire may also result in changes to systemic lupus erythematosus severity

Comparison of the most highly represented sequences in our B-1a cells from TET2-KO and WT mice with the literature revealed interesting findings (Figure 13) [4, 156, 210]. Yang *et al.* investigated the B-1a IgH repertoire as it progressed from neonate to adult and found that the CDR3 sequence ARFYYYGSSYAMDY was one of the most abundant sequences in B-1a cells from healthy 2-month-old B6 mice [210]. Consistent with their findings, RHYYGSSYYAMDY, a sequence with only minor variation, was the third-most replicated in B-1a cells from our similarly aged WT mice. Holodick *et al.* found that the CDR3 sequence MRYGNYWYFDV makes up almost 40% of peritoneal B-1a sequences in SLE mice [4]. This identical sequence was the top replicated sequence in our B-1a cells from WT mice at ~8% of all sequences, and MRYSNYWYFDV, a sequence with only minor variation, was the second-most replicated sequence in our B-1a cells from WT mice at 2% of all sequences. Intriguingly, this sequence MRYGNYWYFDV accounted for ~6%, MRYSNYWYFDV accounted for ~6%, and MRYGDYWYFDV accounted for ~4% of all CDR3s in the B-1a cells from TET2-KO mice, suggesting that TET2 may have minor influence on the pool of IgMs in SLE based

on heavy chain CDR3 sequence [108, 120, 129, 143]. Consistent with this finding, the CDR3 sequence MRYGSSYWYFDV, in the top twelve of CDR3s for SLE mice was highly similar to sequence MRYSSYWYFDV which was also the seventh-most abundant sequence in the B-1a cells from TET2-KO mice (Figure 4C) [4]. Due to this commonality in CDR3 sequences from B-1a cells from TET2-KO mice with B-1a cells from SLE models, it could be fruitful to investigate targeted therapy against B-1a cells with TET2-KO to see if used in an SLE model, then SLE severity is attenuated. While several of the sequences we found common to the literature had minor variations, it should be noted that even a minor variation in the CDR3 sequence can have a large impact on binding specificity due to polarity, charge, and other R-group properties. Despite this, the finding of different specificities replicated in the B-1a cells from TET2-KO mice is novel and bears further investigation for more mechanistic insights. Additional research into CDR3 sequences associated with other disease models as they become available will continue to reveal potential connections that loss of TET2 plays in CDR3 specificity and Ig production.

TET2 influence of Ig production and BCR heterogeneity may provide targets for autoimmune therapeutics

Taken together, our data reveals that loss of TET2 influences Ig production and BCR repertoire, particularly in B-1a cells. The recent evidence implicating TET2 in the pathogenesis of CVD [86, 87, 110, 111] and SLE [125, 127, 234-236], and our data suggesting that TET2 may regulate the pool of antigen-specific IgM produced by B-1

cells, underscores the need for further study of the impact and mechanisms whereby TET2 regulates B-1 cells, especially in the context of diseases involving chronic and systemic inflammation. In addition, these findings raise the possibility that function-attenuating somatic mutations in TET2 observed in clonal hematopoiesis of indeterminate potential (CHIP) and hematological malignancies [86, 96, 237-239] may serve as genetic biomarkers of chronic inflammatory diseases like atherosclerosis and SLE and provide new insights into disease pathogenesis and potential targeted therapeutics.

Figure 21. Future directions to advance knowledge of the role of TET2 in B-1 cell function and disease. Experiments continuing use of the global knockout of TET2 should focus on assessing antibody and proliferative response to challenge with LPS or an MDA-LDL mimotope. Additionally, while a recent presentation by Yoshimoto and colleagues at 2024 AAI Meeting revealed that transfer of fetal-derived B-1 cells from TET2-KO mice into a clonal hematopoiesis model of TET2 deficiency fed a WD resulted in reduced atherosclerosis progression, but the mechanism remains to be determined. Figure made with BioRender

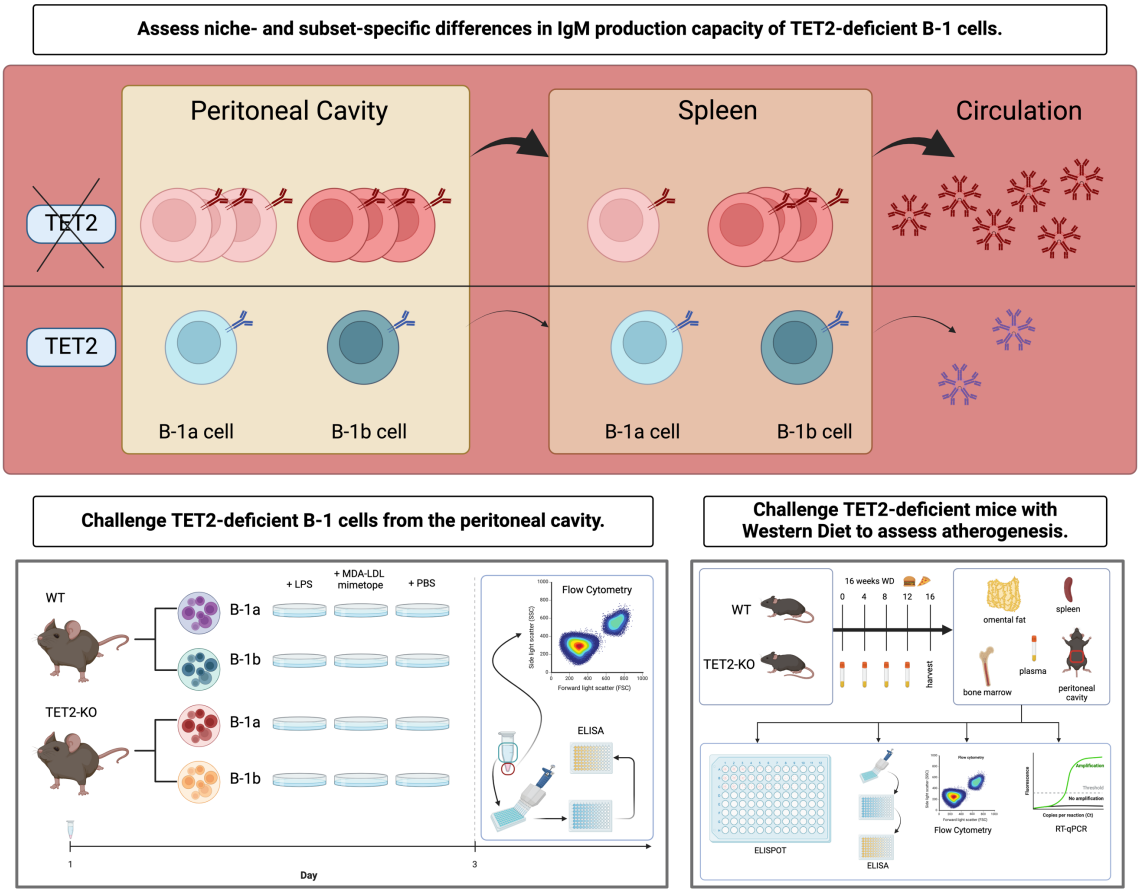
Assess niche- and subset-specific differences in IgM production capacity of TET2-deficient B-1 cells.
Peritoneal Cavity
Spleen
Circulation
TET2
TET2
B-1a cell
B-1b cell
B-1a cell
B-1b cell
Challenge TET2-deficient B-1 cells from the peritoneal cavity.
Challenge TET2-deficient mice with Western Diet to assess atherogenesis.
WT
TET2-KO
+ LPS
+ MDA-LDL mimetope
+ PBS
B-1a
B-1b
B-1a
B-1b
Flow Cytometry
ELISA
Day
1
3
16 weeks WD
0
4
8
12
16
harvest
omental fat
spleen
plasma
bone marrow
peritoneal cavity
ELISPOT
ELISA
Flow Cytometry
RT-qPCR

Literature Cited

1. Wang, Y., et al., *B Cell Development and Maturation.* Adv Exp Med Biol, 2020. **1254**: p. 1-22.

2. Pattarabanjird, T., et al., *B-1b Cells Possess Unique bHLH-Driven P62-Dependent Self-Renewal and Atheroprotection.* Circ Res, 2022. **130**(7): p. 981-993.

3. Deenen, G.J. and F.G. Kroese, *Kinetics of peritoneal B-1a cells (CD5 B cells) in young adult mice.* Eur J Immunol, 1993. **23**(1): p. 12-6.

4. Holodick, N.E., et al., *Expansion of B-1a Cells with Germline Heavy Chain Sequence in Lupus Mice.* Front Immunol, 2016. **7**: p. 108.

5. Kreslavsky, T., et al., *Essential role for the transcription factor Bhlhe41 in regulating the development, self-renewal and BCR repertoire of B-1a cells.* Nat Immunol, 2017. **18**(4): p. 442-455.

6. Kristiansen, T.A., et al., *Cellular Barcoding Links B-1a B Cell Potential to a Fetal Hematopoietic Stem Cell State at the Single-Cell Level.* Immunity, 2016. **45**(2): p. 346-57.

7. McHeyzer-Williams, L.J. and M.G. McHeyzer-Williams, *Antigen-specific memory B cell development.* Annu Rev Immunol, 2005. **23**: p. 487-513.

8. Holodick, N.E., T. Vizconde, and T.L. Rothstein, *B-1a cell diversity: nontemplated addition in B-1a cell Ig is determined by progenitor population and developmental location.* J Immunol, 2014. **192**(5): p. 2432-41.

9. Montecino-Rodriguez, E. and K. Dorshkind, *B-1 B cell development in the fetus and adult.* Immunity, 2012. **36**(1): p. 13-21.

10. Montecino-Rodriguez, E., H. Leathers, and K. Dorshkind, *Identification of a B-1 B cell-specified progenitor.* Nat Immunol, 2006. **7**(3): p. 293-301.

11. Baumgarth, N., *The double life of a B-1 cell: self-reactivity selects for protective effector functions.* Nat Rev Immunol, 2011. **11**(1): p. 34-46.

12. Taylor, C.L., et al., *Extramedullary hematopoiesis causing paraparesis in congenital cyanotic heart disease.* Neurology, 1998. **51**(2): p. 636-7.

13. Kawahara, T., et al., *Peritoneal cavity B cells are precursors of splenic IgM natural antibody-producing cells.* J Immunol, 2003. **171**(10): p. 5406-14.

14. Ha, S.A., et al., *Regulation of B1 cell migration by signals through Toll-like receptors.* J Exp Med, 2006. **203**(11): p. 2541-50.

15. Alugupalli, K.R. and R.M. Gerstein, *Divide and conquer: division of labor by B-1 B cells.* Immunity, 2005. **23**(1): p. 1-2.

16. Haas, K.M., et al., *B-1a and B-1b cells exhibit distinct developmental requirements and have unique functional roles in innate and adaptive immunity to S. pneumoniae.* Immunity, 2005. **23**(1): p. 7-18.

17. Choi, Y.S. and N. Baumgarth, *Dual role for B-1a cells in immunity to influenza virus infection.* J Exp Med, 2008. **205**(13): p. 3053-64.

18. Cole, L.E., et al., *Antigen-specific B-1a antibodies induced by Francisella tularensis LPS provide long-term protection against F. tularensis LVS challenge.* Proc Natl Acad Sci U S A, 2009. **106**(11): p. 4343-8.

19. Baumgarth, N., et al., *Innate and acquired humoral immunities to influenza virus are mediated by distinct arms of the immune system.* Proc Natl Acad Sci U S A, 1999. **96**(5): p. 2250-5.

20. Hooijkaas, H., et al., *Isotypes and specificities of immunoglobulins produced by germ-free mice fed chemically defined ultrafiltered "antigen-free" diet.* Eur J Immunol, 1984. **14**(12): p. 1127-30.

21. Chou, M.Y., et al., *Oxidation-specific epitopes are dominant targets of innate natural antibodies in mice and humans.* J Clin Invest, 2009. **119**(5): p. 1335-49.

22. Ogden, C.A., et al., *IGM is required for efficient complement mediated phagocytosis of apoptotic cells in vivo.* Autoimmunity, 2005. **38**(4): p. 259-64.

23. Alugupalli, K.R., et al., *B1b lymphocytes confer T cell-independent long-lasting immunity.* Immunity, 2004. **21**(3): p. 379-90.

24. Choi, Y.S., et al., *B-1 cells in the bone marrow are a significant source of natural IgM.* Eur J Immunol, 2012. **42**(1): p. 120-9.

25. Holodick, N.E., J.R. Tumang, and T.L. Rothstein, *Immunoglobulin secretion by B1 cells: differential intensity and IRF4-dependence of spontaneous IgM secretion by peritoneal and splenic B1 cells.* Eur J Immunol, 2010. **40**(11): p. 3007-16.

26. Holodick, N.E., T. Vizconde, and T.L. Rothstein, *Splenic B-1a Cells Expressing CD138 Spontaneously Secrete Large Amounts of Immunoglobulin in Naive Mice.* Front Immunol, 2014. **5**: p. 129.

27. Ouchida, R., et al., *Critical role of the IgM Fc receptor in IgM homeostasis, B-cell survival, and humoral immune responses.* Proc Natl Acad Sci U S A, 2012. **109**(40): p. E2699-706.

28. Ait-Oufella, H., et al., *Recent advances on the role of cytokines in atherosclerosis.* Arterioscler Thromb Vasc Biol, 2011. **31**(5): p. 969-79.

29. Zhang, H., et al., *Serum IgG subclasses in autoimmune diseases.* Medicine (Baltimore), 2015. **94**(2): p. e387.

30. Wang, H. and M.J. Schlomchik, *Regulation of autoreactive anti-IgG (rheumatoid factor) B cells in normal and autoimmune mice.* Immunol Res, 1999. **19**(2-3): p. 259-70.

31. Jaskowski, T.D., et al., *Prevalence of IgG autoantibody against F-actin in patients suspected of having autoimmune or acute viral hepatitis.* J Clin Lab Anal, 2007. **21**(4): p. 249-53.

32. Hurez, V., et al., *Pooled normal human polyspecific IgM contains neutralizing anti-idiotypes to IgG autoantibodies of autoimmune patients and protects from experimental autoimmune disease.* Blood, 1997. **90**(10): p. 4004-13.

33. Fries, L.F., C.M. Brickman, and M.M. Frank, *Monocyte receptors for the Fc portion of IgG increase in number in autoimmune hemolytic anemia and other hemolytic states and are decreased by glucocorticoid therapy.* J Immunol, 1983. **131**(3): p. 1240-5.

34. Amendt, T. and H. Jumaa, *Memory IgM protects endogenous insulin from autoimmune destruction.* EMBO J, 2021. **40**(17): p. e107621.

35. Appelgren, D., et al., *Marginal-Zone B-Cells Are Main Producers of IgM in Humans, and Are Reduced in Patients With Autoimmune Vasculitis.* Front Immunol, 2018. **9**: p. 2242.

36. Boross, P., et al., *The inhibiting Fc receptor for IgG, FcgammaRIIB, is a modifier of autoimmune susceptibility.* J Immunol, 2011. **187**(3): p. 1304-13.

37. Karsten, C.M. and J. Kohl, *The immunoglobulin, IgG Fc receptor and complement triangle in autoimmune diseases.* Immunobiology, 2012. **217**(11): p. 1067-79.

38. Diaz-Jouanen, E., et al., *Immune complexes in autoimmune diseases. Differences in immune complexes detected by cellular receptors for complement and for Fc domains of IgG.* Rev Invest Clin, 1980. **32**(2): p. 153-63.

39. Zouali, M., R. Jefferis, and A. Eyquem, *IgG subclass distribution of autoantibodies to DNA and to nuclear ribonucleoproteins in autoimmune diseases.* Immunology, 1984. **51**(3): p. 595-600.

40. Buhre, J.S., M. Becker, and M. Ehlers, *IgG subclass and Fc glycosylation shifts are linked to the transition from pre- to inflammatory autoimmune conditions.* Front Immunol, 2022. **13**: p. 1006939.

41. Ballow, M., *The IgG molecule as a biological immune response modifier: mechanisms of action of intravenous immune serum globulin in autoimmune and inflammatory disorders.* J Allergy Clin Immunol, 2011. **127**(2): p. 315-23; quiz 324-5.

42. Andren, M., et al., *IgG Fc receptor polymorphisms and association with autoimmune disease.* Eur J Immunol, 2005. **35**(10): p. 3020-9.

43. Sondermann, P., *The FcgammaR/IgG Interaction as Target for the Treatment of Autoimmune Diseases.* J Clin Immunol, 2016. **36 Suppl 1**: p. 95-9.

44. Campochiaro, C., et al., *Autoimmunity and immunodeficiency at the crossroad: autoimmune disorders as the presenting feature of selective IgM deficiency.* BMJ Case Rep, 2019. **12**(1).

45. Boes, M., et al., *Accelerated development of IgG autoantibodies and autoimmune disease in the absence of secreted IgM.* Proc Natl Acad Sci U S A, 2000. **97**(3): p. 1184-9.

46. Arnett, D.K., et al., *2019 ACC/AHA Guideline on the Primary Prevention of Cardiovascular Disease: A Report of the American College of Cardiology/American Heart Association Task Force on Clinical Practice Guidelines.* Circulation, 2019. **140**(11): p. e596-e646.

47. Sherer, Y. and Y. Shoenfeld, *Mechanisms of disease: atherosclerosis in autoimmune diseases.* Nat Clin Pract Rheumatol, 2006. **2**(2): p. 99-106.

48. Matsuura, E., et al., *Is atherosclerosis an autoimmune disease?* BMC Med, 2014. **12**: p. 47.

49. Cinoku, II, C.P. Mavragani, and H.M. Moutsopoulos, *Atherosclerosis: Beyond the lipid storage hypothesis. The role of autoimmunity.* Eur J Clin Invest, 2020. **50**(2): p. e13195.

50. Sima, P., L. Vannucci, and V. Vetvicka, *Atherosclerosis as autoimmune disease.* Ann Transl Med, 2018. **6**(7): p. 116.

51. Palinski, W., et al., *Low density lipoprotein undergoes oxidative modification in vivo.* Proc Natl Acad Sci U S A, 1989. **86**(4): p. 1372-6.

52. Libby, P., A.H. Lichtman, and G.K. Hansson, *Immune effector mechanisms implicated in atherosclerosis: from mice to humans.* Immunity, 2013. **38**(6): p. 1092-104.

53. Tsiantoulas, D., et al., *B cells and humoral immunity in atherosclerosis.* Circ Res, 2014. **114**(11): p. 1743-56.

54. Upadhye, A., J.M. Sturek, and C.A. McNamara, *2019 Russell Ross Memorial Lecture in Vascular Biology: B Lymphocyte-Mediated Protective Immunity in Atherosclerosis.* Arterioscler Thromb Vasc Biol, 2020. **40**(2): p. 309-322.

55. Tay, C., et al., *B Cell and CD4 T Cell Interactions Promote Development of Atherosclerosis.* Front Immunol, 2019. **10**: p. 3046.

56. Ait-Oufella, H., et al., *B cell depletion reduces the development of atherosclerosis in mice.* J Exp Med, 2010. **207**(8): p. 1579-87.

57. Bagchi-Chakraborty, J., et al., *B Cell Fcgamma Receptor IIb Modulates Atherosclerosis in Male and Female Mice by Controlling Adaptive Germinal Center and Innate B-1-Cell Responses.* Arterioscler Thromb Vasc Biol, 2019. **39**(7): p. 1379-1389.

58. Perry, H.M., T.P. Bender, and C.A. McNamara, *B cell subsets in atherosclerosis.* Front Immunol, 2012. **3**: p. 373.

59. Tsiantoulas, D., et al., *B Cell-Activating Factor Neutralization Aggravates Atherosclerosis.* Circulation, 2018. **138**(20): p. 2263-2273.

60. Srikakulapu, P. and C.A. McNamara, *B cells and atherosclerosis.* Am J Physiol Heart Circ Physiol, 2017. **312**(5): p. H1060-H1067.

61. Rosenfeld, S.M., et al., *B-1b Cells Secrete Atheroprotective IgM and Attenuate Atherosclerosis.* Circ Res, 2015. **117**(3): p. e28-39.

62. Major, A.S., S. Fazio, and M.F. Linton, *B-lymphocyte deficiency increases atherosclerosis in LDL receptor-null mice.* Arterioscler Thromb Vasc Biol, 2002. **22**(11): p. 1892-8.

63. Kyaw, T., et al., *B1a B lymphocytes are atheroprotective by secreting natural IgM that increases IgM deposits and reduces necrotic cores in atherosclerotic lesions.* Circ Res, 2011. **109**(8): p. 830-40.

64. Sage, A.P., et al., *BAFF receptor deficiency reduces the development of atherosclerosis in mice--brief report.* Arterioscler Thromb Vasc Biol, 2012. **32**(7): p. 1573-6.

65. Kyaw, T., et al., *BAFF receptor mAb treatment ameliorates development and progression of atherosclerosis in hyperlipidemic ApoE(-/-) mice.* PLoS One, 2013. **8**(4): p. e60430.

66. Kyaw, T., et al., *Conventional B2 B cell depletion ameliorates whereas its adoptive transfer aggravates atherosclerosis.* J Immunol, 2010. **185**(7): p. 4410-9.

67. Kyaw, T., et al., *Depletion of B2 but not B1a B cells in BAFF receptor-deficient ApoE mice attenuates atherosclerosis by potently ameliorating arterial inflammation.* PLoS One, 2012. **7**(1): p. e29371.

68. Tay, C., et al., *Follicular B Cells Promote Atherosclerosis via T Cell-Mediated Differentiation Into Plasma Cells and Secreting Pathogenic Immunoglobulin G.* Arterioscler Thromb Vasc Biol, 2018. **38**(5): p. e71-e84.

69. Sage, A.P. and Z. Mallat, *Multiple potential roles for B cells in atherosclerosis.* Ann Med, 2014. **46**(5): p. 297-303.

70. Caligiuri, G., et al., *Protective immunity against atherosclerosis carried by B cells of hypercholesterolemic mice.* J Clin Invest, 2002. **109**(6): p. 745-53.

71. Kyaw, T., et al., *Protective role of natural IgM-producing B1a cells in atherosclerosis.* Trends Cardiovasc Med, 2012. **22**(2): p. 48-53.

72. Perry, H.M. and C.A. McNamara, *Refining the role of B cells in atherosclerosis.* Arterioscler Thromb Vasc Biol, 2012. **32**(7): p. 1548-9.

73. Tsimikas, S., et al., *Relationship of IgG and IgM autoantibodies to oxidized low density lipoprotein with coronary artery disease and cardiovascular events.* J Lipid Res, 2007. **48**(2): p. 425-33.

74. Chang, M.K., et al., *Monoclonal antibodies against oxidized low-density lipoprotein bind to apoptotic cells and inhibit their phagocytosis by elicited macrophages: evidence that oxidation-specific epitopes mediate macrophage recognition.* Proc Natl Acad Sci U S A, 1999. **96**(11): p. 6353-8.

75. Horkko, S., et al., *Monoclonal autoantibodies specific for oxidized phospholipids or oxidized phospholipid-protein adducts inhibit macrophage uptake of oxidized low-density lipoproteins.* J Clin Invest, 1999. **103**(1): p. 117-28.

76. de Faire, U. and J. Frostegard, *Natural antibodies against phosphorylcholine in cardiovascular disease.* Ann N Y Acad Sci, 2009. **1173**: p. 292-300.

77. Shaw, P.X., et al., *Natural antibodies with the T15 idiotype may act in atherosclerosis, apoptotic clearance, and protective immunity.* J Clin Invest, 2000. **105**(12): p. 1731-40.

78. Tsimikas, S., et al., *Oxidation-specific biomarkers, prospective 15-year cardiovascular and stroke outcomes, and net reclassification of cardiovascular events.* J Am Coll Cardiol, 2012. **60**(21): p. 2218-29.

79. Leibundgut, G., J.L. Witztum, and S. Tsimikas, *Oxidation-specific epitopes and immunological responses: Translational biotheranostic implications for atherosclerosis.* Curr Opin Pharmacol, 2013. **13**(2): p. 168-79.

80. Lewis, M.J., et al., *Immunoglobulin M is required for protection against atherosclerosis in low-density lipoprotein receptor-deficient mice.* Circulation, 2009. **120**(5): p. 417-26.

81. Ravandi, A., et al., *Relationship of IgG and IgM autoantibodies and immune complexes to oxidized LDL with markers of oxidation and inflammation and cardiovascular events: results from the EPIC-Norfolk Study.* J Lipid Res, 2011. **52**(10): p. 1829-36.

82. Griffin, D.O., N.E. Holodick, and T.L. Rothstein, *Human B1 cells in umbilical cord and adult peripheral blood express the novel phenotype CD20+ CD27+ CD43+ CD70.* J Exp Med, 2011. **208**(1): p. 67-80.

83. Prasad, A., et al., *Relationship of Autoantibodies to MDA-LDL and ApoB-Immune Complexes to Sex, Ethnicity, Subclinical Atherosclerosis, and Cardiovascular Events.* Arterioscler Thromb Vasc Biol, 2017. **37**(6): p. 1213-1221.

84. Khamis, R.Y., et al., *High Serum Immunoglobulin G and M Levels Predict Freedom From Adverse Cardiovascular Events in Hypertension: A Nested Case-Control Substudy of the Anglo-Scandinavian Cardiac Outcomes Trial.* EBioMedicine, 2016. **9**: p. 372-380.

85. van den Berg, V.J., et al., *IgM anti-malondialdehyde low density lipoprotein antibody levels indicate coronary heart disease and necrotic core characteristics in the Nordic Diltiazem (NORDIL) study and the Integrated Imaging and Biomarker Study 3 (IBIS-3).* EBioMedicine, 2018. **36**: p. 63-72.

86. Jaiswal, S., et al., *Age-related clonal hematopoiesis associated with adverse outcomes.* N Engl J Med, 2014. **371**(26): p. 2488-98.

87. Jaiswal, S., et al., *Clonal Hematopoiesis and Risk of Atherosclerotic Cardiovascular Disease.* N Engl J Med, 2017. **377**(2): p. 111-121.

88. Jaiswal, S. and P. Libby, *Clonal haematopoiesis: connecting ageing and inflammation in cardiovascular disease.* Nat Rev Cardiol, 2020. **17**(3): p. 137-144.

89. Libby, P. and B.L. Ebert, *CHIP (Clonal Hematopoiesis of Indeterminate Potential): Potent and Newly Recognized Contributor to Cardiovascular Risk.* Circulation, 2018. **138**(7): p. 666-668.

90. Fuster, J.J. and K. Walsh, *Somatic Mutations and Clonal Hematopoiesis: Unexpected Potential New Drivers of Age-Related Cardiovascular Disease.* Circ Res, 2018. **122**(3): p. 523-532.

91. Sano, S., Y. Wang, and K. Walsh, *Clonal Hematopoiesis and Its Impact on Cardiovascular Disease.* Circ J, 2018. **83**(1): p. 2-11.

92. Evans, M.A., S. Sano, and K. Walsh, *Cardiovascular Disease, Aging, and Clonal Hematopoiesis.* Annu Rev Pathol, 2020. **15**: p. 419-438.

93. Aviv, A., *Clonal Hematopoiesis Confers Predisposition to Both Cardiovascular Disease and Cancer.* Ann Intern Med, 2019. **170**(5): p. 356.

94. Amoros-Perez, M. and J.J. Fuster, *Clonal hematopoiesis driven by somatic mutations: A new player in atherosclerotic cardiovascular disease.* Atherosclerosis, 2020. **297**: p. 120-126.

95. Kumar, P., et al., *Clonal Hematopoiesis of Indeterminate Potential and Cardiovascular Disease.* Curr Oncol Rep, 2020. **22**(9): p. 87.

96. Haybar, H., et al., *Clonal hematopoiesis: Genes and underlying mechanisms in cardiovascular disease development.* J Cell Physiol, 2019. **234**(6): p. 8396-8401.

97. Calvillo-Arguelles, O., et al., *Connections Between Clonal Hematopoiesis, Cardiovascular Disease, and Cancer: A Review.* JAMA Cardiol, 2019. **4**(4): p. 380-387.

98. Burns, S.S. and R. Kapur, *Putative Mechanisms Underlying Cardiovascular Disease Associated with Clonal Hematopoiesis of Indeterminate Potential.* Stem Cell Reports, 2020. **15**(2): p. 292-306.

99. Paramo Fernandez, J.A., *Atherosclerosis and clonal hematopoyesis: A new risk factor.* Clin Investig Arterioscler, 2018. **30**(3): p. 133-136.

100. Jung, C., M.A. Evans, and K. Walsh, *Genetics of age-related clonal hematopoiesis and atherosclerotic cardiovascular disease.* Curr Opin Cardiol, 2020.

101. Dorsheimer, L., et al., *Association of Mutations Contributing to Clonal Hematopoiesis With Prognosis in Chronic Ischemic Heart Failure.* JAMA Cardiol, 2019. **4**(1): p. 25-33.

102. Cassinat, B., C. Harrison, and J.J. Kiladjian, *Clonal Hematopoiesis and Atherosclerosis.* N Engl J Med, 2017. **377**(14): p. 1400-1.

103. Natarajan, P., S. Jaiswal, and S. Kathiresan, *Clonal Hematopoiesis: Somatic Mutations in Blood Cells and Atherosclerosis.* Circ Genom Precis Med, 2018. **11**(7): p. e001926.

104. Miyazaki-Akita, A., et al., *17beta-estradiol antagonizes the down-regulation of endothelial nitric-oxide synthase and GTP cyclohydrolase I by high glucose: relevance to postmenopausal diabetic cardiovascular disease.* J Pharmacol Exp Ther, 2007. **320**(2): p. 591-8.

105. Rasmussen, K.D. and K. Helin, *Role of TET enzymes in DNA methylation, development, and cancer.* Genes Dev, 2016. **30**(7): p. 733-50.

106. Nakajima, H. and H. Kunimoto, *TET2 as an epigenetic master regulator for normal and malignant hematopoiesis.* Cancer Sci, 2014. **105**(9): p. 1093-9.

107. Pan, F., et al., *The TET2 interactors and their links to hematological malignancies.* IUBMB Life, 2015. **67**(6): p. 438-45.

108. Lio, C.J., et al., *TET enzymes augment activation-induced deaminase (AID) expression via 5-hydroxymethylcytosine modifications at the Aicda superenhancer.* Sci Immunol, 2019. **4**(34).

109. Lio, C.-W., et al., *Tet2 and Tet3 cooperate with B-lineage transcription factors to regulate DNA modification and chromatin accessibility.* eLife, 2016. **5**: p. e18290.

110. Fuster, J.J., et al., *Clonal hematopoiesis associated with TET2 deficiency accelerates atherosclerosis development in mice.* Science, 2017. **355**(6327): p. 842-847.

111. Sano, S., et al., *Tet2-Mediated Clonal Hematopoiesis Accelerates Heart Failure Through a Mechanism Involving the IL-1beta/NLRP3 Inflammasome.* J Am Coll Cardiol, 2018. **71**(8): p. 875-886.

112. Ko, M., et al., *Ten-Eleven-Translocation 2 (TET2) negatively regulates homeostasis and differentiation of hematopoietic stem cells in mice.* Proc Natl Acad Sci U S A, 2011. **108**(35): p. 14566-71.

113. Kunimoto, H., et al., *Tet2 disruption leads to enhanced self-renewal and altered differentiation of fetal liver hematopoietic stem cells.* Sci Rep, 2012. **2**: p. 273.

114. Moran-Crusio, K., et al., *Tet2 loss leads to increased hematopoietic stem cell self-renewal and myeloid transformation.* Cancer Cell, 2011. **20**(1): p. 11-24.

115. Moreno, C.R., et al., *Morphomolecular Characterization of Serum Nanovesicles From Microbiomes Differentiates Stable and Infarcted Atherosclerotic Patients.* Front Cardiovasc Med, 2021. **8**: p. 694851.

116. Cull, A.H., et al., *Tet2 restrains inflammatory gene expression in macrophages.* Exp Hematol, 2017. **55**: p. 56-70 e13.

117. Zhang, W., et al., *TET2 Expression in Bone Marrow Mononuclear Cells of Patients with Myelodysplastic Syndromes and Its Clinical Significances.* Cancer Biol Med, 2012. **9**(1): p. 34-7.

118. Zhang, W., et al., *Down-regulation of TET2 in CD3(+) and CD34(+) cells of myelodysplastic syndromes and enhances CD34(+) cells proliferation.* Int J Clin Exp Pathol, 2015. **8**(9): p. 10840-6.

119. Li, Z., et al., *Deletion of Tet2 in mice leads to dysregulated hematopoietic stem cells and subsequent development of myeloid malignancies.* Blood, 2011. **118**(17): p. 4509-18.

120. Rasmussen, K.D., et al., *TET2 binding to enhancers facilitates transcription factor recruitment in hematopoietic cells.* Genome Res, 2019. **29**(4): p. 564-575.

121. Zhao, H., et al., *The synergy of Vitamin C with decitabine activates TET2 in leukemic cells and significantly improves overall survival in elderly patients with acute myeloid leukemia.* Leuk Res, 2018. **66**: p. 1-7.

122. Rasmussen, K.D., et al., *Loss of TET2 in hematopoietic cells leads to DNA hypermethylation of active enhancers and induction of leukemogenesis.* Genes Dev, 2015. **29**(9): p. 910-22.

123. Qu, K., et al., *Vitamin C down-regulate apo(a) expression via Tet2-dependent DNA demethylation in HepG2 cells.* Int J Biol Macromol, 2017. **98**: p. 637-645.

124. Tanaka, S., et al., *Tet2 and Tet3 in B cells are required to repress CD86 and prevent autoimmunity.* Nat Immunol, 2020. **21**(8): p. 950-961.

125. Wu, H., et al., *High salt promotes autoimmunity by TET2-induced DNA demethylation and driving the differentiation of Tfh cells.* Sci Rep, 2016. **6**: p. 28065.

126. Zhao, Z., et al., *The catalytic activity of TET2 is essential for its myeloid malignancy-suppressive function in hematopoietic stem/progenitor cells.* Leukemia, 2016. **30**(8): p. 1784-1788.

127. Wu, H., et al., *The IL-21-TET2-AIM2-c-MAF pathway drives the T follicular helper cell response in lupus-like disease.* Clin Transl Med, 2022. **12**(3): p. e781.

128. Wang, Y., et al., *Tet2-mediated clonal hematopoiesis in nonconditioned mice accelerates age-associated cardiac dysfunction.* JCI Insight, 2020. **5**(6).

129. Zhang, Q., et al., *Tet2 is required to resolve inflammation by recruiting Hdac2 to specifically repress IL-6.* Nature, 2015. **525**(7569): p. 389-393.

130. Garcia-Gomez, A., et al., *TET2- and TDG-mediated changes are required for the acquisition of distinct histone modifications in divergent terminal differentiation of myeloid cells.* Nucleic Acids Res, 2017. **45**(17): p. 10002-10017.

131. Li, R., et al., *TET2 Loss Dysregulates the Behavior of Bone Marrow Mesenchymal Stromal Cells and Accelerates Tet2(-/-)-Driven Myeloid Malignancy Progression.* Stem Cell Reports, 2018. **10**(1): p. 166-179.

132. Kallin, E.M., et al., *Tet2 facilitates the derepression of myeloid target genes during CEBPalpha-induced transdifferentiation of pre-B cells.* Mol Cell, 2012. **48**(2): p. 266-76.

133. Pan, W., et al., *The DNA Methylcytosine Dioxygenase Tet2 Sustains Immunosuppressive Function of Tumor-Infiltrating Myeloid Cells to Promote Melanoma Progression.* Immunity, 2017. **47**(2): p. 284-297 e5.

134. Tsagaratou, A., et al., *Dissecting the dynamic changes of 5-hydroxymethylcytosine in T-cell development and differentiation.* Proc Natl Acad Sci U S A, 2014. **111**(32): p. E3306-15.

135. Ichiyama, K., et al., *The methylcytosine dioxygenase Tet2 promotes DNA demethylation and activation of cytokine gene expression in T cells.* Immunity, 2015. **42**(4): p. 613-26.

136. Carty, S.A., et al., *The Loss of TET2 Promotes CD8(+) T Cell Memory Differentiation.* J Immunol, 2018. **200**(1): p. 82-91.

137. Nakatsukasa, H., et al., *Loss of TET proteins in regulatory T cells promotes abnormal proliferation, Foxp3 destabilization and IL-17 expression.* Int Immunol, 2019. **31**(5): p. 335-347.

138. Orlanski, S., et al., *Tissue-specific DNA demethylation is required for proper B-cell differentiation and function.* Proc Natl Acad Sci U S A, 2016. **113**(18): p. 5018-23.

139. Schoeler, K., et al., *TET enzymes control antibody production and shape the mutational landscape in germinal centre B cells.* FEBS J, 2019. **286**(18): p. 3566-3581.

140. Dominguez, P.M., et al., *TET2 Deficiency Causes Germinal Center Hyperplasia, Impairs Plasma Cell Differentiation, and Promotes B-cell Lymphomagenesis.* Cancer Discov, 2018. **8**(12): p. 1632-1653.

141. Rosikiewicz, W., et al., *TET2 deficiency reprograms the germinal center B cell epigenome and silences genes linked to lymphomagenesis.* Sci Adv, 2020. **6**(25): p. eaay5872.

142. Arioka, Y., et al., *Activation-induced cytidine deaminase alters the subcellular localization of Tet family proteins.* PLoS One, 2012. **7**(9): p. e45031.

143. Jiao, J., et al., *AID and TET2 co-operation modulates FANCA expression by active demethylation in diffuse large B cell lymphoma.* Clin Exp Immunol, 2019. **195**(2): p. 190-201.

144. Quivoron, C., et al., *TET2 inactivation results in pleiotropic hematopoietic abnormalities in mouse and is a recurrent event during human lymphomagenesis.* Cancer Cell, 2011. **20**(1): p. 25-38.

145. Chen, S., *Ultrafast one-pass FASTQ data preprocessing, quality control, and deduplication using fastp.* iMeta, 2023. **2**(2): p. e107.

146. Dobin, A., et al., *STAR: ultrafast universal RNA-seq aligner.* Bioinformatics, 2013. **29**(1): p. 15-21.

147. Liao, Y., G.K. Smyth, and W. Shi, *featureCounts: an efficient general purpose program for assigning sequence reads to genomic features.* Bioinformatics, 2014. **30**(7): p. 923-30.

148. Love, M.I., W. Huber, and S. Anders, *Moderated estimation of fold change and dispersion for RNA-seq data with DESeq2.* Genome Biol, 2014. **15**(12): p. 550.

149. Wu, T., et al., *clusterProfiler 4.0: A universal enrichment tool for interpreting omics data.* Innovation (Camb), 2021. **2**(3): p. 100141.

150. Ashburner, M., et al., *Gene ontology: tool for the unification of biology. The Gene Ontology Consortium.* Nat Genet, 2000. **25**(1): p. 25-9.

151. Peng, K., et al., *Rigorous benchmarking of T-cell receptor repertoire profiling methods for cancer RNA sequencing.* Briefings in Bioinformatics, 2023. **24**(4).

152. Gu, Z., et al., *circlize Implements and enhances circular visualization in R.* Bioinformatics, 2014. **30**(19): p. 2811-2.

153. Holodick, N.E., et al., *Age-Related Decline in Natural IgM Function: Diversification and Selection of the B-1a Cell Pool with Age.* J Immunol, 2016. **196**(10): p. 4348-57.

154. Upadhye, A., et al., *Diversification and CXCR4-Dependent Establishment of the Bone Marrow B-1a Cell Pool Governs Atheroprotective IgM Production Linked to Human Coronary Atherosclerosis.* Circ Res, 2019. **125**(10): p. e55-e70.

155. Srikakulapu, P., et al., *B-1b Cells Have Unique Functional Traits Compared to B-1a Cells at Homeostasis and in Aged Hyperlipidemic Mice With Atherosclerosis.* Front Immunol, 2022. **13**: p. 909475.

156. Prohaska, T.A., et al., *Massively Parallel Sequencing of Peritoneal and Splenic B Cell Repertoires Highlights Unique Properties of B-1 Cell Antibodies.* J Immunol, 2018. **200**(5): p. 1702-1717.

157. Chen, L., et al., *LncRNA MAGI2-AS3 inhibits the self-renewal of leukaemic stem cells by promoting TET2-dependent DNA demethylation of the LRIG1 promoter in acute myeloid leukaemia.* RNA Biol, 2020. **17**(6): p. 784-793.

158. Zhang, W., et al., *[TET2 and DLK1 gene expression and their clinical significance in bone marrow CD(3)(+) T cells of patients with*

myelodysplastic syndrome]. Zhonghua Nei Ke Za Zhi, 2012. **51**(7): p. 543-6.

159. Sun, J., et al., *SIRT1 Activation Disrupts Maintenance of Myelodysplastic Syndrome Stem and Progenitor Cells by Restoring TET2 Function.* Cell Stem Cell, 2018. **23**(3): p. 355-369 e9.

160. Kubuki, Y., et al., *TET2 mutation in diffuse large B-cell lymphoma.* J Clin Exp Hematop, 2017. **56**(3): p. 145-149.

161. Zhao, Z., et al., *Combined Loss of Tet1 and Tet2 Promotes B Cell, but Not Myeloid Malignancies, in Mice.* Cell Rep, 2015. **13**(8): p. 1692-704.

162. Mouly, E., et al., *B-cell tumor development in Tet2-deficient mice.* Blood Adv, 2018. **2**(6): p. 703-714.

163. Song, L., et al., *TRUST4: immune repertoire reconstruction from bulk and single-cell RNA-seq data.* Nat Methods, 2021. **18**(6): p. 627-630.

164. Giudicelli, V., D. Chaume, and M.P. Lefranc, *IMGT/GENE-DB: a comprehensive database for human and mouse immunoglobulin and T cell receptor genes.* Nucleic Acids Res, 2005. **33**(Database issue): p. D256-61.

165. Xu, J.L. and M.M. Davis, *Diversity in the CDR3 Region of VH Is Sufficient for Most Antibody Specificities.* Immunity, 2000. **13**(1): p. 37-45.

166. Tsuji, N., T.L. Rothstein, and N.E. Holodick, *Antigen Receptor Specificity and Cell Location Influence the Diversification and Selection of the B-1a Cell Pool with Age.* J Immunol, 2020. **205**(3): p. 741-759.

167. Kretschmer, K., et al., *The selection of marginal zone B cells differs from that of B-1a cells.* J Immunol, 2003. **171**(12): p. 6495-501.

168. Hardy, R.R., C.J. Wei, and K. Hayakawa, *Selection during development of VH11+ B cells: a model for natural autoantibody-producing CD5+ B cells.* Immunol Rev, 2004. **197**: p. 60-74.

169. Berland, R. and H.H. Wortis, *Origins and functions of B-1 cells with notes on the role of CD5.* Annu Rev Immunol, 2002. **20**: p. 253-300.

170. Yoshimoto, M., *The ontogeny of murine B-1a cells.* Int J Hematol, 2020. **111**(5): p. 622-627.

171. Stall, A.M., et al., *Characteristics and development of the murine B-1b (Ly-1 B sister) cell population.* Ann N Y Acad Sci, 1992. **651**: p. 33-43.

172. del Barrio, L., et al., *Production of anti-LPS IgM by B1a B cells depends on IL-1β and is protective against lung infection with Francisella tularensis LVS.* PLoS Pathog, 2015. **11**(3): p. e1004706.

173. Aziz, M., M. Brenner, and P. Wang, *Therapeutic Potential of B-1a Cells in COVID-19.* Shock, 2020. **54**(5): p. 586-594.

174. Askenase, P.W., et al., *A subset of AID-dependent B-1a cells initiates hypersensitivity and pneumococcal pneumonia resistance.* Ann N Y Acad Sci, 2015. **1362**: p. 200-14.

175. Viau, M., et al., *Staphylococcal protein a deletes B-1a and marginal zone B lymphocytes expressing human immunoglobulins: an immune evasion mechanism.* J Immunol, 2005. **175**(11): p. 7719-27.

176. Aziz, M., et al., *B-1a cells protect mice from sepsis-induced acute lung injury.* Mol Med, 2018. **24**(1): p. 26.

177. Gruber, S., et al., *Sialic Acid-Binding Immunoglobulin-like Lectin G Promotes Atherosclerosis and Liver Inflammation by Suppressing the Protective Functions of B-1 Cells.* Cell Rep, 2016. **14**(10): p. 2348-61.

178. Papac-Milicevic, N., C.J. Busch, and C.J. Binder, *Malondialdehyde Epitopes as Targets of Immunity and the Implications for Atherosclerosis.* Adv Immunol, 2016. **131**: p. 1-59.

179. Karvonen, J., et al., *Immunoglobulin M type of autoantibodies to oxidized low-density lipoprotein has an inverse relation to carotid artery atherosclerosis.* Circulation, 2003. **108**(17): p. 2107-12.

180. Palinski, W., E. Miller, and J.L. Witztum, *Immunization of low density lipoprotein (LDL) receptor-deficient rabbits with homologous malondialdehyde-modified LDL reduces atherogenesis.* Proc Natl Acad Sci U S A, 1995. **92**(3): p. 821-5.

181. George, J., et al., *Hyperimmunization of apo-E-deficient mice with homologous malondialdehyde low-density lipoprotein suppresses early atherogenesis.* Atherosclerosis, 1998. **138**(1): p. 147-52.

182. Shaw, P.X., et al., *Human-derived anti-oxidized LDL autoantibody blocks uptake of oxidized LDL by macrophages and localizes to atherosclerotic lesions in vivo.* Arterioscler Thromb Vasc Biol, 2001. **21**(8): p. 1333-9.

183. Harmon, D.B., et al., *Protective Role for B-1b B Cells and IgM in Obesity-Associated Inflammation, Glucose Intolerance, and Insulin Resistance.* Arterioscler Thromb Vasc Biol, 2016. **36**(4): p. 682-91.

184. Coltro, G., et al., *Clinical, molecular, and prognostic correlates of number, type, and functional localization of TET2 mutations in chronic myelomonocytic leukemia (CMML)-a study of 1084 patients.* Leukemia, 2020. **34**(5): p. 1407-1421.

185. Stremenova Spegarova, J., et al., *Germline TET2 loss of function causes childhood immunodeficiency and lymphoma.* Blood, 2020. **136**(9): p. 1055-1066.

186. Bussaglia, E., et al., *TET2 missense variants in human neoplasia. A proposal of structural and functional classification.* Molecular Genetics & Genomic Medicine, 2019. **7**(7): p. e00772.

187. Grasset, E.K., et al., *Sterile inflammation in the spleen during atherosclerosis provides oxidation-specific epitopes that induce a protective B-cell response.* Proc Natl Acad Sci U S A, 2015. **112**(16): p. E2030-8.

188. Miller, Y.I., et al., *Oxidation-Specific Epitopes Are Danger-Associated Molecular Patterns Recognized by Pattern Recognition Receptors of Innate Immunity.* Circulation Research, 2011. **108**(2): p. 235-248.

189. Binder, C.J., N. Papac-Milicevic, and J.L. Witztum, *Innate sensing of oxidation-specific epitopes in health and disease.* Nat Rev Immunol, 2016. **16**(8): p. 485-97.

190. Steinberg, D. and J.L. Witztum, *Oxidized low-density lipoprotein and atherosclerosis.* Arterioscler Thromb Vasc Biol, 2010. **30**(12): p. 2311-6.

191. Witztum, J.L. and A.H. Lichtman, *The influence of innate and adaptive immune responses on atherosclerosis.* Annu Rev Pathol, 2014. **9**: p. 73-102.

192. Que, X., et al., *Oxidized phospholipids are proinflammatory and proatherogenic in hypercholesterolaemic mice.* Nature, 2018. **558**(7709): p. 301-306.

193. Kretschmer, K., et al., *Maintenance of peritoneal B-1a lymphocytes in the absence of the spleen.* J Immunol, 2004. **173**(1): p. 197-204.

194. Duber, S., et al., *Induction of B-cell development in adult mice reveals the ability of bone marrow to produce B-1a cells.* Blood, 2009. **114**(24): p. 4960-7.

195. Ghosn, E.E. and Y. Yang, *Hematopoietic stem cell-independent B-1a lineage.* Ann N Y Acad Sci, 2015. **1362**: p. 23-38.

196. Xu, Z., et al., *Mechanisms of peritoneal B-1a cells accumulation induced by murine lupus susceptibility locus Sle2.* J Immunol, 2004. **173**(10): p. 6050-8.

197. Pan, F., et al., *Tet2 loss leads to hypermutagenicity in haematopoietic stem/progenitor cells.* Nat Commun, 2017. **8**: p. 15102.

198. Zhang, X., et al., *DNMT3A and TET2 compete and cooperate to repress lineage-specific transcription factors in hematopoietic stem cells.* Nat Genet, 2016. **48**(9): p. 1014-23.

199. Casali, P. and E.W. Schettino, *Structure and function of natural antibodies.* Curr Top Microbiol Immunol, 1996. **210**: p. 167-79.

200. Hayakawa, K., et al., *Positive selection of natural autoreactive B cells.* Science, 1999. **285**(5424): p. 113-6.

201. Hayakawa, K., et al., *Positive selection of anti-thy-1 autoreactive B-1 cells and natural serum autoantibody production independent from bone marrow B cell development.* J Exp Med, 2003. **197**(1): p. 87-99.

202. Hardy, R.R. and K. Hayakawa, *Positive and negative selection of natural autoreactive B cells.* Adv Exp Med Biol, 2012. **750**: p. 227-38.

203. Bolotin, D.A., et al., *MiXCR: software for comprehensive adaptive immunity profiling.* Nature Methods, 2015. **12**(5): p. 380-381.

204. Upadhyay, A.A., et al., *BALDR: a computational pipeline for paired heavy and light chain immunoglobulin reconstruction in single-cell RNA-seq data.* Genome Medicine, 2018. **10**(1): p. 20.

205. Liu, K.J., M.A. Zelazowska, and K.M. McBride, *The Longitudinal Analysis of Convergent Antibody VDJ Regions in SARS-CoV-2-Positive Patients Using RNA-Seq.* Viruses, 2023. **15**(6): p. 1253.

206. Song, L., et al., *Comprehensive Characterizations of Immune Receptor Repertoire in Tumors and Cancer Immunotherapy Studies.* Cancer Immunol Res, 2022. **10**(7): p. 788-799.

207. Zhang, Y. and T.Y. Lee, *Revealing the Immune Heterogeneity between Systemic Lupus Erythematosus and Rheumatoid Arthritis Based on Multi-Omics Data Analysis.* Int J Mol Sci, 2022. **23**(9).

208. Kretschmer, K., H. Engel, and S. Weiss, *Strong antigenic selection shaping the immunoglobulin heavy chain repertoire of B-1a lymphocytes in lambda 2(315) transgenic mice.* Eur J Immunol, 2002. **32**(8): p. 2317-27.

209. Andrews, S.F., et al., *Global analysis of B cell selection using an immunoglobulin light chain-mediated model of autoreactivity.* J Exp Med, 2013. **210**(1): p. 125-42.

210. Yang, Y., et al., *Distinct mechanisms define murine B cell lineage immunoglobulin heavy chain (IgH) repertoires.* Elife, 2015. **4**: p. e09083.

211. Tornberg, U.C. and D. Holmberg, *B-1a, B-1b and B-2 B cells display unique VHDJH repertoires formed at different stages of ontogeny and under different selection pressures.* EMBO J, 1995. **14**(8): p. 1680-9.

212. Aoki-Ota, M., et al., *Skewed primary Igkappa repertoire and V-J joining in C57BL/6 mice: implications for recombination accessibility and receptor editing.* J Immunol, 2012. **188**(5): p. 2305-15.

213. Jaffe, D.B., et al., *Functional antibodies exhibit light chain coherence.* Nature, 2022. **611**(7935): p. 352-357.

214. Nguyen, T.T. and N. Baumgarth, *Natural IgM and the Development of B Cell-Mediated Autoimmune Diseases.* Crit Rev Immunol, 2016. **36**(2): p. 163-177.

215. Wong, J.B., et al., *B-1a cells acquire their unique characteristics by bypassing the pre-BCR selection stage.* Nat Commun, 2019. **10**(1): p. 4768.

216. Alayed, K., et al., *TET2 mutations, myelodysplastic features, and a distinct immunoprofile characterize blastic plasmacytoid dendritic cell neoplasm in the bone marrow.* Am J Hematol, 2013. **88**(12): p. 1055-61.

217. Ito, K., et al., *Non-catalytic Roles of Tet2 Are Essential to Regulate Hematopoietic Stem and Progenitor Cell Homeostasis.* Cell Rep, 2019. **28**(10): p. 2480-2490 e4.

218. Wille, C.K., et al., *Restricted TET2 Expression in Germinal Center Type B Cells Promotes Stringent Epstein-Barr Virus Latency.* J Virol, 2017. **91**(5).

219. Kitabatake, M., et al., *Transgenic overexpression of G5PR that is normally augmented in centrocytes impairs the enrichment of high-affinity antigen-specific B cells, increases peritoneal B-1a cells, and induces autoimmunity in aged female mice.* J Immunol, 2012. **189**(3): p. 1193-201.

220. Pao, L.I., et al., *B cell-specific deletion of protein-tyrosine phosphatase Shp1 promotes B-1a cell development and causes systemic autoimmunity.* Immunity, 2007. **27**(1): p. 35-48.

221. Iciek, L.A., et al., *B-1 cells in systemic autoimmune responses: IgM+, Fc epsilon Rdull B cells are lost during chronic graft-versus-host disease but not in murine AIDS or collagen-induced arthritis.* Immunol Invest, 1994. **23**(4-5): p. 293-311.

222. Palinski, W., et al., *Cloning of monoclonal autoantibodies to epitopes of oxidized lipoproteins from apolipoprotein E-deficient mice. Demonstration of epitopes of oxidized low density lipoprotein in human plasma.* J Clin Invest, 1996. **98**(3): p. 800-14.

223. Kobayashi, K., et al., *The role of innate and adaptive immunity to oxidized low-density lipoprotein in the development of atherosclerosis.* Ann N Y Acad Sci, 2005. **1051**: p. 442-54.

224. Hosseini, H., et al., *Phosphatidylserine liposomes mimic apoptotic cells to attenuate atherosclerosis by expanding polyreactive IgM producing B1a lymphocytes.* Cardiovasc Res, 2015. **106**(3): p. 443-52.

225. Srikakulapu, P., et al., *Perivascular Adipose Tissue Harbors Atheroprotective IgM-Producing B Cells.* Front Physiol, 2017. **8**: p. 719.

226. Deroissart, J. and C.J. Binder, *Mapping the functions of IgM antibodies in atherosclerotic cardiovascular disease.* Nat Rev Cardiol, 2023. **20**(7): p. 433-434.

227. Taleb, A., et al., *High immunoglobulin-M levels to oxidation-specific epitopes are associated with lower risk of acute myocardial infarction.* J Lipid Res, 2023. **64**(6): p. 100391.

228. Tsimikas, S., et al., *Human oxidation-specific antibodies reduce foam cell formation and atherosclerosis progression.* J Am Coll Cardiol, 2011. **58**(16): p. 1715-27.

229. Liu, Y., et al., *TET2: A Novel Epigenetic Regulator and Potential Intervention Target for Atherosclerosis.* DNA Cell Biol, 2018. **37**(6): p. 517-523.

230. Zadeh, F.J., et al., *The role of molecular mechanism of Ten-Eleven Translocation2 (TET2) family proteins in pathogenesis of cardiovascular diseases (CVDs).* Mol Biol Rep, 2020. **47**(7): p. 5503-5509.

231. Ordonez, C., et al., *Both B-1a and B-1b cells exposed to Mycobacterium tuberculosis lipids differentiate into IgM antibody-secreting cells.* Immunology, 2018.

232. Veneri, D., et al., *Changes of human B and B-1a peripheral blood lymphocytes with age.* Hematology, 2007. **12**(4): p. 337-41.

233. Anania, C., et al., *Increased prevalence of vulnerable atherosclerotic plaques and low levels of natural IgM antibodies against phosphorylcholine in patients with systemic lupus erythematosus.* Arthritis Res Ther, 2010. **12**(6): p. R214.

234. Sung, W.Y., et al., *Methylation of TET2 Promoter Is Associated with Global Hypomethylation and Hypohydroxymethylation in Peripheral Blood Mononuclear Cells of Systemic Lupus Erythematosus Patients.* Diagnostics (Basel), 2022. **12**(12).

235. Zhao, M., et al., *Increased 5-hydroxymethylcytosine in CD4(+) T cells in systemic lupus erythematosus.* J Autoimmun, 2016. **69**: p. 64-73.

236. Cheng, H.H., et al., *AHR/TET2/NT5E axis downregulation is associated with the risk of systemic lupus erythematosus and its progression.* Immunology, 2023. **168**(4): p. 654-670.

237. Cai, Z., et al., *Inhibition of Inflammatory Signaling in Tet2 Mutant Preleukemic Cells Mitigates Stress-Induced Abnormalities and Clonal Hematopoiesis.* Cell Stem Cell, 2018. **23**(6): p. 833-849 e5.

238. Steensma, D.P., et al., *Clonal hematopoiesis of indeterminate potential and its distinction from myelodysplastic syndromes.* Blood, 2015. **126**(1): p. 9-16.

239. Swierczek, S. and J.T. Prchal, *Clonal hematopoiesis in hematological disorders: Three different scenarios.* Exp Hematol, 2020. **83**: p. 57-65.

240. Scharer, C.D., et al., *Antibody-secreting cell destiny emerges during the initial stages of B-cell activation.* Nature Communications, 2020. **11**(1): p. 3989.

241. Venturi, G.M., et al., *Leukocyte migration is regulated by L-selectin endoproteolytic release.* Immunity, 2003. **19**(5): p. 713-24.

242. Morrison, V.L., et al., *TLR-mediated loss of CD62L focuses B cell traffic to the spleen during Salmonella typhimurium infection.* J Immunol, 2010. **185**(5): p. 2737-46.

243. Elgueta, R., et al., *CCR6-dependent positioning of memory B cells is essential for their ability to mount a recall response to antigen.* J Immunol, 2015. **194**(2): p. 505-13.

244. Förster, R., et al., *CCR7 Coordinates the Primary Immune Response by Establishing Functional Microenvironments in Secondary Lymphoid Organs.* Cell, 1999. **99**(1): p. 23-33.

245. Förster, R., et al., *A Putative Chemokine Receptor, BLR1, Directs B Cell Migration to Defined Lymphoid Organs and Specific Anatomic Compartments of the Spleen.* Cell, 1996. **87**(6): p. 1037-1047.

246. Kothari, H., et al., *Association of D-dimer with Plaque Characteristics and Plasma Biomarkers of Oxidation-Specific Epitopes in Stable Subjects with Coronary Artery Disease.* J Cardiovasc Transl Res, 2018. **11**(3): p. 221-229.

247. Binder, C.J., et al., *Pneumococcal vaccination decreases atherosclerotic lesion formation: molecular mimicry between Streptococcus pneumoniae and oxidized LDL.* Nat Med, 2003. **9**(6): p. 736-43.

Appendix 1: Loss of TET2 reduces CCR6 RNA expression

Rationale

One of the differentially expressed genes (Figure 8C) , *Sell*, also known as CD62L, is known for its role in cell adhesion and mediating migration of leukocytes to secondary lymphoid organs and sites of infection, and its expression can also influence B cell fate [240-242]. Loss of CD62L in B cells allows for antibody-secreting cells to remain in circulation until they rehome in the bone marrow [240]. From our RNASeq data set, CD62L was downregulated in B-1a cells from TET2-KO mice compared to WT (Figure 8C). This was confirmed with flow cytometry on B-1 cells from the peritoneal cavity (Figure 8D). During *Salmonella* infection, loss of CD62L prioritizes B cell trafficking to the spleen [242]. Perhaps a similar mechanism is in play with loss of TET2, as there is elevated B-1b cell number and frequency in the spleen of TET2-KO mice compared to WT. Another differentially expressed gene, *Ccr6*, was downregulated in B-1a cells from TET2-KO mice compared to WT. CCR6 expression enables B cells to migrate to specific sites where its ligand CCL20 is expressed, such as inflamed tissues or sites of infection. If there is decreased cell-surface expression of CCR6, B cell trafficking could be impaired. To determine if the mechanism of elevated cell number in the peritoneal cavity could be due to inhibited cell migration, we assessed additional surface expression of chemokines involved in leukocyte migration, including CCR6 which had reduced RNA expression. We also analyzed *Ccr6* DNA methylation to see if hypermethylation could contribute to the observed reduction in RNA expression.

Methods

Mice

All animal protocols were approved by the Animal Care and Use Committee at the University of Virginia. TET2-KO mice [112] were provided by Dr. Kenneth Walsh (University of Virginia). The model was generated by Ko *et al.* and targeted the endogenous *TET2* locus to create a conditional allele that enabled the deletion of exons 8, 9, and 10, the catalytic region of TET2 [112]. Mice were maintained on a 12-h light/dark schedule in a specific pathogen-free animal facility and given food (standard chow diet, Tekland 7012) and water *ad libitum*. The number of mice included in each study is indicated in the figures or the associated legends.

Sample Preparations for Flow Cytometry

Bone marrow, spleen, and peritoneal cavity cells were processed for flow cytometry as previously described [61]. Briefly, following sacrifice by CO_2 overdose, peritoneal cells were harvested by flushing the peritoneal cavity with 10 mL FACS buffer (PBS containing 1% BSA, 0.05% NaN_3). The spleen and one femur and tibia were removed. Spleens and flushed bone marrow were filtered through a 70 μm cell strainer. Red blood cells were lysed from single-cell suspensions of bone marrow and spleen using a lysis buffer containing 155 mM NH_4Cl, 10 mM $KHCO_3$, and 0.1 mM EDTA. Cell surface Fc receptors were blocked using anti-CD16/32 (clone:93, 4 eBioscience), then cells were stained with fluorescently conjugated antibodies against cell surface markers. Cells were stained with fixable Live/Dead Fixable Blue (Fisher) for dead cell

discrimination, then fixed in 2% PFA in PBS. Clone and fluorophore information for the flow cytometry antibodies used in murine experiments to immunophenotype B cell subsets and chemokine expression can be found in Table 3.

All flow cytometry was conducted at the University of Virginia Flow Cytometry Core Facility. Immunophenotyping was performed on an Aurora Borealis 5-laser (Cytek) cytometer. Data analysis and flow plots were generated using OMIQ software (Dotmatics). Representative flow plots were chosen based on the samples whose population frequencies were closest to the mean for that group. Gates on flow plots were set using fluorescence minus one (FMO) controls.

Table 3. Murine chemokine immunophenotyping panel used for flow cytometry of the peritoneal cavity, bone marrow, and spleen.

Marker	**Fluorophore**	**Clone**	**Vendor**
CXCR3	BUV395	CXCR3-173	BD
CD45	BUV496	I3/2.3	BD
CXCR5	BUV615	2G8	BD
CD23	BUV737	B3B4	BD
CD44	BUV805	IM7	BD
CCR6	BV421	29-2L17	BioLegend
IgD	efluor450	11-26c	eBioscience
Ly6C	BV480	RB6-8C5	BD
CD8	BV510	53-6.7	BioLegend
CD62L	BV570	MEL-14	BioLegend
CD5	BV605	53-7.3	BD
CD127	BV650	A7R34	BioLegend
CXCR4	BV711	2B11/CXCR4	BD
CD138	BV750	281-2	BD
CCR7	BV785	4B12	BD
CD25	BB515	PC61	BD
B220	Spark Blue 550	RA3-6B2	BioLegend
CD4	PerCP	RM4-5	BD
CD11b	PerCP-Cy5.5	M1/70	BD
CD37	PE	Duno85	BioLegend
IgM	PE-CF594	R6-60.2	BD
F4-80	PE-Cy7	BM8	eBioscience
CD21	APC	7G6	BD
CD11c	AF647	N418	BioLegend
CD24	R718	30-F1	BD
CD19	APC-efl780	1D3	eBioscience
NK1.1	APC-F810	S17016D	BioLegend
Live/Dead Fixable Blue			Fisher

DNA Methylation Assay

Peritoneal B-1a, B-1b, and B-2 cells obtained from *TET2*-KO and *TET2*-WT C57BL/6 mice were sort-purified directly into RLT Plus Buffer (Qiagen). RNA and DNA were extracted using the Qiagen AllPrep kit. The purified DNA was subjected to bisulfite conversion and the samples were run on Illumina mouse methylation bead chip arrays.

Results

CCR6 RNA expression is reduced in peritoneal B-1 cells from TET2-KO but not WT mice

RNAseq analysis of peritoneal B-1a, B-1b, and B-2 cells from TET2-KO and WT mice revealed reduced chemokine receptor CCR6 expression in B-1a (-4.879-fold change, 1.803E-08 padj.) and B-1b cells (-2.170-fold change, 0.3477 padj.) from the TET2-KO mice compared to WT (data not shown). Further, methylation analysis showed significant hypermethylation of CCR6 in B-1a and B-1b cells from TET2-KO mice compared to WT (Figure 22).

TET2 deficiency in B-1 cells results in subset- and niche-specific changes to chemokine receptor expression compared to WT controls

In a pilot experiment with a limited sample size, we observed reduced surface expression of CCR7 (CC motif chemokine receptor 7) in peritoneal B-1b cells from

TET2-KO mice (p-value = 0.0286), and reduced surface expression of CXCR5 (CXC motif chemokine receptor 5 in B-1a (p-value = 0.0286) and B-1b cells (p-value = 0.0286) from the peritoneal cavity of TET2-KO mice compared to WT (Figure 23). Interestingly, in both the splenic and BM B-1b cells from TET2-KO mice, there was a trending decrease in CXCR5 expression (p-value = 0.0571). CCR7 and CXCR5 are chemokines involved in directing B cells to the spleen and other secondary lymphoid organs, and to the BM [243]. Reduced CCR7 and CXCR5 expression should result in impaired trafficking to the spleen [244, 245]. Yet, we saw elevated B-1b cell number and frequency from TET2-KO mice compared to WT in the spleen (Figure 4). Additional studies looking into proliferation and cell survival are needed to clarify the mechanism responsible for the elevated cell numbers in these specific B-1 niches.

Conclusions

We determined that loss of TET2 increases hypermethylation of CCR6 and suppresses CCR6 RNA expression in B-1 cells. Changes in chemokine expression may result in impaired or altered lymphocyte trafficking across the three niches where B-1 cells are primarily located. Aberrant B-1 cell trafficking could lead to the accumulation of peritoneal B-1 cell subtypes. It must be noted that this study only had an n of 4 mice, and bears repeating with a larger study size which can be determined with power analysis using the data generated from this experiment. Further investigation using *in vitro* migration assays and adoptive transfer to measure migration of peritoneal B-1 cells from

TET2 mice is needed before causal connections can be reported to explain the increased peritoneal B-1 cell number in TET2-KO mice.

Figure 22. Differential methylation in B-1a, B-1b, and B-2 cells from TET-KO mice compared to WT controls. (**A**) Gene annotated CpGs displayed methylation differences in the B-1 cell subsets from TET2-KO and WT mice. (**B**) B-1a cells from the peritoneal cavity of TET2-KO mice exhibited increased DNA methylation at the CCR6 gene. (**C**) Integrative analysis identified CCR6 as a gene that contributes to chemotaxis inhibition due to DNA methylation. Significance was determined using two-tailed Mann-Whitney U-tests.

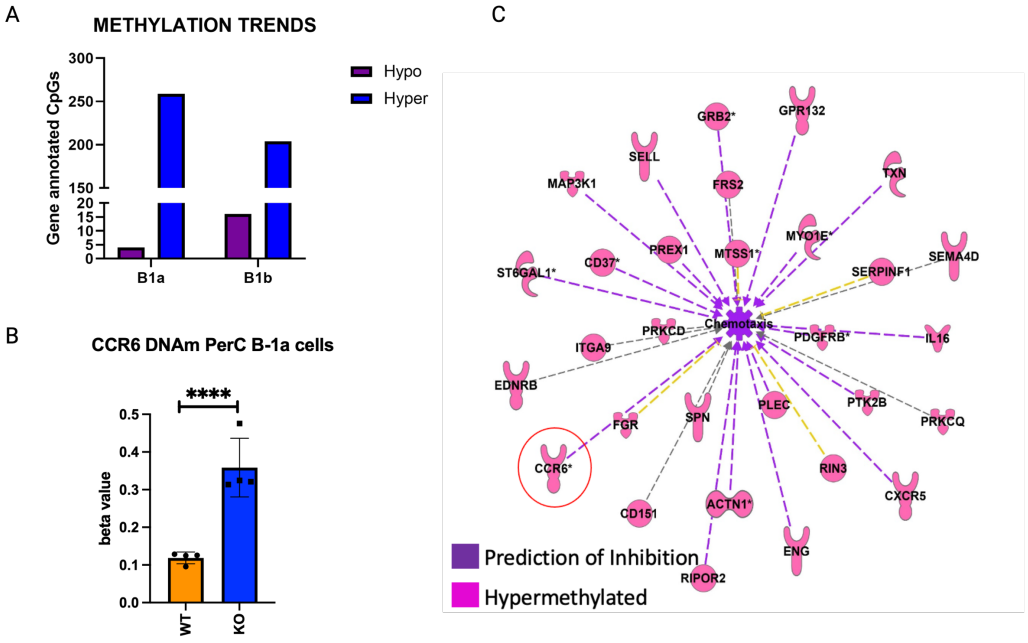
A
METHYLATION TRENDS
Gene annotated CpGs
300
250
200
150
20
15
10
5
0
B1a
B1b
Hypo
Hyper
B
CCR6 DNAm PerC B-1a cells
****
beta value
0.5
0.4
0.3
0.2
0.1
0.0
WT
KO
C
GRB2*
GPR132
SELL
MAP3K1
FRS2
TXN
MYO1E*
PREX1
MTSS1*
CD37*
SEMA4D
ST6GAL1*
SERPINF1
PRKCD
Chemotaxis
PDGFRB*
IL16
ITGA9
EDNRB
PLEC
PTK2B
PRKCQ
FGR
SPN
CCR6*
RIN3
CXCR5
ACTN1*
CD151
ENG
RIPOR2
Prediction of Inhibition
Hypermethylated

Figure 23. Chemokine receptor expression in B-1 cells from TET2-KO and WT mice. (**A - D**), Bar chart displaying Median Fluorescence Intensity (MFI) of CCR6 (**A**), CCR7 (**B**), CXCR4 (**C**), and CXCR5 (**D**) in B-1a cells and B-1b cells from the peritoneal cavity (**left**), the BM (**middle**), or the spleen (**right**) of TET2-KO (n = 4) and WT (n = 4) mice. Blue and orange represent WT and TET2-KO mice, respectively. Significance was determined with two-tailed Mann-Whitney U-tests (* $p < 0.05$).

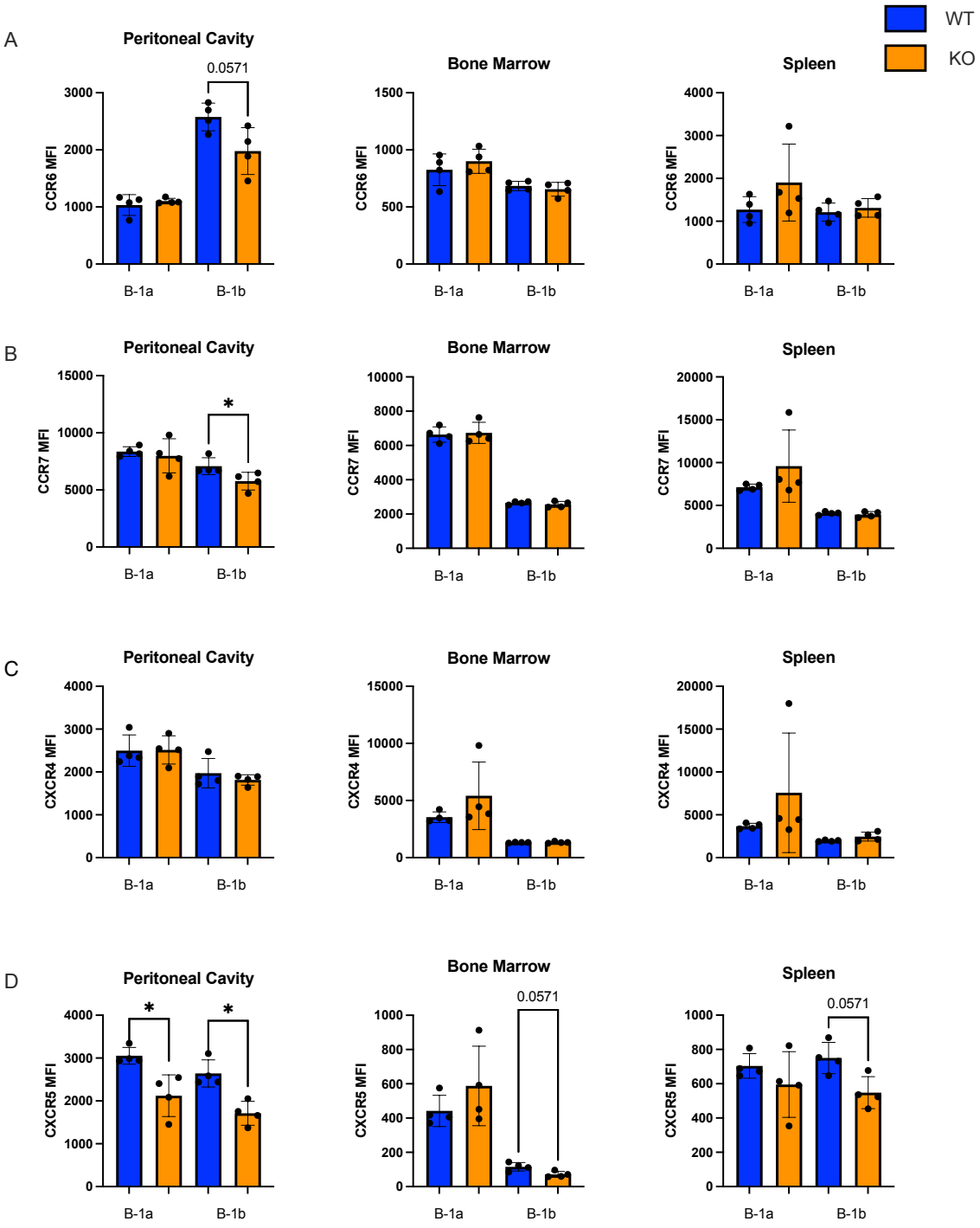
WT
KO
A
Peritoneal Cavity
Bone Marrow
Spleen
CCR6 MFI
0.0571
B-1a
B-1b
B
CCR7 MFI
*
C
CXCR4 MFI
D
CXCR5 MFI

Appendix 2: IgM to OSEs levels in mice with TET2-KO and humans with TET2 mutations compared to WT

Rationale

Malondialdehyde-modified low-density lipoprotein (MDA-LDL) and Copper-oxidized LDL (Cu-oxLDL) are oxidation-specific epitopes (OSEs) that IgM binds to, preventing uptake by macrophages and plaque generation in atherosclerosis. E06 is a T15 idiotype IgM natural antibody (Nab) exclusively produced by B-1 cells, which recognizes the phosphocholine (PC) head group in oxidized phospholipids on the surface of apoptotic cells, and the PC present on the cell wall of *Streptococcus pneumoniae* thus facilitating apoptotic cell clearance and protection from infectious pathogens [77]. The increase in V_H11 and V_H12 pairing that are typical for B-1a cells producing natural antibodies is consistent with the increase in IgM to OSEs in the plasma (Figure 16). Elevated levels of IgM to OSEs have been previously correlated with a reduced risk of acute myocardial infarction [227, 232], ASCVD [85, 177-182], and a diminished risk of fatty liver disease [177, 233, 234]. Additionally, consequences of metabolic dysregulation such as obesity-associated inflammation, glucose intolerance, and insulin resistance are less severe with elevated IgM to OSE [81, 183]. This association implies a protective function of those IgMs in the context of inflammatory diseases, such as atherosclerosis. We used ELISA to evaluate several IgM to OSEs in both mice and humans with TET2 deficiency.

Methods

Human Subjects

Fifty-eight human subjects were recruited for study through the Cardiac Catheterization laboratory at the University of Virginia as previously described [246]. All participants provided written informed consent prior to enrollment, and the study was approved by the Human IRB Committee at UVA.

Sample Preparation and Archer VariantPlex Myeloid Panel Sequencing

Peripheral blood mononuclear cells and B cell subsets were sort-purified from whole blood. DNA was extracted using Zymopure Plasmid Mini Prep kit and stored in EDTA-free UltraPure water. Briefly, DNA was fragmented before undergoing end repair, ligation, PCR, and barcoding. Library concentration was quantified using the KAPA Universal Library Quantification Kit, diluted to an appropriate concentration, and then libraries were pooled at equimolar concentrations. Sequencing was performed on the Illumina MiSeq. Libraries were de-multiplexed, and data was analyzed with Archer Analysis.

Mice

All animal protocols were approved by the Animal Care and Use Committee at the University of Virginia. TET2-KO mice [112] were provided by Dr. Kenneth Walsh (University of Virginia). The model was generated by Ko *et al.* and targeted the

endogenous *TET2* locus to create a conditional allele that enabled the deletion of exons 8, 9, and 10, the catalytic region of TET2 [112]. Mice were maintained on a 12-h light/dark schedule in a specific pathogen-free animal facility and given food (standard chow diet, Tekland 7012) and water *ad libitum*. The number of mice included in each study is indicated in the figures or the associated legends.

ELISA for quantification of IgM to OSEs in mice and humans

Levels of IgM antibodies specific for MDA-LDL, Cu-oxLDL, PC-BSA, and T15-E06 idiotype in mouse plasma were determined as previously described [61, 247]. Levels of IgM or IgG against MDA-LDL in human plasma were measured by chemiluminescent ELISA as previously described [81].

Results

MDA-LDL IgM is elevated in both mice and humans with TET2 deficiency

Interestingly, plasma levels of IgM specific to OSE to malondialdehyde-modified low-density lipoprotein (MDA-LDL) showed a statistically significant increase in both mice and humans with TET2 deficiency (Figure 24). Cu-oxLDL, PC-BSA, and T15-E06 idiotype exhibited no differences in mice. Total IgM and IgG levels were not changed in humans. Total IgM, but not IgG, was elevated in mice with TET2-KO compared to WT.

Figure 23. IgM to OSE levels in TET2-KO and WT mice and humans with mutations in TET2. Enzyme-linked immunosorbent assay (ELISA) of total IgM (**A**), IgM to MDA-LDL (**B**), total IgG (**C**) from plasma of TET2-KO (n = 26) and WT (n = 26) mice. ELISA of human total IgM (**D**) and IgM to MDA-LDL (**E**) from the plasma of humans with TET2 mutations (n = 13) or with functional TET2 (n=45). ELISA of IgM to Cu-oxLDL (**F**), IgM to T15-E06 (**G**), and IgM PC-BSA (**H)** from plasma of TET2-KO (n = 26) and WT (n = 26) mice. Blue and orange represent WT and TET2-KO mice, respectively. The data is not normalized to total IgM. Significance was determined with two-tailed Mann-Whitney U-tests (* $p < 0.05$).

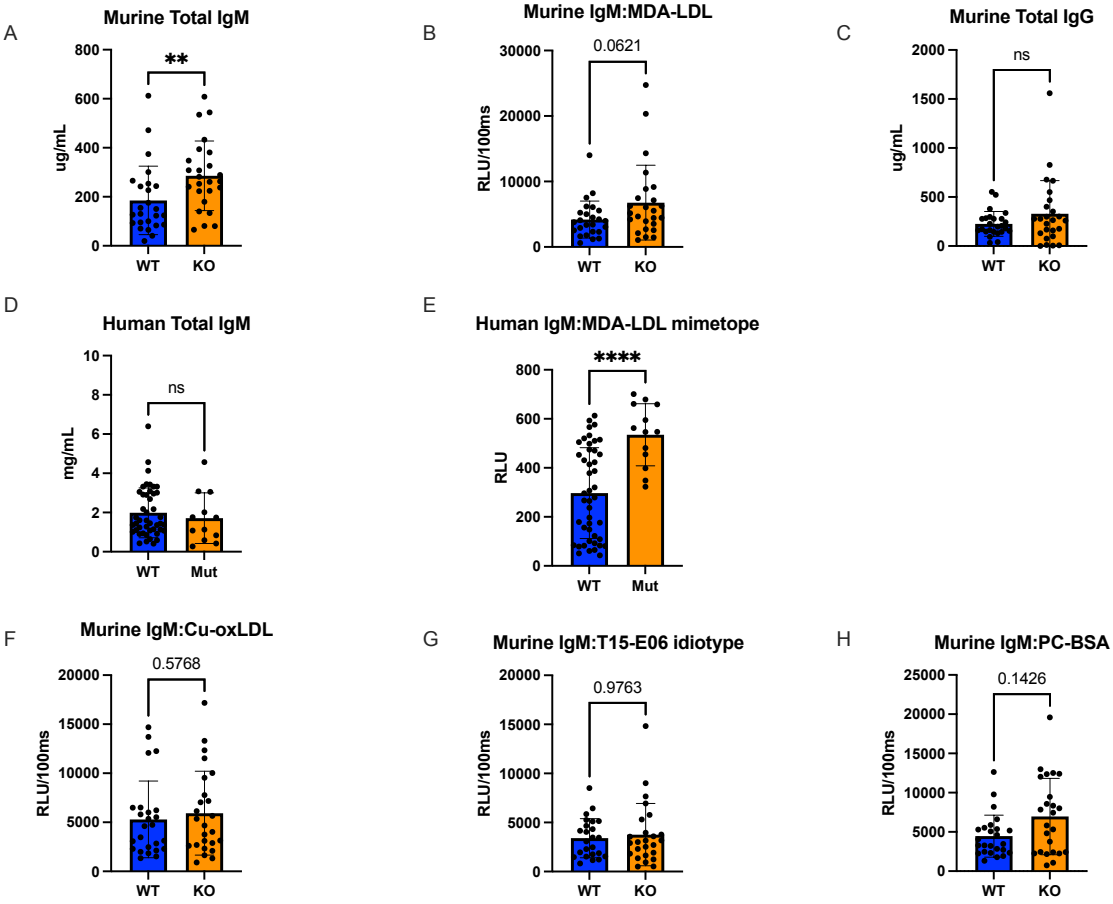
A
Murine Total IgM
ug/mL
800
600
400
200
0
**
WT
KO
B
Murine IgM:MDA-LDL
RLU/100ms
30000
20000
10000
0
0.0621
WT
KO
C
Murine Total IgG
ug/mL
2000
1500
1000
500
0
ns
WT
KO
D
Human Total IgM
mg/mL
10
8
6
4
2
0
ns
WT
Mut
E
Human IgM:MDA-LDL mimetope
RLU
800
600
400
200
0
****
WT
Mut
F
Murine IgM:Cu-oxLDL
RLU/100ms
20000
15000
10000
5000
0
0.5768
WT
KO
G
Murine IgM:T15-E06 idiotype
RLU/100ms
20000
15000
10000
5000
0
0.9763
WT
KO
H
Murine IgM:PC-BSA
RLU/100ms
25000
20000
15000
10000
5000
0
0.1426
WT
KO

Conclusions

The observed rise in protective IgM to OSEs following the global loss of TET2 is at odds with previously shown deleterious effects of loss-of-function TET2 mutation in cardiovascular disease [86, 110, 111, 128, 235]. The investigation into whether this phenomenon is B cell-specific needs further study. It is also important to note that the mouse model is a total knockout of the TET2 gene while the data generated from human PBMCs covers an array of TET2 mutations. Importantly, the level of MDA-LDL-IgM in humans with TET2 mutations is elevated despite no difference in total IgM, suggesting that the increase in IgM-OSE is due to antibody repertoire and not due to an overall increase in total IgM production. Nevertheless, understanding the mechanisms underlying the production of these protective IgM in the context of TET2 mutations holds the potential for identifying cell-targeted therapies in the treatment of inflammatory diseases, such as atherosclerosis.